University of Calgary

PRISM Repository **https://prism.ucalgary.ca**

The Vault Open Theses and Dissertations

2021-05-05

Crystal Chemistry of Wulfenite (PbMoO4) and Wolframite ([Fe,Mn]WO4)

Umbsaar, Darren Andrew

Umbsaar, D. A. (2021). Crystal Chemistry of Wulfenite (PbMoO4) and Wolframite ([Fe,Mn]WO4) (Master's thesis, University of Calgary, Calgary, Canada). Retrieved from https://prism.ucalgary.ca. http://hdl.handle.net/1880/113407

Downloaded from PRISM Repository, University of Calgary

UNIVERSITY OF CALGARY

Crystal Chemistry of Wulfenite ($PbMoO_4$) and Wolframite ($[Fe,Mn]WO_4$)

by

Darren Andrew Umbsaar

A THESIS
SUBMITTED TO THE FACULTY OF GRADUATE STUDIES
IN PARTIAL FULFILMENT OF THE REQUIREMENTS FOR THE
DEGREE OF MASTER OF SCIENCE

GRADUATE PROGRAM IN GEOLOGY AND GEOPHYSICS

CALGARY, ALBERTA

MAY, 2021

© Darren Andrew Umbsaar 2021

Abstract

This study examines the crystal chemistry of some natural simple molybdate and tungstate minerals, namely wulfenite ($PbMoO_4$) and wolframite ($[Fe,Mn]WO_4$). Historically, these mineral species have been a challenge to analyze through X-ray diffraction (XRD) methods, due to the presence of large atoms (Pb, Mo, and W) within the structure. These large atoms dominate in scattering X-rays, and Pb also has high absorption, making it a challenge to accurately determine the position of the oxygen atoms, which are much lighter and do not contribute to the diffraction pattern as strongly. Wulfenite samples that are analyzed in this study are from: (1) Laurion, Greece; (2) Red Cloud Mine, Arizona; (3) Glove Mine, Arizona; (4) Taco Mine, Utah; (5) Mezica Mine, Slovenia; (6) Touissit, Morocco; and (7) Los Lamentos, Mexico. Wolframite samples that are analyzed in this study are from: (1) Tong Wah (Tae Wha) mine, Korea; (2) Oregon Mine, Boulder, Colorado; (3) Silverton, Colorado; and (4) Pasto Bueno, Peru. These minerals were examined using the electron probe microanalyzer (EPMA), however only the crystal structure of the wulfenites were examined using synchrotron High Resolution Powder X-Ray Diffraction (HRPXRD). The wulfenite samples were very pure, (ranging within $Pb_{0.99\text{-}1.00}Mo_{0.99\text{-}1.00}O_4$) with only trace amounts of V^{5+}, Cr^{6+}, W^{6+}, and S^{6+} detected by the EPMA. Wolframite samples showed a compositional range between $(Mn_{0.65}Fe_{0.37})_{\Sigma 1.02}W_{0.99}O_4$ and $(Mn_{1.00}Fe_{0.00})_{\Sigma 1.00}W_{0.99}O_4$. Each wolframite was quite homogeneous, except for the sample from Oregon Mine, Colorado, whose Mn-contents ranged from 0.746 to 0.864 *apfu* throughout the crystal indicating it may be a multiphase sample.

For the wulfenite samples, structural Rietveld refinements confirmed tetragonal space group $I4_1/a$ and achieved the following reduced χ^2 and overall $R(F^2)$ values: Laurion, Greece (2.055, 0.0798); Red Cloud Mine, Arizona (1.698, 0.0939); Glove Mine, Arizona (1.903, 0.0684); Taco Mine, Utah (1.785, 0.0911); Mezica (Mies) Mine, Slovenia (1.782, 0.1045); Touissit, Morocco (1.958, 0.0827); and Los Lamentos, Mexico (1.589, 0.1046). Wulfenite crystals were homogeneous, single phases, and displayed no hemimorphic morphologies or hemimorphic symmetry reductions, as has been reported by some previous studies. Bond distances were quite similar between samples, however minute variations may be due to trace element substitution in the B-site or crystallinity differences. Edge Length Distortions (ELD) and Tetrahedral Angle Variance (TAV) were calculated to quantify Mo tetrahedral compression.

Acknowledgements

Special thanks to Dr. Sytle Antao of the University of Calgary for supervising this Master's thesis. Thank you for providing guidance, advice, support, and extensive proofreading during my study. It was a pleasure and an honor to complete this project under your supervision. You have given me a much stronger grasp on the study of mineralogy, and I am very grateful for the knowledge you have imparted to me during my time at U of C.

Thanks to Dr. Robert Marr for your crucial assistance in operating the electron microprobe. Your knowledge of the microprobe's intricacies was absolutely essential to the collection of mineral analyses.

Thanks to the beamline 11-BM, Advanced Photon Source (APS) at the Argonne National Laboratory (ANL), whose facility was imperative for the collection of HRPXRD data.

I would also like to say a special thank you to Kaveer Hazrah, my friend and colleague who also was a Master's student with Dr. Antao. I am grateful for your generous help and advice, and for being there to just chat about each other's projects, and to share in both the struggles and triumphs of writing a thesis.

Thank you to my family for supporting me throughout this thesis and during my time at university. You helped clear my head, and gave me the motivation to keep going and a reason to laugh and smile along the way.

Table of Contents

List of Tables

List of Figures

List of Abbreviations and Formulas

Abbreviations:

XRD = X-Ray Diffraction

EPMA = Electron Probe Microanalyzer/analysis

ICP-MS = Inductively-Coupled Plasma Mass Spectrometry

HRPXRD = High Resolution Powder X-Ray Diffraction

Z = Formula Units

BSE image = Back Scatter Electron image

apfu = Atoms per formula unit

Mineral Formulas:

$CaWO_4$ = Scheelite

$CaMoO_4$ = Powellite

$PbWO_4$ = Stolzite

$PbMoO_4$ = Wulfenite

$(Fe,Mn)WO_4$ = Wolframite

$FeWO_4$ = Ferberite

$MnWO_4$ = Hübnerite

CHAPTER 1 – Introduction

1.1 Purpose of Study

This study examines the crystal chemistry of wulfenite ($PbMoO_4$) and wolframite ($[Fe,Mn]WO_4$). There are several goals that this thesis has accomplished:

1. Provide accurate geochemical and structural characterizations of natural wulfenite and wolframite mineral specimens from localities around the globe using electron probe microanalyses (EPMA) and synchrotron high resolution powder X-ray diffraction (HRPXRD) techniques.
2. Compare and contrast this data with geochemical and structural analyses from other authors in an effort to more accurately characterize the structures and compositions of these minerals.

1.2 Organization of Thesis

This thesis is organized into three main sections: Chapter 2 contains a general introduction to the chemistry and structure of molybdate and tungstate minerals of the form ABO_4 (where A = divalent metal cation; B = W^{6+} or Mo^{6+}), as well as a discussion on the analytical challenges associated with X-ray diffraction (XRD) analyses of these large-cation mineral groups. The following chapters are written as mineralogical manuscripts on the chemistry and structure of wulfenite (Chapter 3) and wolframite (Chapter 4). These sections will provide a review of the results of previous studies on those mineral groups as well as comparisons to the EPMA and HRPXRD results from this study. The results of this study were also presented as a poster at the virtual Calgary Geoconvention 2020 (Umbsaar and Antao 2020).

CHAPTER 2 - Introduction to ABO_4 Molybdates and Tungstates

2.1 Crystal Chemistry

For over a century, crystallographers and mineralogists have investigated molybdate and tungstate minerals of the form ABO_4 (where A = divalent metal cation; B = W^{6+} or Mo^{6+}). Powder and/or single crystal XRD experiments on natural and synthetic specimens have provided a rich database of information on these species (Barth 1926; Sleight 1972). These minerals crystallize in two main crystal systems: (1) the tetragonal scheelite-type structure (space group $I4_1/a$, formula units, Z, = 4), and (2) the monoclinic wolframite-type structure (space group $P2/c$, Z = 2), depending on the size of the A cation (Hazen et al. 1985; Maczka et al. 2012). In general, when the A cation radius is >0.90 Å the crystal will form the tetragonal scheelite-type structure, whereas an A cation radius of <0.90 Å will favor the monoclinic wolframite-type structure (Hazen et al. 1985; Macavei and Schulz 1993). Therefore, in scheelite-type minerals the A sites are commonly occupied by larger cations such as Ca^{2+}, Pb^{2+}, Sr^{2+}, Ba^{2+}, Eu^{2+}, or Cd^{2+} whereas the A sites in wolframite-type minerals are commonly occupied by transition metals with smaller ionic radii such as Fe^{2+}, Mn^{2+}, Mg^{2+}, Zn^{2+}, Ni^{2+}, Co^{2+}, or Cu^{2+} (Broch 1930; Sleight 1972; Redfern et al. 1995; Zhuravlev et al. 2011).

2.2 Analytical Challenges

X-ray diffraction experiments on ABO_4 tungstate and molybdate minerals have long been a challenge for a few reasons. Firstly, molybdates and tungstates have inherently large linear absorption coefficients, being composed of large atoms such as Pb, Mo, and W, and therefore may be subject to errors in the X-ray data (Dickinson 1920; Hazen et al. 1985). Furthermore, since the atomic scattering factor, *f*, is proportional to the number of electrons in a species, the large atoms in the structure (namely Pb, Mo, and W) dominate in scattering X-rays, which makes it challenging

to precisely determine the atomic coordinates of oxygen, being a much lighter element with a weaker scattering factor, and therefore a weaker contribution to the overall peak intensity (Leciejewicz 1965). To overcome this, several studies have applied neutron diffraction to precisely determine the oxygen positions in tungstates and molybdates. This is because neutron scattering length is independent of atomic number (O, Pb, Mo, and W are of the same order of magnitude) as opposed to the scattering of X-rays which is related directly to the number of electrons present (David et al. 2002). Successful neutron diffraction studies include structural refinements of scheelite ($CaWO_4$) (Kay et al. 1964), powellite ($CaMoO_4$) (Gurmen et al. 1971), wulfenite ($PbMoO_4$) (Leciejewicz 1965), ferberite ($FeWO_4$) (Ulku 1967), hübnerite ($MnWO_4$) (Dachs et al. 1967), sanmartinite ($ZnWO_4$) (Schofield et al. 1996, 1997), and russellite (Bi_2WO_4) (Knight 1992). However, neutron diffraction has a few drawbacks: (1) the necessity of large sample sizes, since neutrons have a high penetration (David et al. 2002); (2) neutron beams are much weaker in intensity than a synchrotron X-ray source, and therefore have a much lower resolution, and often poorer signal to noise ratio.

2.3 Benefits of Synchrotron HRPXRD

This study is dedicated to accurately determining crystal structure data specifically on the minerals wulfenite ($PbMoO_4$) and wolframite ($[Fe,Mn]WO_4$). In an effort to overcome the aforementioned obstacles involved with conventional, in-house XRD, and to acquire accurate structural data for these minerals, this study uses state-of-the-art synchrotron high resolution powder X-ray diffraction (HRPXRD). The main benefit of synchrotron HRPXRD is its high resolution afforded by the extremely high beam intensity and the finely-tuned monochromatic radiation. This use of strictly monochromatic radiation produces very narrow diffraction peaks,

which helps to distinguish closely spaced peaks and allows for superior peak indexing (cell parameter determination). Common conventional XRD experiments often have problems with peak broadening and overlap since these XRD sources cannot produce a sufficiently powerful monochromatic beam. Additionally, the intensity of the synchrotron source means that more data points are collected, and it therefore produces a more detailed diffraction pattern overall. Therefore, in this study, synchrotron HRPXRD was the method of choice, which is especially important in analyzing minerals with high absorption coefficients.

CHAPTER 3 – Wulfenite Crystal Chemistry

3.1 Introduction

Wulfenite ($PbMoO_4$) is a member of the scheelite-type group of molybdates and tungstates, which have the general formula: ABO_4, where A is a divalent metal cation with an ionic radius >0.90 Å (commonly Ca^{2+}, Pb^{2+}, Sr^{2+}, Ba^{2+}, Eu^{2+}, or Cd^{2+}) and B is a highly charged cation (W^{6+} or Mo^{6+}) (Sleight 1972; Hazen et al. 1985). This mineral group has tetragonal symmetry ($a = b \neq c$; $\alpha = \beta = \gamma = 90^{\circ}$) and belongs to space group $I4_1/a$ with four formula units per unit cell ($Z = 4$) (Barth 1926). This space group symbol indicates that it is a body-centered (*I*-type) lattice, and the cell contents can be generated with a 4-fold screw axis oriented perpendicular to an *a*-glide plane. Wulfenite has a variety of possible crystal habits, with the most common being tabular, square beveled, or bipyramidal crystals. It is a relatively soft mineral (Moh's Hardness = 3) with a vitreous lustre, and occurs in a myriad of colours including: (commonly) brown, yellow, orange, red and (rarer) green, blue, white, grey, and black (Bideaux 1990). Optical and infrared spectroscopic studies have determined that Cr^{6+} substituting for Mo^{6+} causes yellow to red colours (Haberlandt and Schroll 1949). Experiments on Cr^{6+}-doped wulfenite crystals showed that even 0.002 *apfu* of Cr^{6+} substituting for Mo^{6+} was sufficient to produce an orange colour, and values above 0.01 *apfu* produced a red color (Talla et al. 2013). Other authors suggest substitution of V, Cu, and over-stoichiometric Pb are possible sources of red colouration, whereas As may cause yellow to green coloration (Bideaux 1990; Recnik et al. 2014).

Wulfenite ($PbMoO_4$) usually occurs as a secondary mineral formed in shallow, oxidized zones of lead-zinc hydrothermal sulfide deposits. Typically, oxidizing groundwater percolates through the host rock and breaks down primary sulfides such as galena (PbS), sphalerite (ZnS), and molybdenite (MoS_2) to generate Pb^{2+} and MoO_4^{2-} ions in solution, which recombine under

oxidizing conditions to precipitate wulfenite (Olson 1966; Bideaux 1990; Vesselinov 1996). Some of the scheelite-type molybdates and tungstates possess unique photoluminescent properties such as fluorescence and phosphorescence, making them suitable materials for industrial products such as scintillators, radiation detectors, solid-state laser sources, acousto-optic devices *etc*. (Pinnow et al. 1969; Blasse 1997; Nakamura et al. 2002; Vernaleken et al. 2007; Sczancoski et al. 2009; Bomio et al. 2013). As such, knowledge of the fundamental structure and chemistry of this mineral group may be beneficial to industrial applications, however these precise applications are beyond the scope of this thesis.

Table 3.1: Structural data for stolzite ($PbWO_4$) and wulfenite ($PbMoO_4$) listed with increasing *V* within each series

Reference	Locality	Composition	*a*/Å	*c*/Å	*V*/Å^3	B-O/Å	A-O1/Å	A-O2/Å	<A-O>/Å	<O-O>/Å	<O-B-O>/°
Chipaux et al. (2001)^{P,S}	Syn (yellow)	$PbWO_4$	5.43241(48)	12.04817(106)	355.55(9)*	1.799*	2.582*	2.628*	2.605*	2.938*	109.48*
Xu et al. (1995)^{P,N}	Yaogangxian, China	$Pb_{1.03}Mg_{0.02}W_{0.98}O_4$	5.44503(3)	12.0495(1)	357.248(7)*	1.780*	2.591*	2.608*	2.599*	2.902*	109.77*
Moreau et al. (1996)^{S,S}	Syn	$PbWO_4$	5.456(2)	12.020(2)	357.81(32)*	1.795(8)	2.580(8)	2.637(8)	2.609(6)*	2.931*	109.49*
Moreiras et al. (1991)^{S,N}	La Tala, Spain	not given	5.455(1)	12.039(1)	358.2(2)	1.780(24)	2.627(24)	3.094(23)	2.861(17)*	2.906(25)*	109.50*
Hazen et al. (1985)^{S,S}	Syn	$PbWO_4$	5.4595(3)	12.0432(7)	358.96(6)						
Swanson et al. (1957)^{P,S}	Syn	$PbWO_4$	5.4616	12.046	359.32*						
Sleight (1972)^{P,S}	Syn	$PbWO_4$	5.4622	12.048	359.4						
Laishevtseva et al. (1989)^{U,S}	Syn	$PbWO_4$	5.462(2)	12.05(15)	359.4						
Chipaux et al. (2001)^{P,S}	Syn (bottom)	$PbWO_4$	5.46462(49)	12.04787(109)	359.77(10)*	1.773*	2.613*	2.652*	2.633*	2.894*	109.49*
Thresiamma et al. (2008)^{P,S}	Syn	$PbWO_4$	5.4680	12.0593	360.56*						
Chipaux et al. (2001)^{P,S}	Syn (top)	$PbWO_4$	5.46979(52)	12.06339(117)	360.92(10)*	1.776*	2.613*	2.657*	2.635*	2.899*	109.48*
Hibbs et al. (2000)^{S,N}	San Francisco Mine, Mexico	$Pb_{1.00}(Mo_{0.90}W_{0.10})O_4$	5.436(2)	12.068(8)	356.6(5)	1.775(5)	2.611(5)	2.627(5)	2.619(4)*	2.898*	109.50(17)*
Secco et al. (2008)^{S,N}	Biella, Italy	$Pb_{1.00}(Mo_{0.99}W_{0.01})O_4$	5.433(1)	12.098(1)	357.1(2)	1.776(6)	2.601(7)	2.636(6)	2.619(5)*	2.900*	109.49*
Leciejewicz (1965)^{S,N}	Los Lamentos, Mexico	not given	5.4312(16)	12.1065(39)	357.12(33)*	1.772(6)	2.610	2.630	2.620*	2.895*	109.39(75)*
Lugli et al. (1999)^{S,N}	Monte Cengio, Italy	$Pb_{1.00}Mo_{1.00}O_4$	5.434(1)	12.107(1)	357.5(2)*	1.769(3)	2.611(3)	2.636(3)	2.624(2)*	2.888(4)*	109.50(9)*
Secco et al. (2008)^{S,N}	Biella, Italy	$Pb_{1.00}(Mo_{0.84}W_{0.16})O_4$	5.434(2)	12.106(2)	357.5(3)	1.781(11)	2.606(11)	2.626(10)	2.616(7)*	2.908*	109.49*
Laishevtseva et al. (1989)^{U,S}	Syn	$PbMoO_4$	5.436(2)	12.10(15)	357.6						
Hazen et al. (1985)^{S,S}	Syn	$PbMoO_4$	5.4351(3)	12.1056(8)	357.60(6)						
Sleight (1972)^{P,S}	Syn	$PbMoO_4$	5.4355	12.108	357.7						
Secco et al. (2008)^{S,N}	Biella, Italy	$Pb_{1.00}(Mo_{0.54}W_{0.46})O_4$	5.442(1)	12.078(1)	357.7(2)	1.767(10)	2.609(9)	2.647(10)	2.628(7)*	2.886*	109.48*
Swanson et al. (1957)^{P,S}	Syn	$PbMoO_4$	5.435	12.11	357.72*						

$V = a^2c$

*Calculated when not given in paper

Superscript Notation: 1st letter ^{P} = Powder XRD or ^{S} = Single Crystal XRD; 2nd letter ^{N} = Natural specimen, ^{S} = Synthetic specimen, ^{U} = Unknown/Not given

3.2 Previous X-Ray Diffraction Work on Scheelite-type Minerals

3.2.1 Background

This section will discuss the body of work collected by previous studies on scheelite-type molybdates and tungstates.

The structures of scheelite-type molybdates and tungstates have been investigated for over a century. The first documented XRD study of scheelite ($CaWO_4$) and wulfenite ($PbMoO_4$) was performed by Dickinson (1920); he determined that these minerals have a tetragonal unit cell ($a = b \neq c$; $\alpha = \beta = \gamma = 90^\circ$) and possess axial ratios (c/a) of 1.549 and 1.563, respectively. Dickinson (1920) stated that the unit cell was a face-centred lattice, however this was later found to be incorrect. Vegard (1926) undertook an investigation of the structure of scheelite and powellite in which he determined that scheelite, powellite, stolzite, and wulfenite are isomorphous and belong to space group $I4_1/a$, containing 8 formula units per unit cell (Z = 8). Theoretical structure factors were calculated in an effort to determine the oxygen atomic coordinates, and although he tried many possibilities, he encountered oxygen atomic arrangements producing either incorrect peak intensities, or too high symmetry (Vegard 1926). He concluded with remarks about the coordination of the Ca and W atoms: each Ca atom is in contact with 8 O atoms, each O touches two Ca atoms, one W atom, and two other O atoms, while each W atom is in a tetrahedral coordination with 4 O, which are slightly compressed parallel to the c-axis. While Vegard (1926) determined the correct space group, $I4_1/a$, Barth (1926) noted that a simpler lattice containing only 4 formula units (Z = 4) exists by rotating the X and Y axes 45° about the Z axis. As a result, the axial ratio *(c/a)* of scheelite increases from ~1.53 to ~2.17 and the cell volume decreases by 50% (Barth 1926). Henceforth, authors following Barth (1926) report unit cell dimensions of all scheelite-type minerals using the smaller, simplest, body-centred lattice ($I4_1/a$, Z = 4). During these

early years, some other authors (Vegard and Refsum 1927; Aanerud 1931) also performed XRD analyses to determine cell parameters of common scheelite-type tungstates and molybdates containing A cations of Ca, Pb, Sr, and Ba.

As mentioned previously, a common difficulty experienced by early workers on tungstate and molybdate minerals was the accurate determination of oxygen atomic coordinates in the presence of large atoms Pb, W, and Mo (Dickinson 1920; Vegard 1926). To address this obstacle, Sillen and Nylander (1943) undertook a thorough investigation on the oxygen positions in scheelite-type molybdates and tungstates. Assuming the ions behaved as "rigid spheres", they proceeded to calculate the possible arrangements of atoms that were compatible with the variation of *a* and *c* parameters in the isomorphous scheelite-type series. They determined the following O atomic coordinates: for $CaWO_4$ and $CaMoO_4$, x = 0.25(2), y = 0.15(2), z = 0.075(15); for $PbWO_4$ and $PbMoO_4$, x = 0.25(2), y = 0.13(2), z = 0.075(15). Moreover, Sillen and Nylander (1943) confirmed the findings of Vegard (1926)—that the B tetrahedra are not regular, but rather slightly compressed perpendicular to the *c* axis. Unfortunately, these early studies by (Vegard 1926; Vegard and Refsum 1927; Aanerud 1931; Sillen and Nylander 1943) presented cell parameters for many scheelite-type minerals that are not very accurate, indicated by large discrepancies in cell parameters (usually much smaller cell volumes) compared to more recent studies, including this study.

In 1964, two independently conducted studies investigated the crystal structure of scheelite ($CaWO_4$) using two methods: XRD (Zalkin and Templeton 1964) and neutron diffraction (Kay et al. 1964). Their results were in excellent agreement, and they found that the W-O tetrahedra were slightly compressed with O-W-O angles of ~107.5° (x4) and ~113.4° (x2), and the 8-coordinated Ca polyhedra consisted of 2 different Ca-O bond lengths with a multiplicity of 4.

A year later, the first complete structural refinement of wulfenite ($PbMoO_4$) (including atom positions and bond distances) was published by Leciejewicz (1965) using single crystal neutron diffraction on a natural specimen from Los Lamentos, Mexico.

Neutron diffraction was also used by Gurmen et al. (1971) to determine the structure of $CaMoO_4$ (powellite), $SrWO_4$, $SrMoO_4$, and $BaWO_4$. They noted that the B-O bond distance is independent of the A species present, for a given B cation. A more recent investigation of powellite was performed by Barbosa et al. (2002), however the bond distances which were calculated from their given atomic coordinates were highly different than those reported by Hazen et al. (1985) and Gurmen et al. (1971), indicating that their results are probably not reliable.

Sleight (1972) published a comprehensive collection of accurate cell parameter measurements for a wide variety of scheelite-type and wolframite-type tungstate and molybdate minerals. In his paper, Sleight (1972) also remarks on some generalities in simple ABO_4 compounds, namely that the cell volume for molybdates is smaller than that of tungstates, while the *c/a* ratio for molybdates is larger than that of tungstates for a given A cation.

Hazen et al. (1985) performed single-crystal X-ray diffraction experiments on scheelite-type compounds $CaMoO_4$, $CaWO_4$, $CdMoO_4$, $PbWO_4$, and $PbMoO_4$, at pressures up to 6 GPa. No phase transitions to monoclinic fergusonite were observed in these conditions, however these compounds experienced anisotropic compression, where the *c*-axis was 1.2-1.9 times more compressible than the *a*-axis (Hazen et al. 1985). This pressure response in the scheelite structure is due to the relatively high rigidity of the Mo and W tetrahedra compared to the more compressible A polyhedra (Hazen et al. 1985; Maczka et al. 2012). The compressibility of the polyhedra is proportional to the polyhedral volume divided by the cation formal charge; this indicates that alkali

scheelite-type compounds such as $NaReO_4$ and $KRuO_4$ compress to a greater degree than tungstates and molybdates with divalent polyhedra (e.g. Ca, Pb, Cd, etc.) (Hazen et al. 1985).

Decades after that of wulfenite, the first structural refinement of the lead-tungstate end-member, stolzite ($PbWO_4$), was accomplished by Moreiras et al. (1991). Subsequently, during the next few years, the structure of stolzite would be refined by several other authors, namely Xu et al. (1995), Moreau et al. (1996), and Chipaux et al. (2001). All of these studies, however, including Moreiras et al. (1991), present structural results which appear to be inaccurate; the details of the qualms associated with these studies are discussed in section *3.2.5.*

Lugli et al. (1999) presented an accurate structural refinement of a natural wulfenite from Monte Cengio, Italy using single crystal XRD. Additionally, Lugli et al. (1999) noted that the isotropic thermal parameters (B_{eq}) of Pb and Mo were smaller than those of Leciejewicz (1965), however $B_{eq(O)}$ was essentially the same between studies. Lugli et al. (1999) reported anisotropic thermal parameters for Pb, Mo, and O as well; they found that the β_{33} component of the Mo atom was significantly higher than β_{11} and β_{22}, allowing the Mo tetrahedra to flatten slightly in the *ab* plane, lengthening the two O-O distances in the tetrahedra that are perpendicular to the $\bar{4}$ axis, which is the only geometric change to the tetrahedra permitted by the space group symmetry (Lugli et al. 1999).

A few more recent structural investigations of wulfenite have been performed by Hibbs et al. (2000), Secco et al. (2008), and Cora et al. (2011) with a special focus on addressing an enigmatic feature called "hemimorphism" reportedly present in certain natural wulfenite samples from localities such as Mezica (Mies) Mine, Slovenia, and The Christmas Gift Mine, Chillagoe, Australia. Hemimorphism implies that the structure is polar (or lacks a mirror plane perpendicular to the 4-fold axis) causing a symmetry reduction from space group $I4_1/a$ to $I\bar{4}$ (Bideaux 1990),

however there exists no consensus on whether or not wulfenite occasionally exists in space group $I\bar{4}$ (Hibbs et al. 2000; Cora et al. 2011). Only a small handful of natural samples of intermediate composition in the wulfenite-stolzite solid solution series have been examined using XRD (Quodling and Cohen 1938; Clark and Sillitoe 1970; Secco et al. 2008), and so far only Hibbs et al. (2000) and Secco et al. (2008) have provided structural data for non-endmember occurrences. Hemimorphism will be discussed in more detail in Chapter *3.1.3.*

3.2.2 Wulfenite Structure

As mentioned previously, the first complete structural refinement (atom positions and bond distances) of wulfenite was accomplished by Leciejewicz (1965) using single crystal neutron diffraction on a natural specimen from Los Lamentos, Mexico, and has since been refined by others (Table 3.1). Wulfenite possesses the same general structure as all scheelite-type ABO_4 compounds. It is composed of cations of Pb and Mo arranged in a close-packed cubic array (Sleight 1972). The Pb^{2+} cations form 8-coordinated polyhedra and have 2 slightly different Pb-O bond distances (Pb-O1 and Pb-O2), each with a multiplicity of 4 (Leciejewicz 1965). Each Pb polyhedron shares 4 edges with adjacent Pb polyhedra which are "piled up" parallel to the **c**-axis (Fig. 3.1) (Damascena Dos Passos et al. 2017). The Mo^{6+} cations occupy tetrahedral sites which are slightly compressed perpendicular to **c**-axis, yet maintain four Mo-O bonds of equal length (Leciejewicz 1965). Meanwhile each Mo tetrahedron is bonded to 8 different Pb sites by sharing 2 other Pb sites per oxygen (Fig. 3.1). The Pb and Mo cations lie in special positions 4b and 4a, respectively, of site symmetry $\bar{4}$ with coordinates (0, ¼, ⅝) and (0, ¼, ⅛), respectively, whereas the O atoms lie in general position 16f with coordinates (*x, y, z*) (Sillen and Nylander 1943; Hazen et al. 1985).

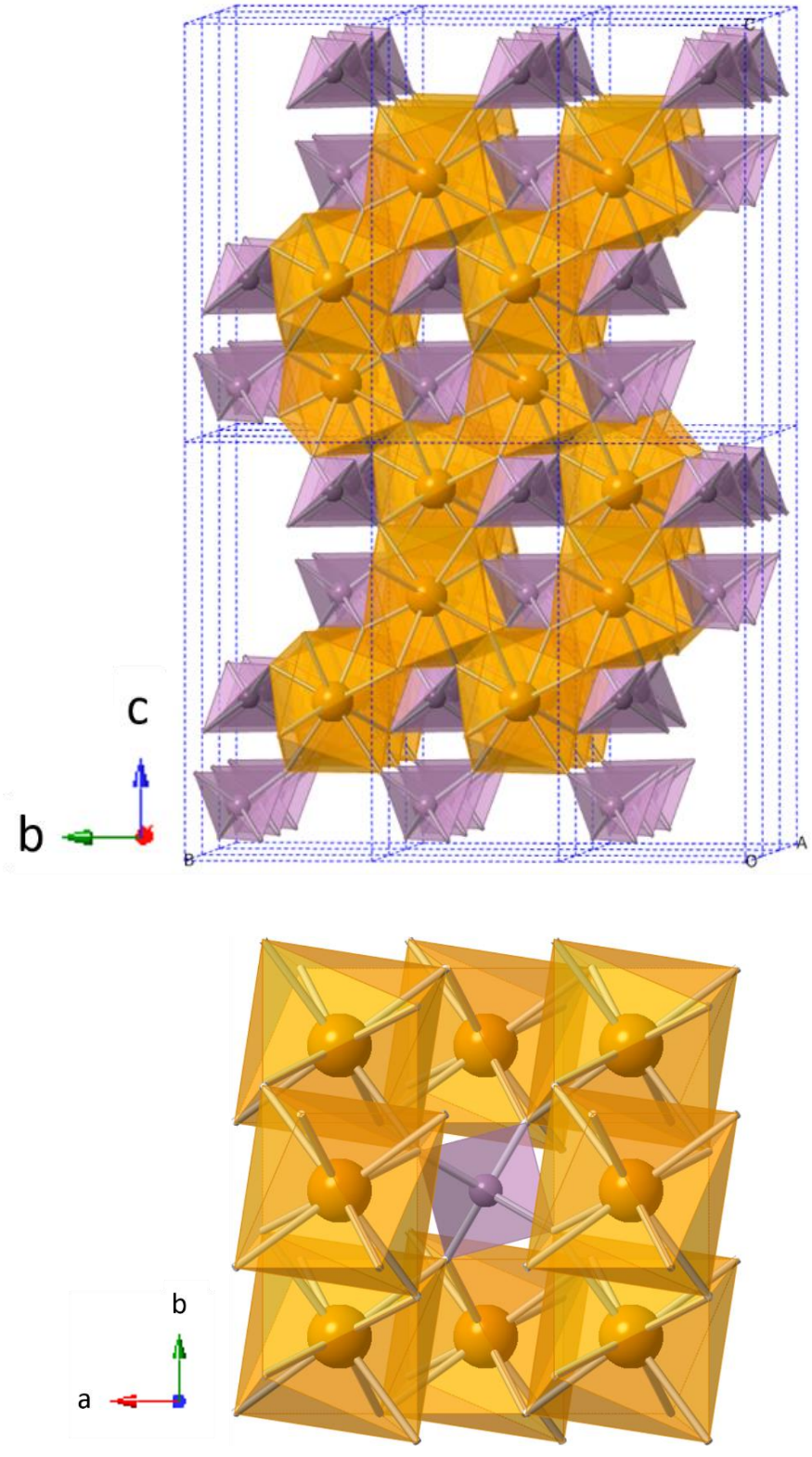

Figure 3.1: (top) Crystal structure of wulfenite viewed down the **a**-axis. (bottom) View down the **c**-axis depicting the corner sharing of the Mo tetrahedra (purple), and the edge sharing of adjacent Pb 8-fold polyhedra (orange).

3.2.3 Wulfenite-Stolzite Solid Solution Series

Wulfenite ($PbMoO_4$) is the Mo-bearing endmember in a solid solution series with its W-bearing counterpart, stolzite ($PbWO_4$), formed by the substitution of W^{6+} for Mo^{6+} (Nakamura et al. 2002). Wulfenite is more common than stolzite, and furthermore only a few studies have documented the occurrence of natural samples of intermediate composition in the wulfenite-stolzite series (Quodling and Cohen 1938; Clark and Sillitoe 1970; Hibbs et al. 2000; Secco et al. 2008). Over a century ago, Ullman (1912) discovered a W-Mo-bearing wulfenite, and named the mineral species "chillagite" after its origin in the Christmas Gift Mine, Chillagoe, Australia. However, years later Quodling and Cohen (1938) investigated a chillagite sample from the same locality with a composition of $3PbWO_4 + 5PbMoO_4$ using XRD, and they concluded that the similarity in ionic radii of W and Mo as well as similar cell parameters of stolzite, chillagite, and wulfenite preclude the possibility of a unique structure. Since then, several studies have confirmed the existence of a complete solid solution series between wulfenite and stolzite using X-ray Diffraction (XRD) on synthetic samples (Oeder et al. 1980; Laishevtseva et al. 1989; Nakamura et al. 2002). The existence of a solid solution series is rationalized by the similar ionic radii and charge of W^{6+} (0.42 Å) and Mo^{6+} (0.41 Å) (Shannon 1976), which facilitates their substitution within the tetrahedral B site (Oeder et al. 1980). Laishevtseva et al. (1989) performed XRD and Raman Spectroscopy on synthesized crystals across a range in the $PbMoO_4$-$PbWO_4$ series. They noted that the substitution of Mo for W increases the *a* parameter from approximately 5.436(2) to 5.462(2), and decreases the *c* parameter from approximately 12.10(15) to 12.05(15). Conversely, the substitution of Ca^{2+} for Pb^{2+} in either of these minerals is limited because the ionic radii of Pb^{2+} (1.29 Å) and Ca^{2+} (1.12 Å) are vastly different, and therefore cannot substitute in high abundance (Oeder et al. 1980; Nakamura et al. 2002). In support of this, Nakamura et al. (2002) performed

XRD experiments on synthetic samples across a compositional range in the **Ca**MoO_4-**Pb**MoO_4 (CP-M) and **Ca**WO_4-**Pb**WO_4 (CP-W) systems (bold added to show substituents) to investigate the extent of these solid solution series. They noted that immiscibility (separation into 2 phases) occurs for most intermediate compositions in the Ca-Pb series based on the splitting of diffraction peak (112). In summary, stolzite and wulfenite form a complete solid solution series via substitution of Mo with W.

3.2.4 The Problem of Hemimorphism

Hemimorphism in wulfenite has been an enigma that has confused mineralogists for decades (Hurlbut 1955; Vesselinov 1996). The term "hemimorphism" means that the crystal morphology appears different depending on which end of the **c**-axis it is viewed along (Fig. 3.2) (Bideaux 1990). This "polarity" in the structure seems to imply the absence of a centre of symmetry, reducing its symmetry from the typical space group $I4_1/a$ to $I\bar{4}$ (Hibbs et al. 2000; Cora et al. 2011). The Mezica (Mies) Mine, Slovenia (Cora et al. 2011; Recnik et al. 2014) and The Christmas Gift Mine, Chillagoe, Queensland, Australia (Hibbs et al. 2000) are the most notable locales to have been documented to form wulfenite possessing this unique property.

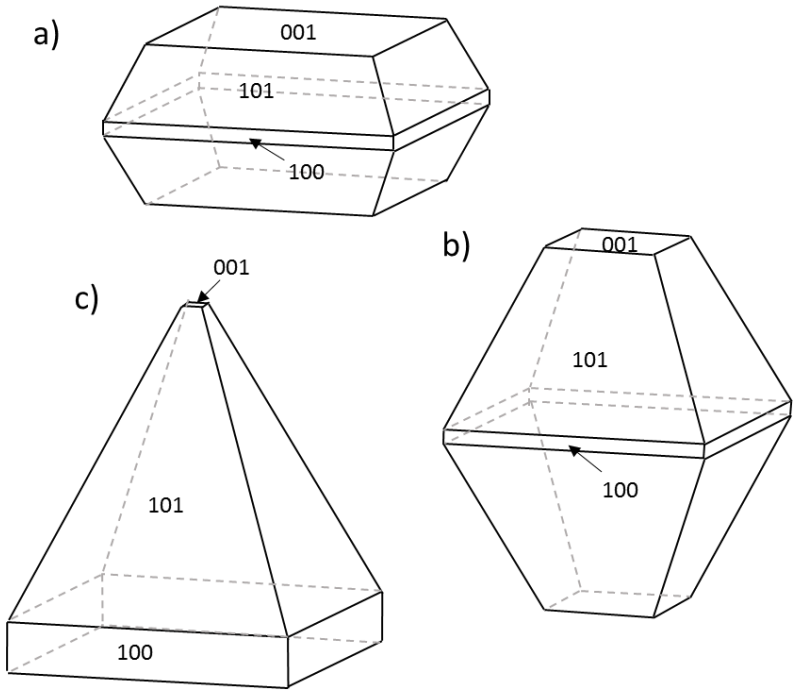

Figure 3.2: a) and b) are common truncated bipyramidal crystal habits seen in wulfenite, whereas c) is a hemimorphic pyramidal habit lacking a mirror plane perpendicular to the 4-fold axis. Adapted from Recnik et al. (2014).

A pyramidal wulfenite sample from the Helena Mine, Slovenia examined by Hurlbut (1955) displayed a feeble piezoelectric response, indicating polarity, which seems to imply that the crystal lacked the expected 4/m symmetry.

Decades later, in an effort to settle the debate, Hibbs et al. (2000) performed single crystal XRD experiments on W-rich wulfenite from Chillagoe, Queensland, Australia with a composition of $PbMo_{0.60}W_{0.40}O_4$. In the XRD trace, they observed 9 reflections in the (*hk*0) zone which were forbidden for space group $I4_1/a$. Additionally, the significant reflections 002, 006, 00 10, 00 14 were observed in the [00*l*] axial direction, precluding the existence of symmetry operations 4_1 (screw axis) and *a* (glide plane), invoking a reduction of symmetry to $I\bar{4}$. Systematic absences were consistent with space group $I\bar{4}$, which permits only the following reflections: $(h+k+l) = 2n$, (which means that $h+k+l$ must be an even number). They did not, however, observe the same

symmetry reduction in a sample of near-endmember composition ($PbMo_{0.90}W_{0.10}O_4$) from Sonora, Mexico. They therefore postulated that wulfenite samples containing significant amounts of both Mo and W (not near-endmember) can display hemimorphism because W and Mo become unequally distributed among the 2a and 2c sites, which may be a more thermodynamically stable arrangement. After reviewing the study by Hibbs et al. (2000), The Commission for New Minerals and Mineral Names (CNMMN) deemed that the name "chillagite" is not warranted as it is a structural variant of wulfenite (Jury et al. 2001). Instead, samples crystallizing in space groups $I4_1/a$ and $I\bar{4}$ are to be called wulfenite-$I4_1/a$ and wulfenite-$I\bar{4}$, respectively (Jury et al. 2001).

Since then, a few more studies have offered both support and also skepticism of the occurrence of wulfenite-$I\bar{4}$. Cora et al. (2011) observed forbidden reflections for space group $I4_1/a$ in a sample from Mezica (Mies) Mine, Slovenia, however unlike Hibbs et al. (2000), their sample was Mo-rich ($Pb_{0.94}Mo_{1.06}O_4$). They suggested the cause of hemimorphism to be ordering of Pb and Mo in the 2b position. One study by Secco et al. (2008), published several years after the study by Hibbs et al. (2000), completely disagrees with the occurrence of a symmetry reduction to wulfenite-$I\bar{4}$. Their study on three natural wulfenites of varying composition in the wulfenite-stolzite series from Biella, Italy found that the so-called "forbidden reflections" seen in the XRD traces were merely artifacts caused by "$\lambda/2$ effects" because those reflections suddenly disappeared upon decreasing the Mo X-ray tube voltage below 34.9kV (Kirschbaum et al. 1997; Secco et al. 2008). Therefore, they maintain that all wulfenite-stolzite compositions possess $I4_1/a$ symmetry.

It has been postulated by Vesselinov (1996) that the hemimorphic morphologies from Mezica Mine, Slovenia are not due to structural differences, but rather arise from local gradients in Pb and Mo concentrations parallel to the crystal's 4-fold axis during growth. This could potentially explain the occasional coexistence of hemimorphic and non-hemimorphic specimens, since the

morphology would depend on the crystal orientation relative to the source of the Pb ions (Recnik et al. 2014). However, it fails to explain hemimorphic crystal growth on limestone and limonite deposits at the mine, and furthermore does not explain why other localities in the world do not also apparently have this reliance on local cation concentrations (Recnik et al. 2014). Interestingly, hemimorphic wulfenite occurs more often on a limonite host compared to limestone and galena, so Recnik et al. (2014) suggests perhaps the presence of iron influences hemimorphic growth. In summary, the cause of hemimorphic morphologies, and whether or not a symmetry reduction to $I\bar{4}$ is involved is a matter of debate.

3.2.5 Reliability of Previous Studies

Literature data on the cell parameters, bond distances, and atomic positions of wulfenite and stolzite show noticeable discrepancies, especially data collected by early investigators such as Vegard and Refsum (1927), Aanerud (1931), Quodling and Cohen (1938), Sillen and Nylander (1943), and Clark and Sillitoe (1970) which have been excluded from Table 3.1 due to their inaccuracy. Even amongst the more recent studies listed in Table 3.1 and plotted in Figures 3.7, 3.9, and 3.10, there is considerable inconsistency, especially for the stolzite endmember. The qualms that the author has with previous structural studies are discussed in this section:

Structural results for stolzite presented by Moreiras et al. (1991), Xu et al. (1995), and Chipaux et al. (2001) may not be reliable for the following reasons: Moreiras et al. (1991) presented single crystal structural data for a natural stolzite from La Tala, Spain using Mo Kα radiation; the large Pb-O1 and Pb-O2 bond distances of 2.627(24) and 3.094(23), respectively, were anomalous, suggesting unreliable results. Xu et al. (1995) presented a powder XRD structural refinement of a natural stolzite from Yaogangxian, Hunan Province, China using Cu Kα radiation, however the distorted O-W-O tetrahedral bond angles of 103° (x4) and 123° (x2) deviate significantly from

other literature values, and their cell volume was even less than that of most wulfenites in literature, which suggests that the data may be unreliable. Xu et al. (1995) also mentioned that the stolzite sample contained tiny inclusions (μm) of an impurity phase (possibly grossular, quartz, or something else), but its intensities on the diffraction trace were less than 2% of that of stolzite and, reportedly, did not impact the refinement. Moreau et al. (1996) used Mo Kα radiation to analyze a single crystal of $PbWO_4$ crystal grown using the Czochralski method, having an exact composition of $PbO + WO_3$. Their structural results seem fairly accurate, however their cell volume was quite small—even less than the wulfenites analyzed in this study. Chipaux et al. (2001) acquired neutron diffraction data on synthetic $PbWO_4$ using the G4.1 two-axis multidetector powder diffractometer at the cold source beamline at the Laboratoire Léon Brillouin (LLB) in France. They presented results for the "top" and "bottom" sides of a synthetic $PbWO_4$ crystal bar, as well as a "yellow sample", which, according to the authors, "[came] from the early stage of the industrial R&D for CMS." The unit cell dimensions and atomic coordinates showed large variability between the "top", "bottom", and "yellow" samples, with cell volumes being 360.92 $Å^3$, 359.77 $Å^3$, and 355.55 $Å^3$, respectively. They postulated that the obvious cell parameter differences may be due to Pb-content decreasing from the "top" to "bottom" of the crystal bar, but they did not support this with any compositional data. The vagueness in sample description and crystal growth methodology, and the significant differences in cell parameters even within the same synthetic crystal bar suggest that the results may not be reliable, or, at least, prevents one from knowing which of their analyses is the most accurate. The least accurate analysis appears to be the "yellow" sample based on the unreasonably small cell volume of 355.55 $Å^3$; the cell volume for stolzite should always be slightly larger than wulfenite based solely on the argument of ionic radii (Sleight 1972).

Fortunately, literature data on wulfenite samples collected in recent decades, on the other hand, show more consistent values than that of stolzite. The wulfenite studies presented in Table 3.1 are all deemed to present reasonably accurate structural and cell data, and seem to not have any outstanding issues to discuss, unlike the stolzite studies. The author speculates that the reason for such variable results for stolzite could be because W (Z = 74) is a much heavier cation than Mo (Z = 42), and is therefore more subject to errors in X-ray data (mentioned in section 2.2) than wulfenite.

3.3. Experimental Methods

3.3.1. Electron Probe Microanalyses (EPMA)

A collection of seven wulfenite samples from various localities (Table 3.2) were quantitatively analyzed using the JEOL JXA-8200 EPMA at the University of Calgary. The JEOL operating program on a Solaris platform was used for ZAF correction and data reduction. The wavelength dispersive spectrometry (WDS) measurements were performed with a voltage of 20 kV, a current of 20 nA, and a beam diameter of 5 μm. The calibration standards used were: Cr = chromite; Pb = pyromorphite; W = scheelite; Ca, Mo = $CaMoO_4$; Zn = ZnO; V = V_2O_5; Ba, S = barite. The average wt. % of oxides (from 10 spot analyses) were used to calculate average atoms per formula unit (*apfu*) on the basis of 4 oxygens (Table 3.3). This compositional data is also represented in bar graphs in Figure 3.4. All spot analyses are tabulated in the Appendix (Tables A1-A7). Additionally, the V_2O_3 (V^{3+}) measurements were converted to V_2O_5 (V^{5+}) by multiplying the wt. % of V_2O_3 by the molar mass ratio, 181.88/149.88. Similarly, the Cr_2O_3 (Cr^{3+}) measurements were converted to CrO_3 (Cr^{6+}) by multiplying the wt. % of Cr_2O_3 by the molar mass ratio 200.00/152.00. These calculations are in accordance with the oxide conversion steps given by Allen and Buseck (1988). The back-scatter electron (BSE) images are shown in Figure 3.3, which depict the approximate locations of each spot analysis.

Table 3.2: Wulfenite samples from discs 1-X and 1-U. Listed from lowest to highest Pb *apfu.*

Sample #	Short form	Name	Mineral	Colour	Locality
1-X-1	1X	VC672	Wulfenite	Yellow	Taco Mine, Lucia, Utah
1-X-2	2X	VC1011	Wulfenite	Orange	Laurion, Greece
1-X-4	4X	VC866	Wulfenite	Black	Glove Mine, Santa Cruz Co, Arizona
1-X-5	5X	UC09955	Wulfenite	Yellow	Touissit, Morocco
1-X-6	6X	UC01598	Wulfenite	Orange	Mezica (Mies) Mine, Slovenia
1-U-7	7U	n/a	Wulfenite	Orange	Los Lamentos, Chihuahua, Mexico
1-U-8	8U	n/a	Wulfenite	Orange	Red Cloud Mine, La Paz County, Arizona

Sample 1X is a yellow, subhedral wulfenite fragment from Taco Mine, Lucia, Utah. It contains several small, dark inclusions of a Ca and Mg-rich mineral (likely dolomite). Small patches of calcite were detected outside of the main crystal. The mineral shows no zoning, and appears homogeneous based on BSE images and the EPMA analyses. On average, trace amounts of WO_3 (0.04 wt. %) and V_2O_5 (0.04 wt. %) are present. It is a nearly pure end-member composition: $Pb_{0.99}Mo_{1.00}O_4$.

Sample 2X is an orange, subhedral-euhedral wulfenite fragment from Laurion, Greece. The crystal is relatively inclusion-free, shows no zonation, and appears homogeneous. On average, trace amounts of V_2O_3 (0.32 wt. %) and CrO_3 (0.05 wt. %) are present; these are the highest abundances of V and Cr out of the selection of wulfenite samples on Disc 1-X. It is a nearly pure end-member composition: $Pb_{1.00}(Mo_{0.99}V_{0.01})O_4$.

Sample 4X is a black, fairly euhedral wulfenite from the Glove Mine, Santa Cruz County, Arizona. The crystal has a few inclusions of quartz, a Na-rich silicate, and some patches of clay minerals. Faint growth lines can be detected in the orientation of tiny inclusions, usually parallel to the crystal faces (Fig. 3.3); compositionally, the crystal is homogeneous and shows no zonation

patterns. The sample also contains a few grains of a Pb-Mn rich mineral were detected (possibly a carbonate); their surfaces appeared heterogeneous, showing a speckled, sand-like appearance at high magnification. On average, the wulfenite contains trace quantities of V_2O_5 (0.07 wt. %). It is a nearly pure end-member composition: $Pb_{0.99}Mo_{1.00}O_4$.

Sample 5X is a yellow, subhedral wulfenite fragment from Touissit, Morocco. The crystal is homogeneous, with only one small inclusion, and shows no zonation. On average, trace amounts of WO_3 (0.15 wt. %) and V_2O_5 (0.06 wt. %) are present. It is a pure end-member composition: $Pb_{1.00}Mo_{1.00}O_4$.

Sample 6X is an orange, subhedral-anhedral wulfenite fragment from the Mezica (Mies) Mine, Slovenia. The crystal is homogeneous, and shows no zonation. On average, trace amounts of WO_3 (0.04 wt. %), V_2O_5 (0.17 wt. %) and SO_3 (0.05 wt. %) are present. It is a nearly pure end-member composition: $Pb_{1.00}Mo_{0.99}O_4$.

Sample 7U is a yellow wulfenite from Los Lamentos, Chihuahua, Mexico. The average composition is very pure with trace amounts of WO_3 (0.06 wt. %) and V_2O_5 (0.05 wt. %) and SO_3 (0.06 wt. %) present. The abundances of WO_3 and SO_3 are rather variable. The composition is almost a pure end member: $Pb_{1.00}Mo_{0.99}O_4$

Sample 8U is an orange wulfenite from Red Cloud Mine, La Paz County, Arizona. The average composition is very pure, with trace amounts of WO_3 (0.14 wt. %) and V_2O_5 (0.01 wt. %) and SO_3 (0.02 wt. %) present. The WO_3 concentrations are quite variable, ranging from 0.00 to 0.40 wt. % within the crystal. The composition is a pure end member: $Pb_{1.00}Mo_{1.00}O_4$

3.3.2 Synchrotron High Resolution Power X-Ray Diffraction (HRPXRD)

Synchrotron High Resolution Powder X-Ray Diffraction (HRPXRD) experiments were performed at beamline 11-BM, Advanced Photon Source (APS), Argonne National Laboratory (ANL). A small fragment (about 2 mm in diameter) of the crystal was crushed to a fine powder using an agate mortar and pestle. The crushed sample was loaded into a Kapton capillary (0.8 mm internal diameter) and rotated during the experiment at a rate of 90 rotations per second. The data were collected at 23°C to a maximum 2θ of about 50° with a step size of 0.001° and a step time of 0.1s per step. The HRPXRD trace was collected with a unique multi-analyzer detection assembly consisting of twelve independent silicon (111) crystal analyzers and $LaCl_3$ scintillation detectors that reduce the angular range to be scanned and result in rapid acquisition of data. A silicon (NIST 640c) and alumina (NIST 676a) standard (ratio of 1/3 Si: 2/3 Al_2O_3 by weight) was used to calibrate the instrument and refine the monochromatic wavelength used in the experiment. Additional details of the experimental set-up are given elsewhere (Antao et al. 2008b; Lee et al. 2008; Wang et al. 2008).

3.3.3 Rietveld Structure Refinements

The HRPXRD traces were modelled using the Rietveld refinement method in the program GSAS (Larson and Von Dreele 2000) and using the EXPGUI interface (Toby 2001). Scattering curves for neutral atoms were used in the refinement. Starting atomic coordinates, cell parameters, and space group $I4_1/a$ were obtained from Leciejewicz (1965). In the program GSAS, the reflection-peak profiles were fitted using type-3 (pseudo-Voigt) functions. Firstly, the background was modelled with a shifted Chebyschev polynomial (5 terms). Full-matrix least-squares refinements varying the scale factor, unit-cell parameters, zero shift, atom coordinates, and

isotropic displacement parameters converged rapidly. The site occupancy factors (*sof*s) for all atoms were kept at 1 considering the fact that these samples are essentially pure end members. The number of data points and the number of observed reflections in the HRPXRD trace together with the Rietveld refinement statistical indicators and unit-cell parameters are given in Table 3.4. The atomic coordinates and isotropic displacement parameters (U_{iso}) are shown in Table 3.5. Selected bond distances and angles are given in Table 3.6. HRPXRD traces are shown in Figure 3.5 with peak intensities increased by a factor of 10 in the $2\theta > 17°$ region. Extraneous data in the region of $2\theta < 2°$ were manually excluded from the XRD traces. The experimental techniques described in this thesis are state-of-the-art. Similar experiments were successfully used by our research group to examine other minerals (Antao and Hassan 2002; Hassan et al. 2003; Hassan et al. 2004; Antao et al. 2005; Antao et al. 2008a; Antao and Hassan 2010; Skinner et al. 2011; Zaman et al. 2012; Antao 2013b, a; Antao and Klincker 2013, 2014; Antao et al. 2015)

Table 3.3: Chemical analyses for wulfenite. Average wt. % of oxides and calculated *apfu* on the basis of 4 oxygen atoms. Samples are listed with increasing Pb-content from left to right.

Sample Oxide	1X wt. %	4X wt. %	6X wt. %	2X wt. %	5X wt. %	7U wt. %	8U wt. %
PbO	60.06(50)	60.27(38)	60.69(31)	60.08(57)	60.75(42)	60.49(25)	60.47(35)
BaO	0.01(1)	0.01(2)	0.01(1)	0.02(3)	0.01(2)	0.01(2)	0.01(2)
CaO	0.00(1)	0.01(1)	0.01(1)	0.01(1)	0.01(1)	n	n
ZnO	0.00(0)	0.01(1)	0.00(1)	0.00(1)	0.00(0)	0.00(0)	0.00(1)
MoO_3	39.29(37)	39.37(23)	39.02(51)	38.30(33)	38.98(52)	38.65(31)	38.68(16)
WO_3	0.04(4)	0.01(3)	0.04(4)	0.02(4)	0.15(7)	0.06(9)	0.14(14)
SO_3	0.01(2)	0.01(2)	0.05(5)	0.03(5)	0.02(3)	0.06(7)	0.02(2)
CrO_3	0.00(0)	0.01(1)	0.00(0)	0.05(5)	0.00(0)	n	n
V_2O_5	0.04(4)	0.07(4)	0.17(7)	0.32(17)	0.06(5)	0.05(2)	0.01(1)
Total	**99.46**	**99.76**	**100.00**	**98.84**	**99.97**	**99.32**	**99.32**
	apfu	*apfu*	*apfu*	*apfu*	*apfu*	*apfu*	*apfu*
Pb^{2+} (1.29 Å)*	0.987(5)	0.988(6)	0.996(11)	0.997(6)	1.000(11)	1.003(6)	1.004(4)
Ba^{2+} (1.42 Å)	0.000(0)	0.000(1)	0.000(0)	0.000(1)	0.000(1)	0.000(0)	0.000(0)
Ca^{2+} (1.12 Å)	0.000(0)	0.001(0)	0.001(1)	0.000(0)	0.001(1)	n	n
Zn^{2+} (0.90 Å)	0.000(0)	0.000(0)	0.000(0)	0.000(0)	0.000(0)	0.000(0)	0.000(0)
ΣA	**0.988**	**0.989**	**0.997**	**0.998**	**1.001**	**1.003**	**1.004**
Mo^{6+} (0.41 Å)	1.001(2)	1.000(1)	0.992(6)	0.986(6)	0.995(5)	0.994(5)	0.995(3)
W^{6+} (0.42 Å)	0.001(1)	0.000(0)	0.001(1)	0.000(1)	0.002(1)	0.001(1)	0.002(2)
S^{6+} (0.12 Å)	0.001(1)	0.001(1)	0.002(2)	0.002(2)	0.001(1)	0.003(3)	0.001(1)
Cr^{6+} (0.26 Å)	0.000(0)	0.000(1)	0.000(0)	0.002(2)	0.000(0)	n	n
V^{5+} (0.36 Å)	0.002(1)	0.003(2)	0.007(3)	0.013(7)	0.002(2)	0.002(1)	0.000(1)
ΣB	**1.004**	**1.004**	**1.002**	**1.003**	**1.000**	**0.999**	**0.999**
Total	**1.992**	**1.993**	**1.999**	**2.001**	**2.001**	**2.002**	**2.003**

*Ionic radii from Shannon (1976)
n = not analyzed for
1X: $Pb_{0.99}Mo_{1.00}O_4$
4X: $Pb_{0.99}Mo_{1.00}O_4$
6X: $Pb_{1.00}Mo_{0.99}O_4$
5X: $Pb_{1.00}Mo_{1.00}O_4$
2X: $Pb_{1.00}(Mo_{0.99}V_{0.01})_{\Sigma 1.00}O_4$
7U: $Pb_{1.00}Mo_{0.99}O_4$
8U: $Pb_{1.00}Mo_{1.00}O_4$

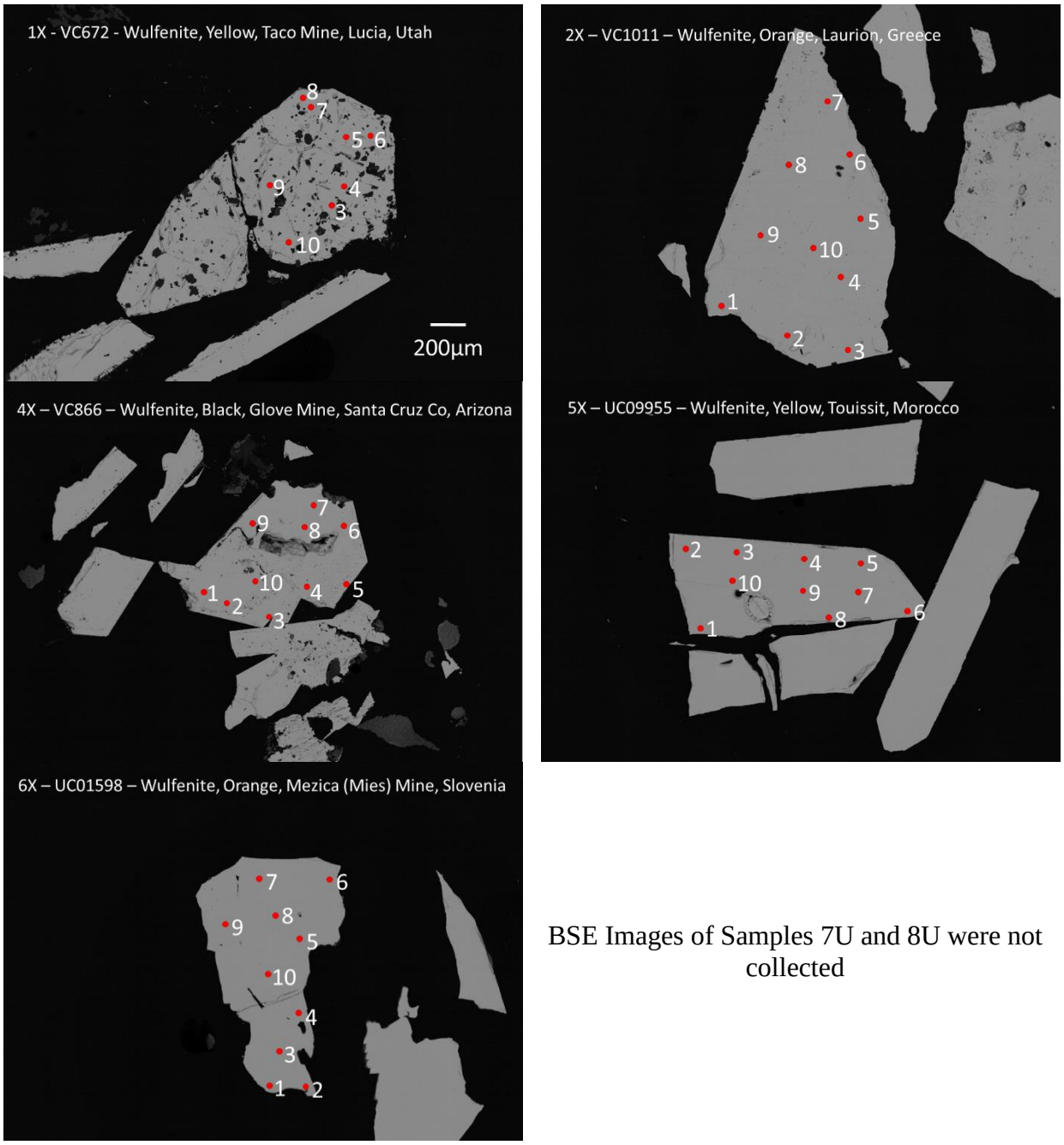

BSE Images of Samples 7U and 8U were not collected

Figure 3.3: Back-scattered electron (BSE) images of wulfenite samples 1X, 2X, 4X, 5X, 6X. Red points on each grain represent approximate locations of quantitative EPMA analyses. According to the BSE images and gathered compositions, the wulfenite grains are all very homogeneous and pure. No zonation or multiphase mixtures were detected.

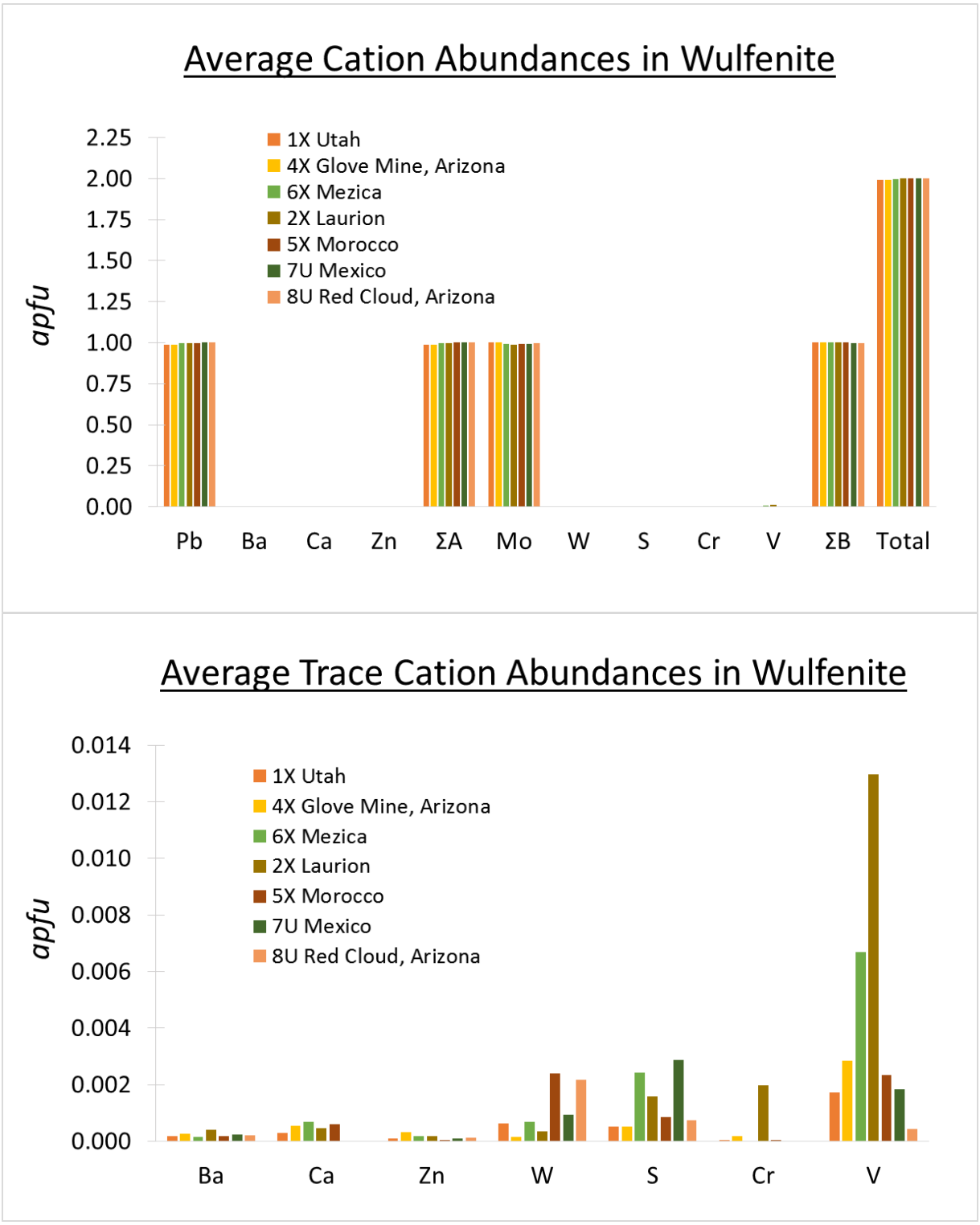

Figure 3.4: Average major and minor (top), and trace (bottom) elemental abundances in wulfenite (on the basis of 4 oxygens).

3.4 Discussion

3.4.1 Variations Among Unit Cell Parameters

In the scheelite-type molybdates and tungstates, the unit cell dimensions are most significantly dictated by the size of the larger, divalent cation species occupying the A site (Sleight 1972; Hazen et al. 1985). Since the ionic radii of Mo^{6+} (0.41 Å) and W^{6+} (0.42 Å) (Shannon 1976) are very similar, and have the same electronic configuration, their substitution in a solid solution series (for a given A cation) only slightly affects the dimensions of the unit cell. Nevertheless, Mo-bearing members have slightly smaller *a* and *V* dimensions, but larger *c* dimensions than their W-bearing counterparts (Sillen and Nylander 1943; Sleight 1972; Laishevtseva et al. 1989). The tetrahedral B-O bond distance remains essentially constant across the series (Oeder et al. 1980). Another rule is that the *c/a* ratio in scheelite-type *molybdates* is always larger than that of scheelite-type *tungstates*, which is due to the fact that the MoO_4^{2-} group is more covalent than the WO_4^{2-} group (Sleight 1972), or perhaps because MoO_4^{2-} tetrahedra are less compressible than the WO_4^{2-} tetrahedra (Oeder et al. 1980).

3.4.2 Structural Results

The cell parameters and selected bond distances for the seven wulfenite samples are compared to literature values of natural and synthetic endmember wulfenite and stolzite (Figs. 3.7-3.9). The same data is also plotted versus *apfu* Mo to help visualize the solid solution series (Fig. 3.10). In general, all wulfenite samples analyzed in this study plot in a relatively tight cluster, and have slightly larger *a*, *c*, and *V* parameters than those of wulfenites reported in literature (Fig. 3.9). Linear trend lines between the wulfenite and stolzite end members are not extremely well correlated, which is contrary to expectation given that this is a simple substitution series with no miscibility gap (Figs. 3.9, 3.10) (Oeder et al. 1980; Laishevtseva et al. 1989). The reason for the

poor correlations is, as previously discussed, a lot of the literature data on stolzite is not very reliable, and the data pool of intermediate compositions in the series is lacking.

There exists some variability in terms of Mo-O and <O-O> lengths, whereas Pb-O and <O-Mo-O> show very consistent values (Fig. 3.7, 3.8). It is difficult to explain the variability in the Mo-O distances, since these are very pure, near endmember compositions with roughly 0.99 to 1.00 *apfu* of Mo in all samples and should, therefore, be very consistent. An explanation could be the substitution of variable amounts of trace metals such as V^{5+}, Cr^{6+}, W^{6+}, or S^{6+} in the tetrahedral Mo (B) site (Table 3.3). For instance, Figure 3.8 shows a positive correlation of B-O distance with V *apfu*. However, since V^{5+} has an ionic radii of 0.36 Å, which is smaller than that of Mo^{6+} (0.41 Å), it seems illogical to be the cause of an increasing B-O bond distance. Tungsten, W (0.42 Å) is slightly larger, and may be a cause for some variability, however its concentrations are incredibly low ≤0.002 *apfu* and do not show a pattern with B-O distance. Moreover, the EPMA is not capable of reliably detecting trace abundances; for more accurate trace element analyses ICP-MS may be required. The MoO_4^{2-} tetrahedra are slightly compressed to varying degrees perpendicular to the **c**-axis, resulting in two distinct O-Mo-O angles ranging from 107.24°-107.98° (x4) and 112.51°-114.02° (x2) (Fig. 3.6). The average O-Mo-O angles (<O-Mo-O>[6]) are all very uniform, ranging from 109.49-109.50°. Additionally, the variation between tetrahedral O-O1 and O-O2 distances confirms that the Mo tetrahedra are compressed to varying degrees in the structure. The Edge Length Distortion (ELD) and Tetrahedral Angle Variance (TAV) were calculated for each wulfenite to gauge the extent of compression of the Mo tetrahedral sites (Table 3.6). There does not seem to be any correlation between TAV or ELD with bond distance, cell parameters, or composition (Fig. 3.11). The reason for this variation of tetrahedral site compression between samples is unknown, but it may be somehow related to the mineral's petrogenesis.

In an ideal, perfectly ordered crystal lattice, the atoms would be fixed exactly at their designated sites (Dunitz et al. 1988). However, in reality the atoms in a mineral are constantly vibrating, meaning they become displaced from the site they occupy to varying degrees, and sometimes even in different amounts in each direction (anisotropic). In this study, only isotropic displacement parameters (U_{iso} x 10^2, $Å^2$) were refined, which assumes that vibrational motion is uniform in all axial directions for each type of atom. A lower U_{iso} value indicates that the atom is more tightly bound to its site in the unit cell, whereas a higher U_{iso} value suggests the atom has a higher probability of being displaced from its position. If a U_{iso} value is extremely large, it means the atom has a diffuse probability distribution over a large area, which could mean that the structural model of the refinement is incorrect (Dunitz et al. 1988). Fortunately, the U_{iso} values in this study are all in an acceptable range, however there is one noticeable difference worth discussing: for all samples except 8U, each atom has a rather similar U_{iso} value, (ranges for Pb = 0.879-0.998; Mo = 0.45-0.62; O = 0.54-0.78). However, sample 8U in particular possesses much lower values for each atom: Pb = 0.668(7); Mo = 0.32(1); and O = 0.31(8) (Fig. 3.12). Explaining the variations in U_{iso} values from just this information alone is not easy; some possible reasons include crystallinity variations (i.e. vacancies/defects or disorder in the lattice) or other substituents in the structure which may affect the vibration of atoms differently. Figure 3.12 shows that the U_{iso} values for Pb and Mo are fairly well-correlated with cell volume, with R-squared values of 0.8879 and 0.8101, respectively, however O shows a much poorer correlation, having an R-squared value of 0.4484 (Fig. 3.12). The fact that sample 8U has a significantly smaller cell volume and smaller U_{iso} values than the rest of the wulfenite specimens seems to suggest that the unit cell itself is more well-ordered and well-crystallized compared to the other wulfenite specimens.

As previously discussed, Mezica Mine, Slovenia is one of the few localities in the world to produce hemimorphic wulfenite specimens (Recnik et al. 2014). Sample 6X, which comes from this locality, was therefore closely examined in hand sample. However, no hemimorphic morphologies could be detected; all crystals appeared bipyramidal in habit. Nevertheless, the possibility of a space group reduction to $I\bar{4}$ was also considered, in accordance with the model put forward by Cora et al. (2011), where Pb and Mo are unequally substituted into the 2b position. It was clear from viewing the XRD traces that there were no unindexed reflections (which would be expected if the unit cell had lower space group symmetry). Moreover, this sample was not Mo-rich (or Pb-deficient), so it seemed unlikely that the model of Cora et al. (2011), could apply to this case. It was therefore concluded that the refinement was best-suited to the common space group $I4_1/a$.

Table 3.4: HRPXRD data and Rietveld refinement statistical indicators for wulfenite samples

	1X – Utah	4X – Glove Mine, AZ	6X – Slovenia	2X – Greece	5X – Morocco	7U – Mexico	8U – Red Cloud Mine, AZ
a/Å	5.43619(2)	5.43655(2)	5.43555(1)	5.43518(2)	5.43605(2)	5.43629(2)	5.43611(1)
c/Å	12.11415(6)	12.11350(6)	12.11877(4)	12.12017(5)	12.11557(5)	12.11445(5)	12.11217(4)
c/a	2.228	2.228	2.230	2.230	2.229	2.228	2.228
V/Å^3	357.999(3)	358.028(3)	358.052(2)	358.044(2)	358.023(2)	358.021(2)	357.930(2)
Reduced χ^2	1.785	1.903	1.782	2.055	1.958	1.589	1.698
*$R(F^2)$	0.0911	0.0684	0.1045	0.0798	0.0827	0.1046	0.0939
Data Points	48071	48071	48071	48071	48071	47995	47995
N_{obs}	915	935	850	893	893	850	844
# of variables	17	17	17	17	17	17	17
λ/Å	0.4127910	0.4127910	0.4127910	0.4127910	0.4127910	0.4142130	0.4142130

R (F^2) = Overall R-structure factor based on observed and calculated structure amplitudes = $\left[\sum(F_o^2 - F_c^2)/\sum(F_o{}^2)\right]^{1/2}$. 2θ range = 2-50°

Table 3.5: Atomic coordinates, isotropic displacement parameters (U_{iso} x 10^2 Å^2) values. Site occupancy factors (*sofs*) for all atoms = 1

	Pb (4b)	Mo (4a)	O (16f)						
			1X	4X	6X	2X	5X	7U	8U
x	0	0	0.2347(4)	0.2330(4)	0.2346(5)	0.2365(4)	0.2339(5)	0.2329(6)	0.2313(5)
y	¼	¼	0.1103(5)	0.1117(4)	0.1104(5)	0.1099(4)	0.1116(5)	0.1094(6)	0.1096(5)
z	⅝	⅛	0.0449(2)	0.0438(2)	0.0438(3)	0.0448(2)	0.0438(2)	0.0458(3)	0.0454(3)
U_{iso}			1X	4X	6X	2X	5X	7U	8U
Pb			0.861(7)	0.960(6)	0.921(7)	0.998(7)	0.879(7)	0.907(8)	0.668(7)
Mo			0.48(1)	0.61(1)	0.57(1)	0.62(1)	0.45(1)	0.52(1)	0.32(1)
O			0.70(7)	0.74(7)	0.54(8)	0.66(7)	0.78(7)	0.74(9)	0.31(8)

Table 3.6: Selected distances (Å) and angles (°) for wulfenite

		1X	4X	6X	2X	5X	7U	8U
Mo-O	x4	1.774(2)	1.772(2)	1.781(3)	1.782(2)	1.775(2)	1.763(3)	1.758(3)
Pb-O1	x4	2.619(3)	2.617(2)	2.615(3)	2.612(2)	2.616(3)	2.617(3)	2.624(3)
Pb-O2	x4	2.625(3)	2.635(2)	2.625(3)	2.621(3)	2.631(3)	2.641(3)	2.642(3)
<Pb-O>[8]		2.622(2)†	2.626(2)	2.620(2)	2.616(2)	2.624(2)	2.629(2)	2.633(2)
O-O1	x4	2.860(4)	2.866(4)	2.878(5)	2.871(4)	2.870(4)	2.839(6)	2.835(5)
O-O2	x2	2.969(5)	2.946(4)	2.968(6)	2.988(4)	2.955(5)	2.958(6)	2.941(6)
<O-O>[6]		2.896(3)	2.893(3)	2.908(4)	2.910(3)	2.898(3)	2.879(4)	2.870(4)
O-Mo-O	x4	107.43(9)	107.98(8)	107.8(1)	107.30(8)	107.88(9)	107.2(1)	107.5(1)
O-Mo-O	x2	113.6(2)	112.5(2)	112.9(2)	113.9 (2)	112.7(2)	114.0(2)	113.5(2)
<O-Mo-O>[6]		109.50(8)	109.49(8)	109.5(1)	109.50(8)	109.49(8)	109.5(1)	109.50(1)
*ELD		1.7(5)	1.2(4)	1.4(5)	1.8(4)	1.3(5)	1.8(6)	1.6(5)
**TAV		10.3(7)	5.5(4)	6.9(6)	11.6(7)	6.2(5)	12.3(9)	9.6(1)

*ELD = Edge Length Distortions (%) $= \frac{100}{n}\sum_{i=1}^{n}\frac{|(O-O)_i-(<O-O>)_m|}{(<O-O>)_m}$ from Renner and Lehmann (1986)

**TAV = Tetrahedral Angle Variance $= \sum_{i=1}^{6}(\theta_i - 109.47)^2/5$ from Robinson et al. (1971)

<Pb-O> $= \frac{4(Pb-O1)+4(Pb-O2)}{8}$

<O-O> $= \frac{4(O-O1)+2(O-O2)}{6}$

<O-Mo-O> $= \frac{4(O-Mo-O)+2(O-Mo-O)}{6}$

†Propagated errors calculated using the general formula: $\Delta z = \sqrt{(\frac{\partial z}{\partial x}\Delta x)^2 + (\frac{\partial z}{\partial y}\Delta y)^2}$

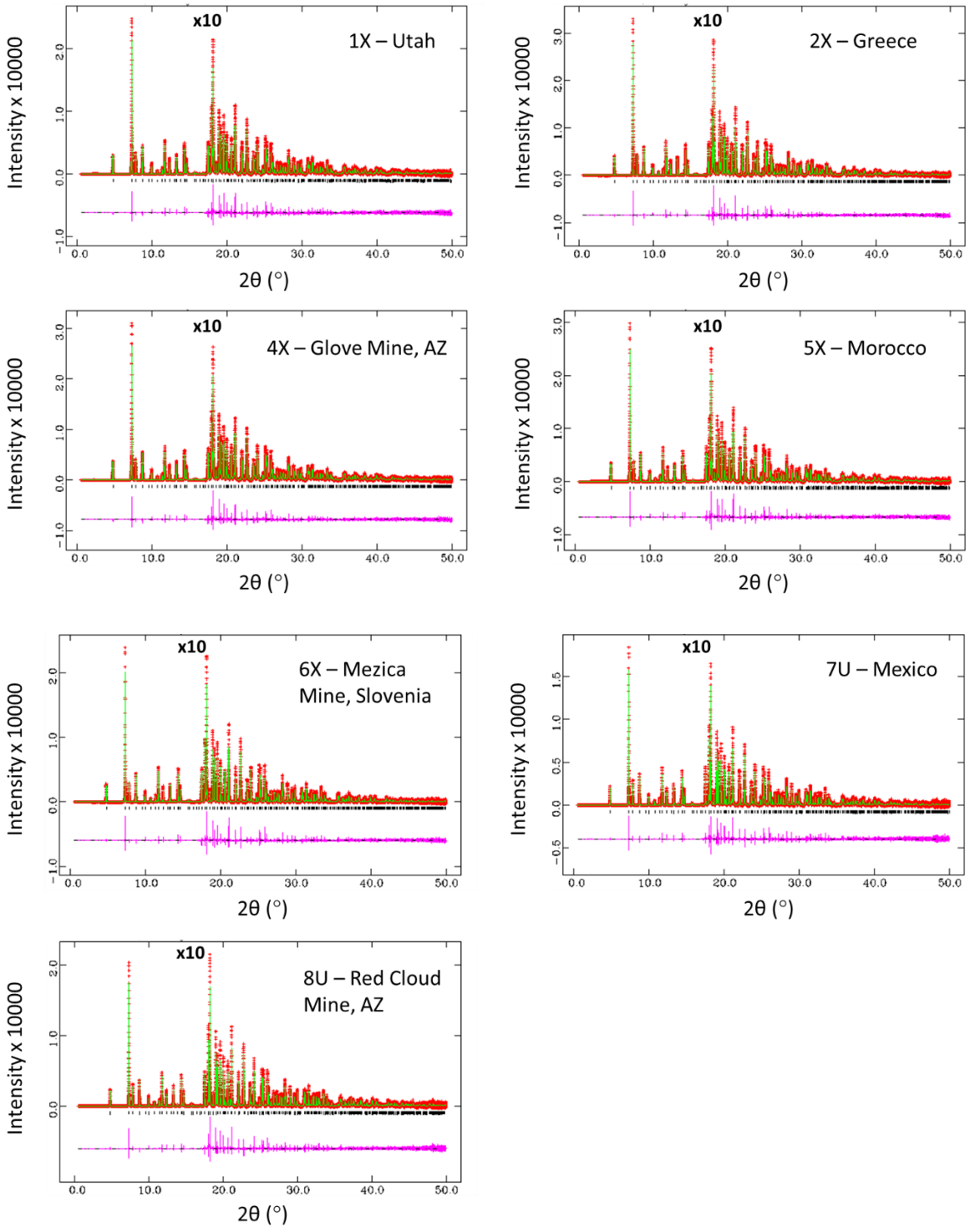

Figure 3.5: HRPXRD traces for wulfenite samples. Red Crosses = observed trace, Green = calculated trace, Pink = difference curve, Black tick marks = reflections. Peak intensities for 2θ > 17° are increased by a factor of 10x to enhance the detail.

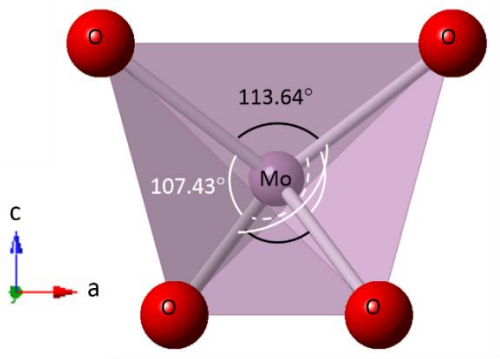

Figure 3.6: The MoO_4^{2-} tetrahedron showing O-Mo-O angles for sample 1X (as an example). Compression occurs parallel to the **c**-axis.

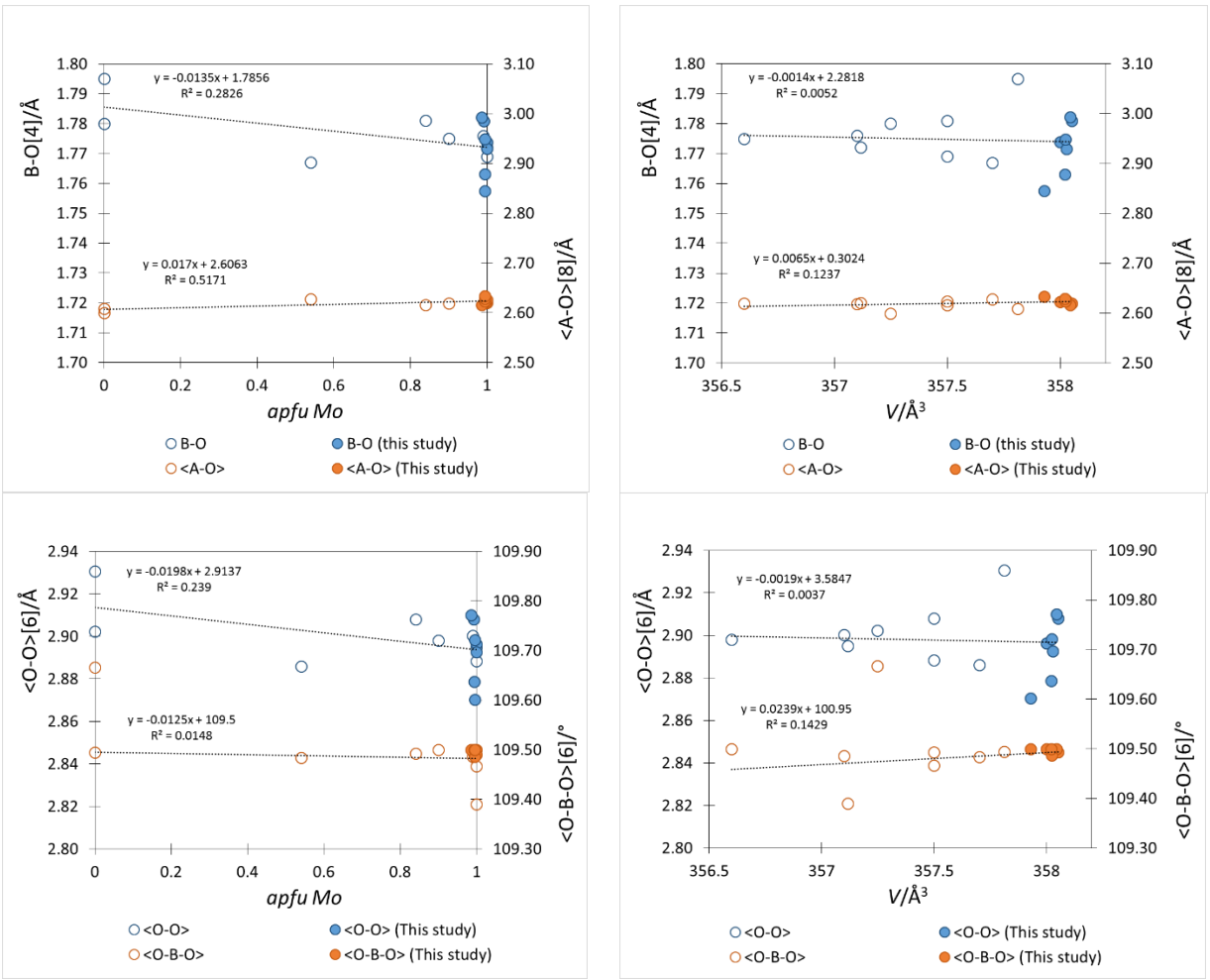

Figure 3.7: Bond distances B-O, <A-O> (average of A-O1 and A-O2), tetrahedral <O-O> bond (average of O-O1 and O-O2), and <O-B-O> angle as a function of *apfu* Mo and Volume, *V*, in the stolzite ($PbWO_4$) and wulfenite ($PbMoO_4$) series. Data comes from this study (filled circles) and literature sources (open circles) listed in Tables 3.6 and 3.1, respectively, excluding Moreiras et al. (1991) and Chipaux et al. (2001).

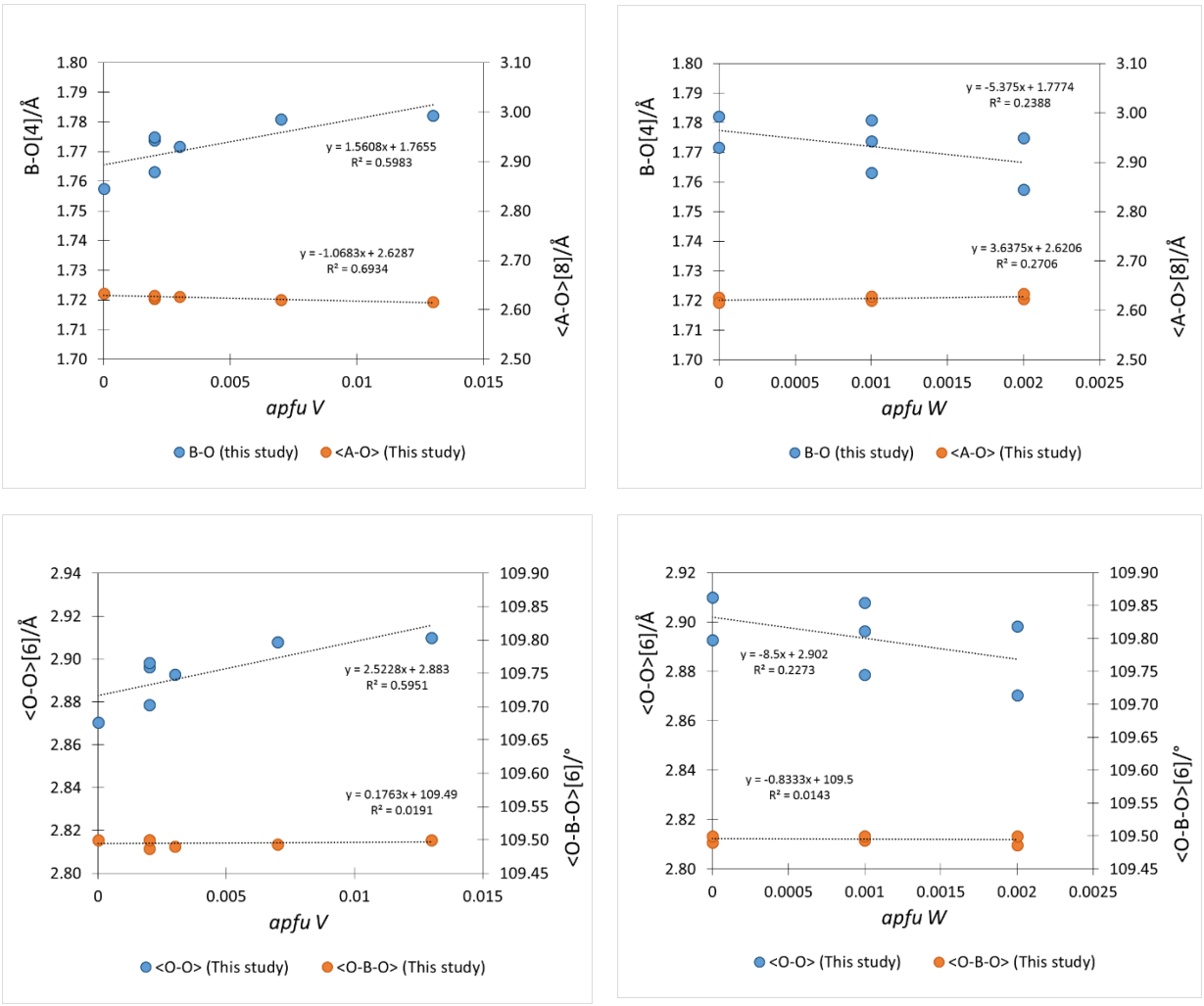

Figure 3.8: Bond distances B-O, <A-O> (average of A-O1 and A-O2), tetrahedral <O-O> bond (average of O-O1 and O-O2), and <O-B-O> angle as a function of *apfu* V and *apfu* W in the stolzite ($PbWO_4$) and wulfenite ($PbMoO_4$) series. Data comes from this study (filled circles) listed in Table 3.6.

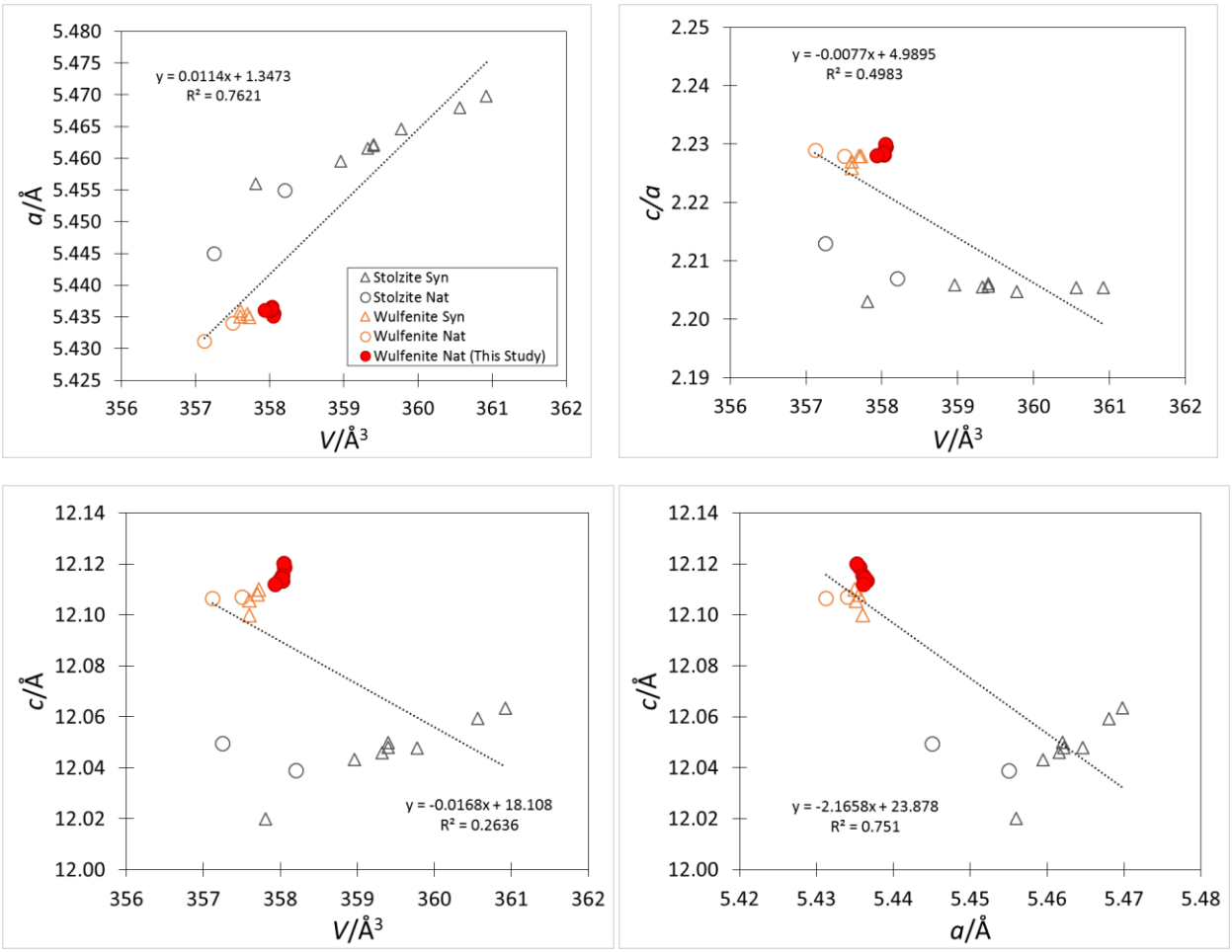

Figure 3.9: Relations among unit-cell parameters *a*, *c*, *c/a*, and *V* between wulfenite ($PbMoO_4$) and stolzite ($PbWO_4$). Data comes from this study (filled red circles) and literature sources (open shapes) listed in Tables 3.4 and 3.1, respectively.

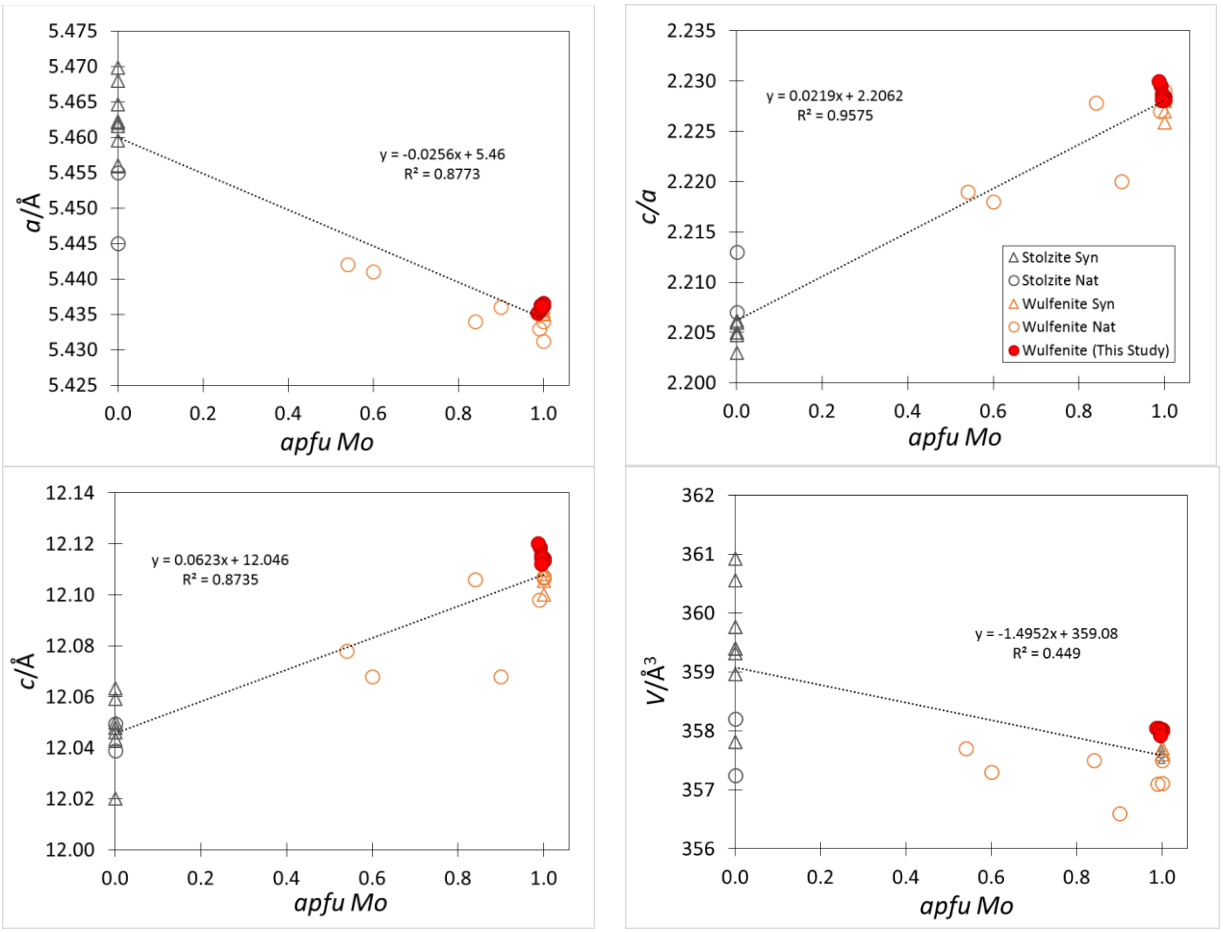

Figure 3.10: Relations among unit-cell parameters *a*, *c*, *c/a*, and *V* between wulfenite ($PbMoO_4$) and stolzite ($PbWO_4$) as a function of Mo-content. Data comes from this study (filled red circles) and literature sources (open shapes) listed in Tables 3.4 and 3.1, respectively.

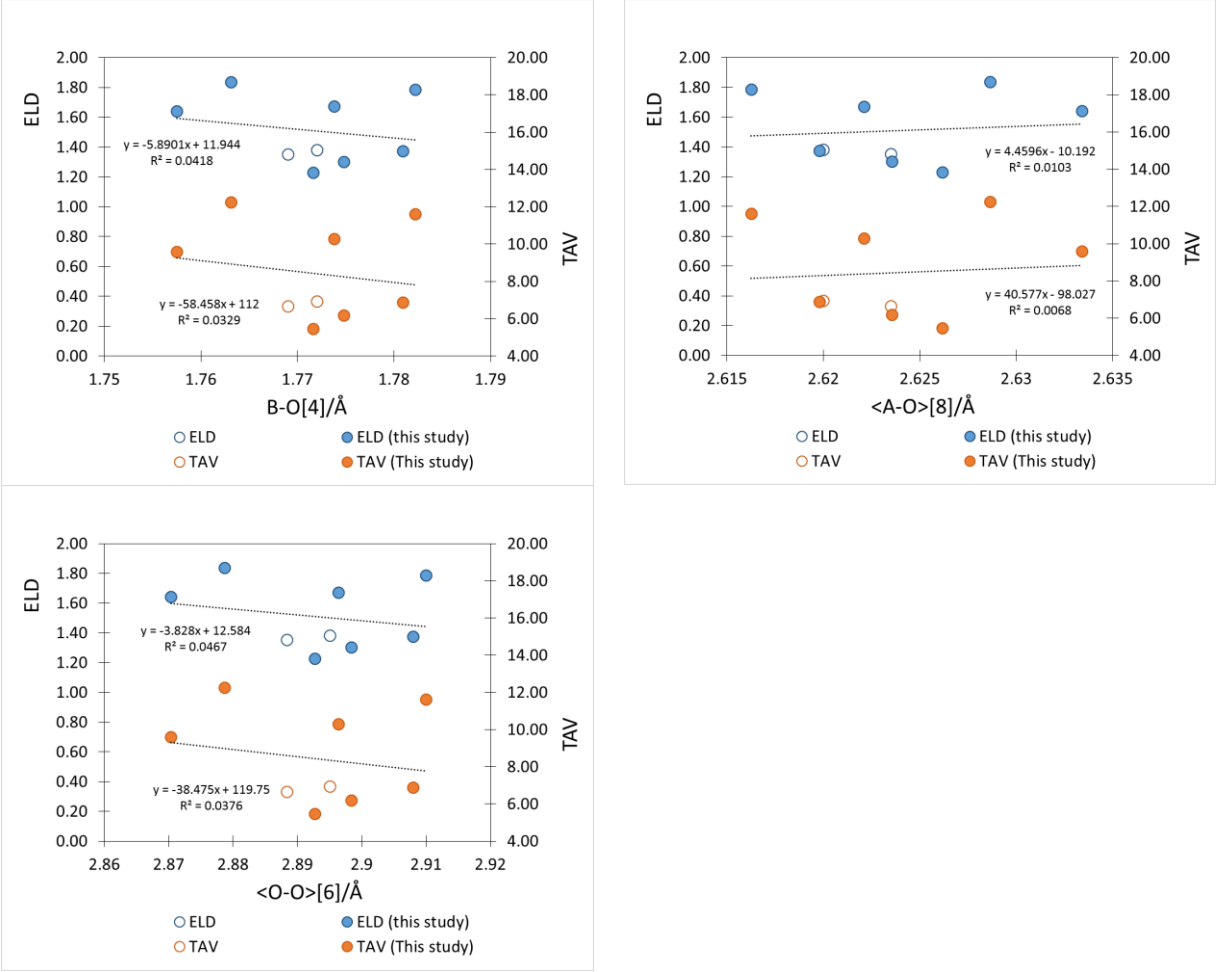

Figure 3.11: Bond distances B-O, <A-O> (average of A-O1 and A-O2), tetrahedral <O-O> bond (average of O-O1 and O-O2), and the larger O-B-O angle in relation to ELD and TAV in the stolzite ($PbWO_4$) and wulfenite ($PbMoO_4$) series. Data comes from this study (filled circles) and Lugli et al. (1999) and Leciejewicz (1965) (open circles)

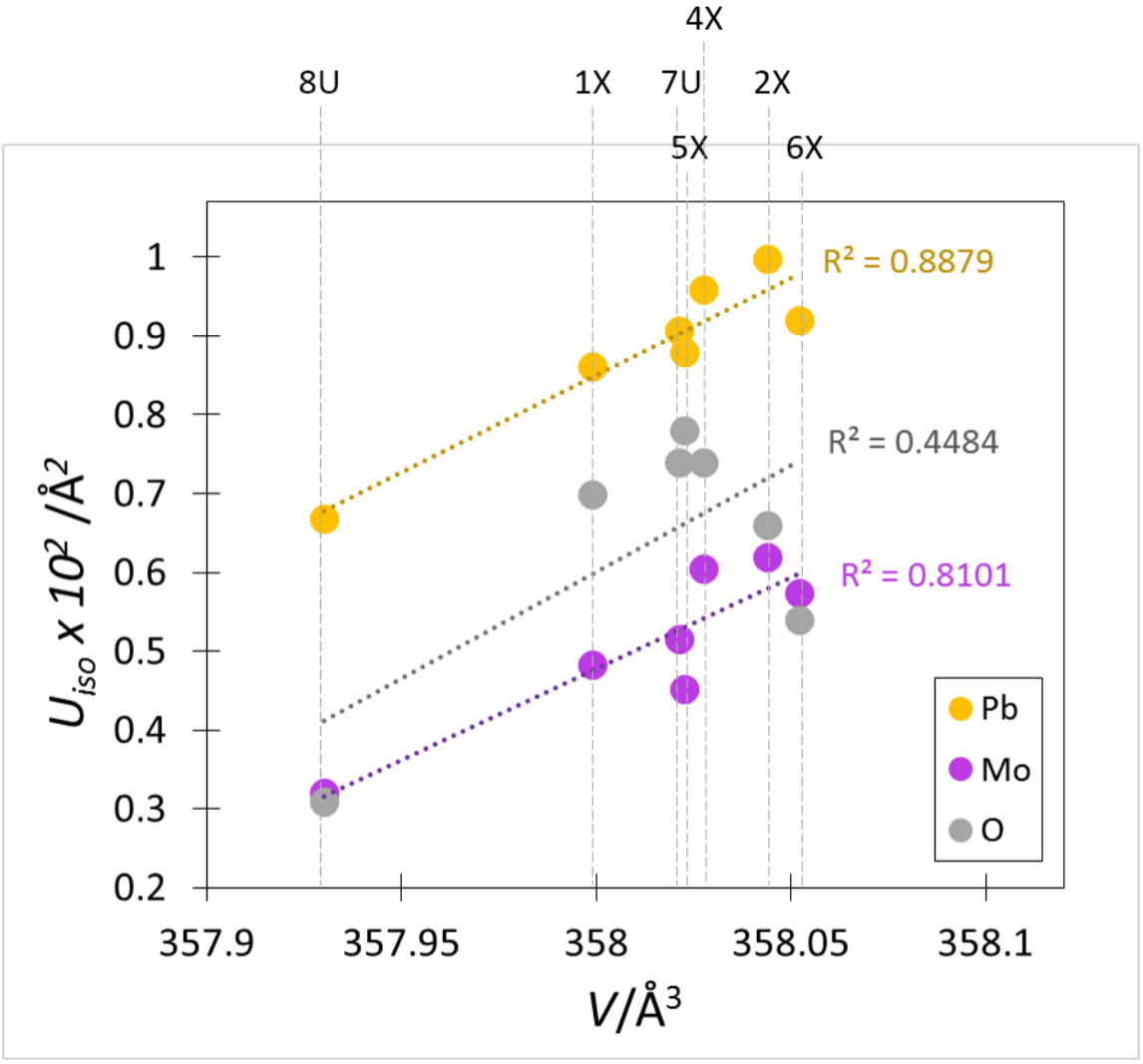

Figure 3.12: U_{iso} x 10^2 (Å^2) values for Pb, Mo, and O atoms versus cell volume, V (Å^3). Data comes from this study (sample names listed above the chart). Correlation coefficients (R-squared values) show the goodness of fit for the trend lines.

CHAPTER 4 – Wolframite Crystal Chemistry

4.1 Introduction

Wolframite ([Fe,Mn]WO_4) is a member of the wolframite-type group of molybdates and tungstates, which have the general formula: ABO_4, where A is a divalent metal cation with an ionic radius <0.90 Å (commonly transition metals such as Fe^{2+}, Mn^{2+}, Mg^{2+}, Zn^{2+}, Ni^{2+}, Co^{2+}, or Cu^{2+}) and B is a highly charged cation (W^{6+} or Mo^{6+}) (Sleight 1972; Hazen et al. 1985). This mineral group has a monoclinic crystal system ($a \neq b \neq c$; $\alpha = \gamma = 90^\circ \neq \beta$) and belongs to space group *P*2/*c* with two formula units per unit cell (Z = 2) (Broch 1930). This space group symbol indicates that it is a primitive (*P*-type) lattice, and the cell contents can be generated with a 2-fold rotation axis oriented perpendicular to a *c*-glide plane. Typical "wolframite" ([Fe,Mn]WO_4) consists of a complete solid solution between Fe and Mn-rich endmembers, which are conventionally defined by the relative abundances of Fe and Mn (Hsu 1976). By the general formula, $Fe_xMn_{1-x}WO_4$, ferberite is defined as $x \geq 0.8$; hübnerite is defined as $x \leq 0.2$, and wolframite is simply an intermediate composition of $0.2 < x < 0.8$ (Fig. 4.1) (Sasaki 1959; Cid-Dresdner and Escobar 1968). Mn^{2+} and Fe^{2+} cations occur in a high spin state in wolframite-type minerals (Mal et al. 2017). Wolframite commonly forms prismatic, tabular to bladed or wedge-shaped crystals, striated along the length and flattened on {100}. It has a moderate hardness (H = 4-4.5), a metallic to adamantine lustre, and ranges from opaque to translucent (Mineral Data Publishing 2005). Most of the time wolframite is black to brown, but the Mn-rich variety, hübnerite, can show a dark crimson, red-brown hue (Mineral Data Publishing 2005).

Wolframite can form in a variety of geologic settings most often spatially associated with highly-fractionated, shallow (≤ 5km) granitic intrusions (Harlaux et al. 2018). Some examples of settings include hydrothermal quartz veins, porphyry systems, stratabound deposits, pegmatite

veins, skarns, and hydrothermally altered granites known as greisens (Brown and Pitfield 2014; Werner et al. 2014; Romer and Kroner 2016). Due to the high degree of magmatic fractionation, these types of deposits are often also enriched in incompatible elements such as Sn, W, Be, Cs, F, B, Li, Rb, Ta, and U (Romer and Kroner 2016). Although the tectonic settings and melt generation mechanisms can vary, the general development of Sn-W deposits which commonly host wolframite can be summarized in a few steps: (1) Intense chemical weathering of sedimentary rocks leaches away feldspar-bound metals (e.g. Na, Ca, Sr, Pb) leaving behind a residue of elements either incorporated or adsorbed by clay minerals (e.g. Li, K, Rb, Cs, Sn, and W); (2) Accumulation of the enriched sedimentary debris at continental margins via fluvial processes; (3) Heating and melting of the enriched sedimentary protoliths through any of a number of processes occurring often at plate margins such as subduction zone magmatism, heat from continental collisions, or crustal extension to generate felsic intrusions with a distinct Sn-W chemical signature (Romer and Kroner 2016).

Wolframite and scheelite are the primary ore minerals mined for tungsten, W, and deposits can be found worldwide. Tungsten is a dense, corrosion-resistant metal with the highest melting point of all metals (3422˚C) (Brown and Pitfield 2014), making it extremely useful in a number of important industrial products including high-strength Fe-W-alloyed steel and incandescent light bulb filaments (Werner et al. 2014). One of the most important industrial uses of W is to synthesize tungsten carbide, WC, whose hardness is second only to diamond, making it an important component in powerful cutting and drilling tools (Werner et al. 2014; Sun et al. 2019).

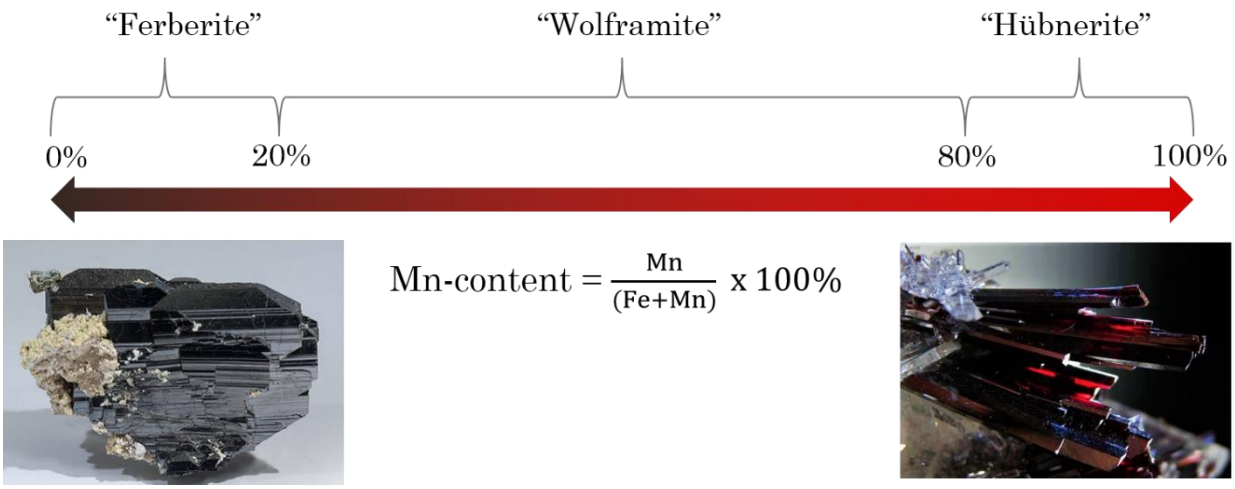

Figure 4.1: Classification of members of the wolframite solid solution series as a function of Mn-content.

Table 4.1: Structural data for wolframite ([Fe,Mn]WO_4). Compositional ranges in the ferberite ($FeWO_4$)—hübnerite ($MnWO_4$) solid solution series listed from Fe-rich to Mn-rich.

Reference	Locality	Composition	*a*/Å	*b*/Å	*c*/Å	*V*/Å^3	*β*/°	<W-O>/Å	<A-O>/Å
Broch (1930)^{P,S}	Syn	$FeWO_4$	4.70(2)	5.69(2)	4.93(2)	131.84(90)*	90.00(13)		
Sasaki (1959)^{P,S}	Syn	$FeWO_4$	4.734(4)	5.708(3)	4.965(4)	134.16(17)*	90.00(3)		
Sleight (1972)^{P,S}	Syn	$FeWO_4$	4.724	5.705	4.961	133.7	90.0		
Hsu (1976)^{U,S}	Syn	$FeWO_4$	4.733(2)	5.709(2)	4.964(3)	134.13(11)*	90.00		
Sasaki (1959)^{P,N}	Otomé, Japan	$(Fe_{1.03}Mn_{0.01})W_{0.99}O_4$	4.737	5.712	4.968	134.42*	90.00		
Sasaki (1959)^{P,N}	Ebisu, Japan	$(Fe_{0.96}Mn_{0.16})W_{0.96}O_4$	4.741	5.711	4.971	134.59*	90.02		
Sugaki et al. (1986)^{P,N}	Tasna Mine, Bolivia	$(Fe_{0.95}Mn_{0.05})W_{1.00}O_4$	4.739(1)	5.718(2)	4.965(1)	134.54(6)*	90.12(3)		
Ulku (1967)^{S,N} XRD	Tirpersdorf, Germany	$(Fe_{0.90}Mn_{0.06})W_{1.00}O_4$	4.730(3)	5.703(2)	4.952(2)	133.58(11)*	90.0	1.938(7)*	2.099(7)*
Ulku (1967)^{S,N} Neutron	Tirpersdorf, Germany	$(Fe_{0.90}Mn_{0.06})W_{1.00}O_4$	//	//	//	//	//	1.940(3)*	2.104(4)*
Cid-Dresdner and Escobar (1968)^{S,N}	Liquinaste, Argentina	$(Fe_{0.885}Mn_{0.055}Mg_{0.06})W_{1.00}O_4$	4.750	5.720	4.970	135.04*	90.17	2.060/1.994*	2.047/2.082*
Pačevski et al. (2007)^{P,N}	Osanica, Serbia	$(Fe_{0.85}Mn_{0.15})W_{1.00}O_4$	4.738(2)	5.707(2)	4.960(2)	134.12(9)	90.08(4)		
Pačevski et al. (2007)^{P,N}	Osanica, Serbia	$(Fe_{0.85}Mn_{0.15})W_{1.00}O_4$	4.741(2)	5.713(1)	4.959(1)	134.32(7)	90.03(3)		
Sasaki (1959)^{P,N}	Funai, Japan	$(Fe_{0.74}Mn_{0.28})W_{0.99}O_4$	4.761	5.720	4.977	135.54*	90.15		
Pačevski et al. (2007)^{P,N}	Osanica, Serbia	$(Fe_{0.71}Mn_{0.29})W_{1.00}O_4$	4.748(1)	5.714(1)	4.961(1)	134.59(5)	90.01(3)		
Sasaki (1959)^{P,N}	Yomei, Japan	$(Fe_{0.54}Mn_{0.47})W_{1.00}O_4$	4.777	5.728	4.982	136.32*	90.30		
Sasaki (1959)^{P,N}	Gessei, Japan	$(Fe_{0.36}Mn_{0.66})W_{0.99}O_4$	4.801	5.741	4.992	137.59*	90.43		
Sasaki (1959)^{P,N}	Hagidaira, Japan	$(Fe_{0.05}Mn_{0.95})W_{1.00}O_4$	4.826	5.755	4.998	138.79*	91.03		
Dachs et al. (1967)^{S,N}	Henderson, North Carolina	$(Fe_{0.03}Mn_{0.97})W_{1.00}O_4$	4.82	5.76	4.97	137.97*	90.88†	1.943*	2.172*
Broch (1930)^{P,S}	Syn	$MnWO_4$	4.84(2)	5.76(2)	4.97(2)	138(1)*	90.88(13)†		
Sasaki (1959)^{P,S}	Syn	$MnWO_4$	4.835(4)	5.758(3)	4.999(4)	139.15(18)*	91.12		
Sleight (1972)^{P,S}	Syn	$MnWO_4$	4.829	5.758	4.996	140.0	91.15		
Hsu (1976)^{U,S}	Syn	$MnWO_4$	4.829(1)	5.759(1)	4.9971(1)	138.94(15)*	91.10(3)		
Macavei and Schulz (1993)^{S,S}	Syn	$MnWO_4$	4.830(1)	5.7603(9)	4.994(1)	138.92(24)	91.14(2)	1.947(6)*	2.177(6)*
Lopez-Moreno et al. (2009)^{Sim}	Simulated	$MnWO_4$	4.796	5.801	5.025	139.8	90.97	1.967*	2.153*
Mal et al. (2017)^{P,S}	Syn	$MnWO_4$	4.8379	5.7656	5.0036	139.5375	91.189	1.970*	2.110*

$V = abcsin(\beta)$

*Calculated when not given in paper

†Obtuse β angle = 180° – acute β angle reported in literature

Superscript Notation: 1st letter ^{P} = Powder XRD or ^{S} = Single Crystal XRD; 2nd letter ^{N} = Natural specimen, ^{S} = Synthetic specimen, ^{U} = unknown/not given in paper, ^{Sim} = simulated

Bond distances reported by Cid-Dresdner and Escobar (1968) are different than those calculated. Notation: Cid-Dresdner and Escobar (1968) values / Calculated values

4.2 Previous X-Ray Diffraction Work on Wolframite-type Minerals

4.2.1 Background

This section will discuss the body of work performed by previous studies on wolframite

Wolframite specimens have been examined by mineralogists for over 150 years. Des Cloizeaux (1850) was among the first to determine the monoclinic character ($a \neq b \neq c$; $\alpha = \gamma = 90^\circ \neq \beta$) of wolframite crystals, which he described as "rhomboïdal oblique" with an obtuse angle between the base and lateral faces (β) of 91.32˚ (Des Cloizeaux 1850). Using crystal indices, Machatschki (1928) calculated the ratio of cell parameters $a : b : c = 0.8263 : 1 : 0.8703$ and determined an acute β angle of 89.40˚. He noted that increasing the size of the divalent cation (Mg < Fe < Mn) caused an increase in *a/b* but a decrease in *c/b* and the acute β angle (increase in obtuse β angle) (Machatschki 1928). Among the very first XRD studies of the wolframite group minerals was a foundational and comprehensive investigation performed by Broch (1930) on the Mn, Fe, Co, Zn, Mg, and Ni tungstates. He found that each of these wolframite-type minerals are isomorphous and belong to the space group *P*2/*c*, and contain 2 formula units per unit cell (Z = 2).

Berman and Campbell (1957) investigated natural wolframites to determine the effect of Fe/Mn abundances on the unit cell parameters as well as thermal stability. They calculated the lattice parameters *a, b,* and *c* by accurately measuring the d-spacings of reflections 030, 022, and 200 for a variety of compositions in the series. Their results show positive linear relationships between d-spacings of reflections 030 and 200 with Mole % MnO. The β angles were calculated from the difference in 2θ values between d_{111} and $d_{\bar{1}11}$ as the difference between them increases with an increasing β angle, which also increases with Mole % MnO. Their results were in good agreement with those of Broch (1930).

Sasaki (1959) conducted XRD experiments similar to Berman and Campbell (1957) on both synthetic and natural wolframite crystals at various compositions in the Fe-Mn solid solution series in an effort to more rapidly and reliably determine the relationships between unit cell parameters and Fe/Mn abundances. Sasaki (1959) analyzed 15 synthetic wolframite samples of different compositions across the whole ferberite to hübnerite series. Cell parameters were determined from the 2θ positions of sharp reflections 011, 110 111, $11\bar{1}$, and 020. He found that the unit cell parameters *a, b, c,* and *β* all increased in smooth linear relationships from Fe towards the Mn endmember. He noted some occasional discrepancies between natural wolframites and the curves derived from synthetic analyses; these discrepancies were attributed to the possible presence of other substituting cations such as trivalent iron (Fe^{3+}), Nb, Ta, Sc, or rare earth elements in the crystal structure. In the synthetic wolframites, the β angle increased with Mn-content from ~90.0˚ @ 0% Mn-content (pure $FeWO_4$) to ~91.1˚ @ 100% Mn-content (pure $MnWO_4$). He noted that, oddly, the *β* angle remained at 90˚ up until 10% Mn-content rather than increasing immediately from 0%.

A few years later, the first complete structural refinement (atom positions and bond distances) of natural ferberite ($FeWO_4$) was accomplished by Ulku (1967) using both neutron diffraction and single crystal XRD. In the same year, the first structural refinement of natural hübnerite ($MnWO_4$) was accomplished by Dachs et al. (1967) using neutron diffraction. At the same time as Ulku (1967), another independent structural refinement of ferberite was completed by Cid-Dresdner and Escobar (1968). The results of the two studies show some differences in atomic coordinates and bond lengths; Cid-Dresdner and Escobar (1968) argue that the refinement of Ulku (1967) may have a problem due to having elevated *R* values in the *(h0l)* projection (where the coordinates of Fe and W are fixed by the space group). Given the lack of modern complete structural studies on

ferberite to compare with, it is difficult to tell which study is the most accurate. A study by Escobar et al. (1971) documents a variety of "light ferberite" from Liquinaste, Argentina with a much lower density of 5.14g/cm^3 compared to the typical mineral density of 7.4g/cm^3. Their XRD results could not detect any observable differences in bond lengths or angles between light and common ferberite, and their cell parameters were very similar. They therefore attribute the lower density to be the result of water and volatile components being trapped in the mineral pores during crystallization, rather than being accommodated into the crystal structure itself.

Sleight (1972) published a comprehensive collection of accurate cell parameter measurements for a wide variety of scheelite-type and wolframite-type tungstate and molybdate minerals.

Soeda et al. (1979) investigated natural wolframite samples from the Chugoku district, Japan to further understand relationships between chemical composition and cell parameters in wolframite. Their results are in agreement with previous studies, however they note that the β angle measurements remained relatively close to 90° regardless of composition. The expansion of the unit cell is most strongly dependent on *a* and *b* parameters.

Macavei and Schulz (1993) performed high pressure experiments as well as structural calculations (atom positions and bond lengths) on several "wolframite-type" compounds including $MgWO_4$, $MnWO_4$, and $CdWO_4$ up to 8GPa. They documented anisotropic compression in the unit cells due to higher compressibility of the A-W distances, but only slight compressibility of the A-A and W-W distances. This means that the **c**-axis (which is parallel to chains of A and W polyhedra) experiences the least compression, whereas the **b**-axis experiences the most compression. The compression of the unit cell is mostly associated with changes in AO_6 polyhedra, which is similar to scheelite-type compounds (Hazen et al. 1985). Their structural results for

synthetic $MnWO_4$ at standard state conditions are in good agreement with results of a natural sample analyzed by Dachs et al. (1967).

4.2.2 Wolframite Structure

The first complete structural refinement (atom positions and bond distances) of ferberite ($FeWO_4$) was accomplished by Ulku (1967) using both neutron diffraction and single crystal XRD, whereas that of hübnerite ($MnWO_4$) was accomplished by Dachs et al. (1967) using neutron diffraction. The wolframite structure can be described as a distorted, closely-packed hexagonal array of oxygens and A^{2+} and W^{6+} octahedra (6-fold coordination) occupying ¼ of the interstices (Fig 4.2) (Sleight 1972; Redfern et al. 1995). The octahedral A and W sites form "zig-zag" chains extending along the **c**-axis (Cid-Dresdner and Escobar 1968; Redfern et al. 1995). Each chain is composed of like octahedra (either only A or only W) sharing two edges per octahedra, which creates alternating layers of repeating O, A, O, W, etc. atoms (Redfern et al. 1995). Each W shares 4 corners with 4 A-site octahedra, which belong to 4 different zig-zag chains (Cid-Dresdner and Escobar 1968). The AO_6 and WO_6 octahedra are highly distorted; 3 unique bond distances with a multiplicity of 2 exist in each octahedra (Cid-Dresdner and Escobar 1968; Lopez-Moreno et al. 2009). The unit cell contains two A atoms (½, y, ¼), two W atoms (0, y, ¼), and eight O atoms that occupy two different general positions O1 (x_1, y_1, z_1), O2 (x_2, y_2, z_2) (Ulku 1967).

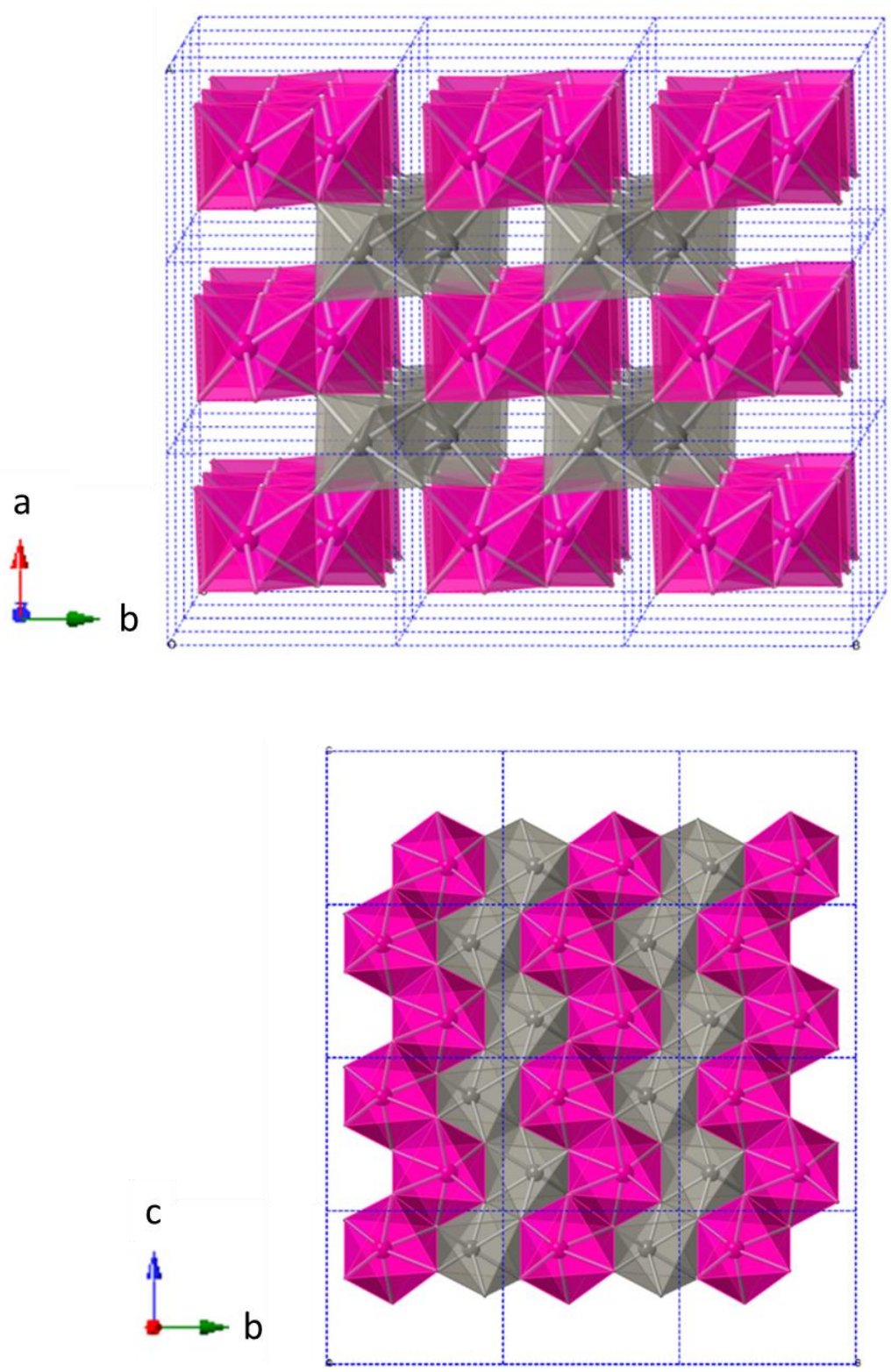

Figure 4.2: (top) Crystal structure of wolframite viewed down **c**-axis. (bottom) View down **a**-axis showing zig-zag chains of A (magenta) and W (grey) octahedra extending along the **c**-axis.

4.2.3 Wolframite Solid Solution Series and Cation Substitution

Natural wolframite-type minerals often exhibit compositional variability due to substitution in the A and B sites (Harlaux et al. 2018). Some of the most common trace metals found in wolframites are A = Ni^{2+}, Co^{2+}, B = V^{3+}, Ti^{4+}, Sn^{4+}, Nb^{5+}, Ta^{5+}, Mo^{6+} (Barkov et al. 2008; Neiva 2008; Harlaux et al. 2018). In some cases, concentrations of Nb^{5+} and Ta^{5+} have been documented to constitute significant wt. % in wolframite (Tindle and Webb 1989). Trivalent iron (Fe^{3+}) has also been noted to occur in small quantities in wolframite, perhaps suggesting the existence of a solid solution series between $FeWO_4$ and a species such as Fe_2WO_6 or $Fe_2(WO_4)_3$ (Clark 1970). Several substitution equations are presented from Harlaux et al. (2018) (Eq. 1 and 2) and Talla et al. (2017) (Eq. 3) to account for the large variability in trace element composition in wolframite. Eq. 1 illustrates the process of charge compensation in A and B sites through substitution of 5+ cations (Nb^{5+} and Ta^{5+}), whereas Eq. 2 shows the substitution of 4+ cations (Ti^{4+}, Sn^{4+}). The [ ] symbols indicate structural vacancies which may compensate for each other to maintain net neutrality (Harlaux et al. 2018). Talla et al. (2017) have even documented the occurrence of OH^- defects in wolframite using infrared (IR) spectroscopy (Eq. 3). Any of a number of possible cations (2+, 3+, 4+, 5+, 6+) may substitute in the A and B sites so long as they have a suitable charge and ionic radii (Harlaux et al. 2018).

$$^{A}(Fe, Mn)^{2+} + {}^{B}[\ ] + 3\ {}^{B}W^{6+} \leftrightarrow {}^{A}[\ ] + 4\ {}^{B}(Nb, Ta)^{5+} \qquad \text{(Eq. 1)}$$

$$^{A}[\ ] + {}^{B}W^{6+} \leftrightarrow {}^{A}(Fe, Mn)^{2+} + {}^{B}(Ti, Sn)^{4+} \qquad \text{(Eq. 2)}$$

$$^{B}W^{6+} + O^{2-} \leftrightarrow {}^{B}(Nb, Ta)^{5+} + OH^{-} \qquad \text{(Eq. 3)}$$

Some studies have identified zoning patterns in natural wolframite specimens (El Agami 2005; Pačevski et al. 2007). El Agami (2005) reports hübnerite from Egypt that displays optical zoning

with some small amounts of chemical zoning. The chemical zones are characterized by hübnerite intergrown with Mn-Fe oxy-hydroxides or wolframite with variable amounts of Fe, Mn and Ca substituted for each other. Pačevski et al. (2007) documented wolframite samples from Osanica, Serbia, one of which displayed striking oscillatory zoning ranging from 8-65 mol% $MnWO_4$ in certain zones of the crystal. Zoning in wolframite may form due to (1) physical-chemical changes in the bulk system during crystal growth (likely cause of abrupt compositional changes); (2) local chemical diffusion near the crystal surface during growth; or (3) decomposition of the Fe-Mn solid solution after crystal growth (Pačevski et al. 2007).

4.3 Experimental Methods

4.3.1 Electron Probe Microanalyses (EPMA)

A collection of four wolframite samples from various localities (Table 4.2) were quantitatively analyzed using the JEOL JXA-8200 EPMA at the University of Calgary. The JEOL operating program on a Solaris platform was used for ZAF correction and data reduction. The wavelength dispersive spectrometry (WDS) measurements were performed with a voltage of 20 kV, a current of 20 nA, and a beam diameter of 5 μm. The calibration standards used were: Mg, Cr = chromite; Pb = pyromorphite; W = scheelite; Mo = $CaMoO_4$; Ni = NiO; Zn = ZnO; V = V_2O_5; Fe, Ti = ilmenite; Ba, S = barite; Mn = UC09059 hübnerite (for wolframite samples). The typical Mn standard, rhodonite, could not be used for calibrating Mn measurements in wolframite because wolframite has a very high mean atomic number. As a result the Z correction was not appropriate, and produced high totals. A solution to this problem was to use a nearly pure Mn-end member hübnerite (UC09059) from the disc as the Mn standard. The average wt. % of oxides (from 10 points) were used to calculate average atoms per formula unit (*apfu*) on the basis of 4 oxygens (Table 4.3). This compositional data is also represented in bar graphs in Figure 4.4. All spot analyses are tabulated in the Appendix (Tables A8-A12). The back-scatter electron (BSE) images are shown in Figure 4.3, which depict the approximate locations of each spot analysis.

Table 4.2: Wolframite samples from discs 1-X and 1-U. Listed from lowest to highest Mn *apfu*.

Sample #	Short form	Name	Mineral	Colour	Locality
1-X-7	7X	VC315	Wolframite	Black	Tong Wah (Tae Wha) mine, Korea
1-X-3	3X	VC758	Wolframite	Black	Oregon mine, Boulder, Colorado
1-X-8	8X	VC692	Hübnerite	Black	Silverton, Colorado
1-X-9	9X	UC09059	Hübnerite	Black	Pasto Bueno, Peru

Sample 3X is a black wolframite from Oregon Mine, Boulder, Colorado. It was originally labelled as a ferberite, although it is enriched in the Mn-component with an average Mn-content of 79.25%, making it nearly a hübnerite. The term "wolframite" will suffice, since it is a Fe-Mn solid solution with Mn content between 20-80%. A clustering of crystals were analyzed; a couple large holes exist within the cluster, as well as some anhedral quartz and iron oxide growths on the crystal edges. Some encrustations of clay minerals were seen mixed with the quartz. On average, FeO (4.93 wt. %) and MnO (18.59 wt. %) are essentially the only divalent cations in the A site, with only trace quantities of ZnO (0.02 wt. %) and NiO (0.02 wt. %). Some SO_3 was present, but is variable. The abundance of Fe and Mn shows some variability amongst the analyzed points, with Fe-content ranging from 0.14-0.26 and Mn-content ranging from 0.75-0.86. This variability may indicate an intergrowth of two or more phases, which will be discussed in more detail in section *4.4.2*. The average composition is a solid solution between Fe and Mn end-members: $(Mn_{0.79}Fe_{0.21})_{\Sigma 1.00}W_{0.99}O_4$.

Sample 7X is a black, subhedral-anhedral wolframite fragment from the Tong Wah (Tae Wha) Mine, Korea. The crystal is homogeneous with a few very tiny inclusions (unknown mineralisation), and shows no zonation. On average, FeO (8.71 wt. %) and MnO (15.14 wt. %) are essentially the only divalent cations in the A site, with only trace quantities of MgO (0.02 wt. %), ZnO (0.02 wt. %), and NiO (0.02 wt. %). SO_3 is present, but in variable amounts. The composition is a solid solution between Fe-Mn endmembers with Mn content between 20-80% so it can be termed a wolframite: $(Mn_{0.65}Fe_{0.37})_{\Sigma 1.02}W_{0.99}O_4$.

Sample 8X is a black, euhedral hübnerite fragment from Silverton, Colorado. The crystal is elongate and prismatic, showing some striations on the upper right edge of the crystal. It is homogeneous, showing no zonation. On average, FeO (1.51 wt. %) and MnO (21.89 wt. %) are

essentially the only divalent cations in the A site, with only trace quantities of NiO (0.03wt. %). SO_3 is present, but variable. The composition is close to a pure hübnerite end-member: $(Mn_{0.94}Fe_{0.06})_{\Sigma 1.00}W_{1.00}O_4$.

Sample 9X is a black, anhedral hübnerite fragment from Pasto Bueno, Peru. The crystal is homogeneous, contains only a few tiny holes and shows no zonation. On average, FeO (0.07 wt. %) and MnO (23.41 wt. %) are essentially the only divalent cations in the A site, with only trace quantities of ZnO (0.04 wt. %) and NiO (0.02 wt. %). SO_3 is present, but variable. The composition is incredibly Mn-rich, and can be considered a pure hübnerite end-member: $(Mn_{1.00}Fe_{0.00})_{\Sigma 1.00}W_{1.00}O_4$.

Table 4.3: Chemical analyses for wolframite. Average wt. % of oxides and calculated *apfu* on the basis of 4 oxygen atoms. Samples are listed with increasing Mn-content from left to right.

Sample Oxide	7X wt. %	3X wt. %	8X wt. %	9X wt. %
MnO	15.14(29)	18.59(99)	21.89(46)	23.41(12)
FeO	8.71(26)	4.93(108)	1.51(56)	0.07(2)
ZnO	0.02(3)	0.02(2)	0.01(1)	0.04(2)
MgO	0.02(2)	0.00(1)	0.00(1)	0.00(1)
NiO	0.02(2)	0.02(2)	0.03(2)	0.02(2)
CaO	0.00(1)	0.01(1)	0.00(0)	0.00(0)
PbO	0.00(0)	0.00(0)	0.00(0)	0.00(0)
WO_3	76.11(33)	76.14(30)	76.29(16)	76.05(39)
MoO_3	0.00(0)	0.00(0)	0.00(0)	0.00(0)
SO_3	0.06(8)	0.12(8)	0.05(9)	0.08(11)
TiO_2	0.02(5)	0.01(3)	0.00(0)	0.01(1)
V_2O_3	0.00(0)	0.00(1)	0.00(0)	0.00(0)
Cr_2O_3	0.01(1)	0.00(0)	0.01(1)	0.00(1)
Total	**100.12**	**99.86**	**99.78**	**99.69**
	apfu	*apfu*	*apfu*	*apfu*
Mn^{2+} (0.83 Å)*	0.645(12)	0.793(44)	0.935(19)	1.000(5)
Fe^{2+} (0.78 Å)	0.367(11)	0.208(45)	0.064(23)	0.003(1)
Zn^{2+} (0.74 Å)	0.001(1)	0.001(1)	0.000(0)	0.002(1)
Mg^{2+} (0.72 Å)	0.001(1)	0.000(1)	0.000(1)	0.000(1)
Ni^{2+} (0.69 Å)	0.001(1)	0.001(1)	0.001(1)	0.001(1)
Ca^{2+} (1.00 Å)	0.000(0)	0.000(1)	0.000(0)	0.000(0)
Pb^{2+} (1.19 Å)	0.000(0)	0.000(0)	0.000(0)	0.000(0)
ΣA	**1.015**	**1.003**	**1.001**	**1.006**
W^{6+} (0.60 Å)	0.992(2)	0.994(2)	0.998(3)	0.994(3)
Mo^{6+} (0.59 Å)	0.000(0)	0.000(0)	0.000(0)	0.000(0)
S^{6+} (0.29 Å)	0.002(3)	0.005(3)	0.002(3)	0.003(4)
Ti^{4+} (0.61 Å)	0.001(2)	0.001(1)	0.000(0)	0.000(0)
V^{3+} (0.64 Å)	0.000(0)	0.000(0)	0.000(0)	0.000(0)
Cr^{3+} (0.62 Å)	0.000(0)	0.000(0)	0.000(0)	0.000(0)
ΣB	**0.995**	**0.999**	**1.000**	**0.998**
Total	**2.010**	**2.002**	**2.001**	**2.004**
%Hu	64(1)	79(4)	94(2)	99.69(8)

*Ionic radii from Shannon (1976)

7X: $(Mn_{0.65}Fe_{0.37})_{\Sigma 1.02}W_{0.99}O_4$

3X: $(Mn_{0.79}Fe_{0.21})_{\Sigma 1.00}W_{0.99}O_4$

8X: $(Mn_{0.94}Fe_{0.06})_{\Sigma 1.00}W_{1.00}O_4$

9X: $(Mn_{1.00}Fe_{0.00})_{\Sigma 1.00}W_{0.99}O_4$

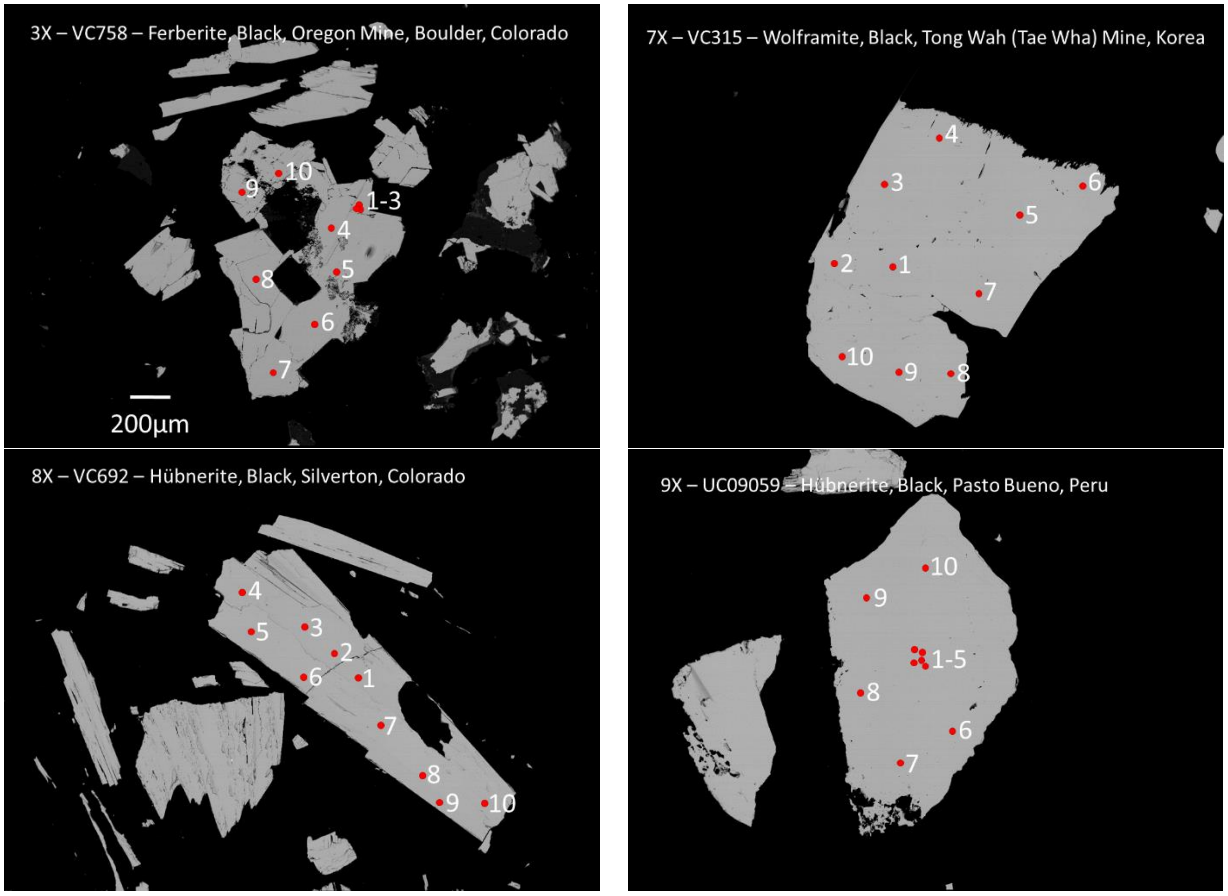

Figure 4.3: Back-scattered electron (BSE) images of wolframite samples: 3X, 7X, 8X, and 9X. Red points on each grain represent approximate locations of quantitative EPMA analyses. According to the BSE images and gathered compositions, the 7X, 8X, and 9X samples are all very homogeneous and pure, however sample 3X shows some variability in Fe, Mn-contents, indicating a potential multiphase mixture.

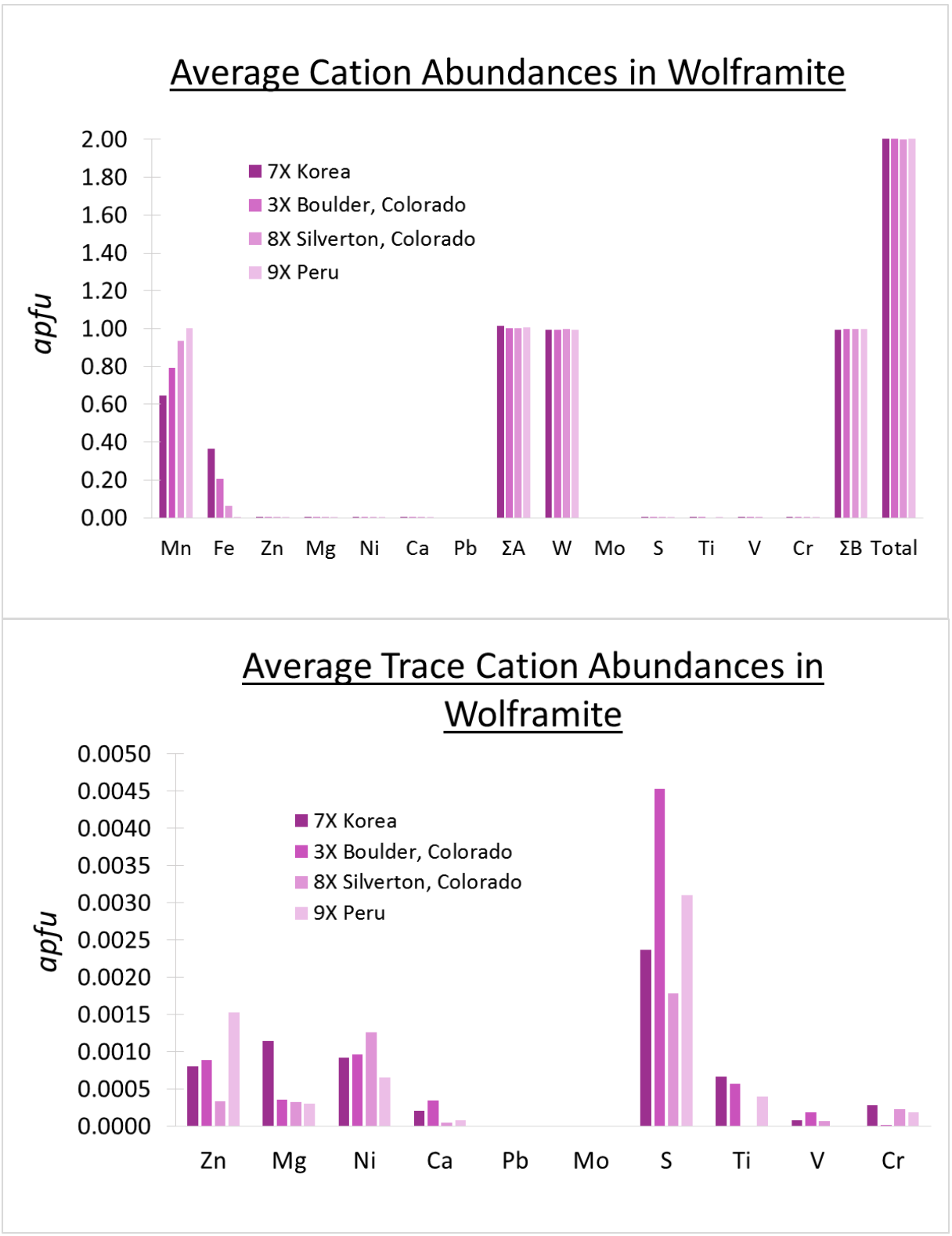

Figure 4.4: Average major and minor (top), and trace (bottom) elemental abundances in wolframite (on the basis of 4 oxygens).

4.4 Discussion

4.4.1 Variations Among Unit Cell Parameters

Due to unforeseen constraints imposed on this project by the COVID-19 pandemic, synchrotron HRPXRD analyses could not be acquired for these wolframite specimens. Below is a discussion of some generalities that previous studies have determined regarding the structures of this mineral group.

In the wolframite series the unit cell dimensions are controlled by the substitution of Fe and Mn. Since the ionic radii of Fe^{2+} (0.78 Å) is slightly less than that of Mn^{2+} (0.83 Å) (Shannon 1976), the unit cell parameters *a, b, c, V,* and *β* are all slightly larger for hübnerite than for ferberite (Sasaki 1959; Soeda et al. 1979). In fact, each cell parameter shows a linear increase in magnitude with increasing Mn-content (Fig 4.6) (Sasaki 1959). Based on the relative slopes of the lines, the *a* parameter is the most sensitive to changes in Mn-content (Soeda et al. 1979; Guillen et al. 1982). Soeda et al. (1979) noted that natural wolframites often deviated from a linear relationship plotted using synthetic wolframites; they attribute this to the substitution of small quantities (~1%) of other cations such as Nb and Y within the structure, indicating a close link between composition and structure. Sasaki (1959) found that in synthetic wolframites, the β angle increased with Mn-content from ~90.0˚ @ 0% Mn-content (pure $FeWO_4$) to ~91.1˚ @ 100% Mn-content (pure $MnWO_4$). Few studies have completed full structural refinements of wolframite specimens. From the few papers that are available regarding the crystal structure, species that are compositionally closer to the hübnerite end-member possess slightly larger A-O and W-O bond distances than the ferberite end-member, which is expected based on the increased lattice size afforded by the substitution of Fe with Mn (Table 4.1). Had this study acquired HRPXRD data, it would have been expected to see noticeable linear trends established between composition and *a, b, c, V, β*

parameters as well as an increase in W-O, A-O bond distances from the most Fe-rich (7X) to the most Mn-rich (9X).

4.4.2 Potential of Multi-phase Wolframite

As previously mentioned, the abundances of Fe and Mn are variable amongst the analyzed points in the wolframite from Boulder, Colorado (3X), with Fe-content ranging from 0.14-0.26 and Mn-content ranging from 0.75-0.86. (Fig. 4.5) This variability seems to indicate an intergrowth of two or more wolframite phases. Table A12 in the Appendix shows the results split into two columns for points with Mn-content > 80% (hübnerite) and points with Mn-content < 80% (wolframite). No obvious patterns can be seen in the trace elements, although S, Zn, and Ti show slightly higher abundances in the "hübnerite"-rich points. The BSE image does not reveal any visible zonation or exsolution lamellae, however the separation of multiple phases must be at a large enough scale since the EPMA is able to resolve those compositional changes throughout the crystal. One reason why any zonation/exsolution in the BSE image is not visible is because the mean atomic numbers of $FeWO_4$ and $MnWO_4$ are incredibly similar, so BSE image brightness contrast is incredibly low, therefore giving the appearance of a homogeneous sample. Another way to test for zoning would be to cut the crystal at different orientations and view under cross-polarized light, as zones of different compositions will go extinct at different positions. Had HRPXRD data been collected for this sample, it would be expected to see some slight diffraction peak splitting due to the presence of different wolframite phases with slightly different unit cell parameters.

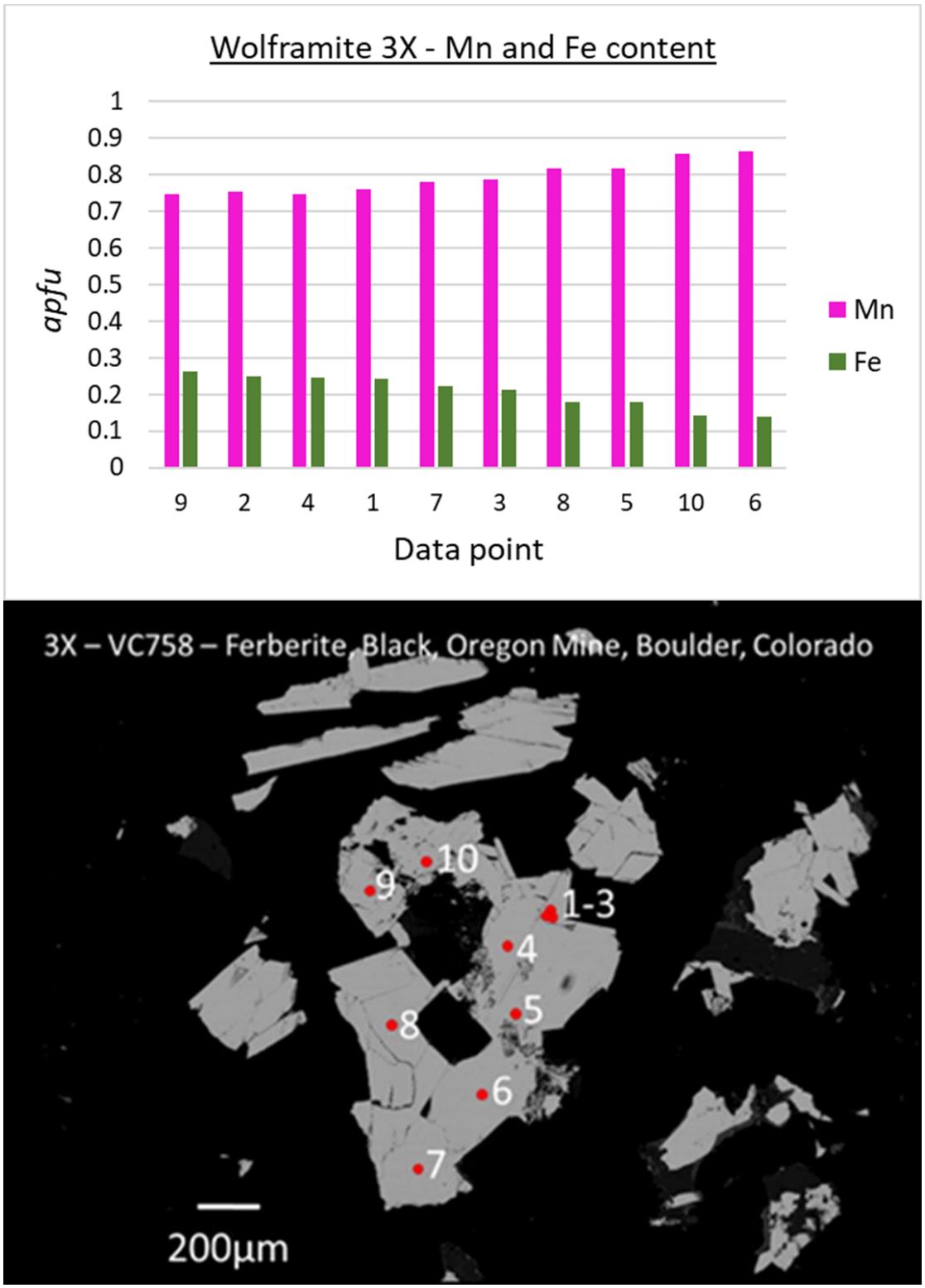

Figure 4.5: Variation in Fe and Mn-contents throughout sample 3X from Boulder Colorado.

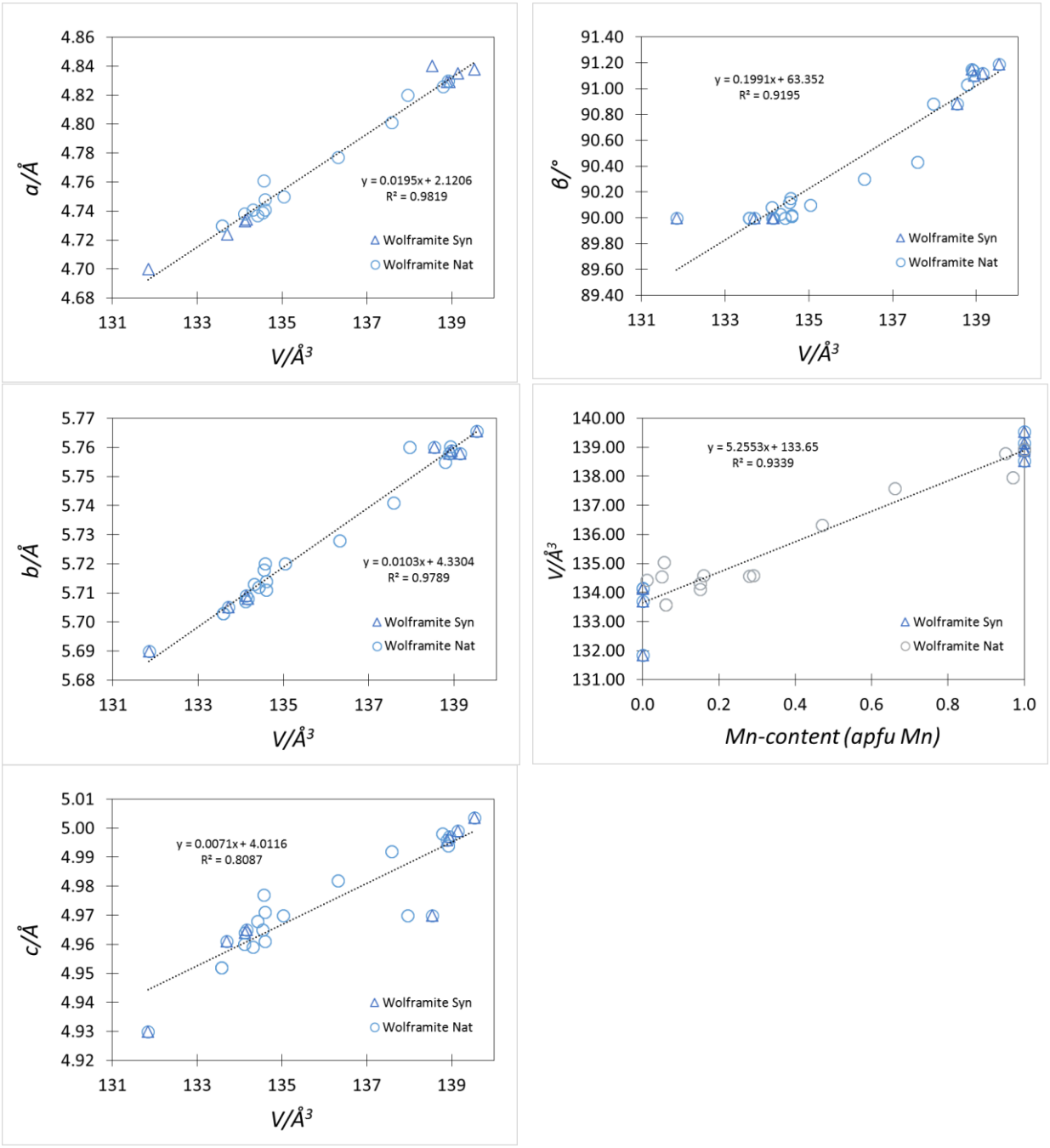

Figure 4.6: Relations among unit-cell parameters *a*, *b*, *c*, *β,* and *V* in the wolframite series. Data comes from both natural (circles) and synthetic (triangles) samples analyzed by the literature sources listed in Table 4.1

CHAPTER 5 – Conclusion

After reviewing the body of previous work conducted using XRD analyses on the wulfenite and wolframite mineral groups, the author presents a few areas for future research:

1) HRPXRD data should be collected for natural stolzite samples, as it is very clear from available literature sources that this mineral species is poorly characterized. Moreover, some natural samples of intermediate compositions in the wulfenite-stolzite series (though rare in nature) would be a benefit to analyze to "fill in the gaps" so to speak. Three localities that the author is aware of that have intermediate compositions are Chillagoe, Queensland, Australia (Hibbs et al. 2000), Copiapo District, Chile (Clark and Sillitoe 1970), and Biella, Italy (Secco et al. 2008).
2) Neutron diffraction data may provide some additional insights into the structure of these minerals. Many of the scheelite and wolframite-type minerals have been successfully characterized using neutron diffraction back in the 1960s and 1970s, but perhaps modern day instrumentation could make improvements. The main challenge is acquiring large enough sample sizes for neutron diffraction.
3) The problem of hemimorphism still remains somewhat of a mystery. The main challenge is acquiring hand samples from the few localities (namely Mezica mine, Slovenia) (Cora et al. 2011; Recnik et al. 2014), and the Christmas Gift mine, Chillagoe, Australia (Hibbs et al. 2000) which display hemimorphic morphologies and are usable for XRD work.
4) A closer look at wolframite sample 3X from Oregon Mine, Boulder, Colorado would be interesting to see if this sample is in fact a multiphase sample. The BSE image, even when adjusted to high contrast, does not show any brightness differences, but the

possibility of a multiphase still remains given the fairly noticeable Fe and Mn concentration changes.

Overall, this project has successfully documented and presented chemical analyses and structural results for a selection of natural wulfenite and wolframite specimens, and integrated these results with the data available from previous researchers.

References

Aanerud, K. (1931) Mischkristallbildung der Scheelitgruppe Durch Fallung von Losungen. Avhandlinger Utgitt Av Det Norske Videnskaps-Akademi Oslo I. Matem-Naturvid, 13, 1–21.

Allen, F.M., and Buseck, P.R. (1988) XRD , FTIR , and TEM studies of optically anisotropic grossular garnets. American Mineralogist, 73, 568–584.

Antao, S.M. (2013a) Is near-endmember birefringent grossular non-cubic? New evidence from synchrotron diffraction. Canadian Mineralogist, 51, 771-784.

Antao, S.M. (2013b) The mystery of birefringent garnet: is the symmetry lower than cubic? Powder Diffraction, 28, 281-288.

Antao, S.M., and Hassan, I. (2002) Thermal analyses of sodalite, tugtupite, danalite, and helvite. Canadian Mineralogist, 40, 163-172.

Antao, S.M., and Hassan, I. (2010) A two-phase intergrowth of genthelvite from Mont Saint-Hilaire, Quebec. Canadian Mineralogist, 48, 1217-1223.

Antao, S.M., Hassan, I., Crichton, W.A., and Parise, J.B. (2005) Effects of high pressure and temperature on cation ordering in magnesioferrite, $MgFe_2O_4$, using in situ synchrotron X-ray powder diffraction up to 1430 K and 6 GPa. American Mineralogist, 90, 1500-1505.

Antao, S.M., Hassan, I., Mulder, W.H., and Lee, P.L. (2008a) The $R\text{-}3c \rightarrow R\text{-}3m$ transition in nitratine, $NaNO_3$, and implications for calcite, $CaCO_3$. Physics and Chemistry of Minerals, 35, 545-557.

Antao, S.M., Hassan, I., Wang, J., Lee, P.L., and Toby, B.H. (2008b) State-of-the-art high-

resolution powder X-ray diffraction (HRPXRD) illustrated with Rietveld structure refinement of quartz, sodalite, tremolite, and meionite. Canadian Mineralogist, 46, 1501-1509.

Antao, S.M., and Klincker, A.M. (2013) Origin of birefringence in andradite from Arizona, Madagascar, and Iran. Physics and Chemistry of Minerals, 40, 575-586.

Antao, S.M., and Klincker, A.M. (2014) Crystal structure of a birefringent andradite-grossular from Crowsnest Pass, Alberta, Canada. Powder Diffraction, 29, 20-27.

Antao, S.M., Mohib, S., Zaman, M., and Marr, R.A. (2015) Ti-rich andradites: chemistry, structure, multi-phases, optical anisotropy, and oscillatory zoning. Canadian Mineralogist, 53, 133-158.

Barbosa, L.B., Reyes Ardila, D., Cusatis, C., and Andreeta, J.P. (2002) Growth and characterization of crack-free scheelite calcium molybdate single crystal fiber. Journal of Crystal Growth, 235, 327–332.

Barkov, A.Y., Martin, R.F., Shi, L., LeBarge, W., and Fedortchouk, Y. (2008) Oscillatory zoning in stanniferous hematite and associated W- and Bi-rich minerals from Canadian Creek, Yukon, Canada. Canadian Mineralogist, 46, 59–72.

Barth, T. (1926) The structure of synthetic, metamict, and recrystallized fergusonite. Norsk Geol. Tids., 427, 23–36.

Berman, J., and Campbell, W.J. (1957) Relationship of composition to thermal stability in the huebnerite-ferberite series of tungstates, 1–14 p.

Bideaux, R.A. (1990) Featured mineral at the 1990 Tucson show: The desert mineral wulfenite.

Rocks and Minerals, 65, 11–30.

Blasse, G. (1997) Classical phosphors: A Pandora's box. Journal of Luminescence, 74, 129–134.

Bomio, M.R.D., Cavalcante, L.S., Almeida, M.A.P., Tranquilin, R.L., Batista, N.C., Pizani, P.S., Siu Li, M., Andres, J., and Longo, E. (2013) Structural refinement, growth mechanism, infrared/Raman spectroscopies and photoluminescence properties of $PbMoO_4$ crystals. Polyhedron, 50, 532–545.

Broch, E.K. (1930) Untersuchungen über Kristallstrukturen des Wolframittypus und des Scheelittypus, 1–61 p. (no. 8. Skrifter (Norske videnskaps-akademi. I--Mat.-naturv. klasse) ; 1929, Ed.). Oslo : I Kommisjon Hos J. Dybwad.

Brown, T., and Pitfield, P. (2014) Tungsten. In Critical Metals Handbook pp. 385–413. John Wiley and Sons.

Chipaux, R., Andre, G., and Cousson, A. (2001) Crystal structure of lead tungstate at 1.4 and 300K. Journal of Alloys and Compounds, 325, 91–94.

Cid-Dresdner, H., and Escobar, C. (1968) The crystal structure of ferberite, $FeWO_4$. Zeitschrift fur Kristallographie, 127, 61–72.

Clark, A.H. (1970) Manganese-iron ratios in wolframite, South Crofty Mine, Cornwall: A discussion. Economic Geology, 65, 889–892.

Clark, A.H., and Sillitoe, R.H. (1970) Tungstenian wulfenites, Mina San Samuel Cachuiyuyo de Llampos, Chile. The American Mineralogist, 55, 2114–2118.

Cora, I., Czugler, M., Dódony, I., and Rečnik, A. (2011) On the symmetry of wulfenite ($Pb[MoO_4]$) from Mežica (Slovenia). Acta Crystallographica Section C: Crystal Structure

Communications, 67, i33–i35.

Dachs, V.H., Stoll, E., and Weitzel, H. (1967) Kristallstruktur und magnetische Ordnung des Hubnerits, $MnWO_4$. Zeitschrift fur Kristallographie, 125, 120–129.

Damascena Dos Passos, R.H., Arab, M., Pereira De Souza, C., and Leroux, C. (2017) $Sr_{1/2}Ce_{5/14}\square_{1/7}WO_4$: A new modulated ternary scheelite compound. Acta Crystallographica Section B: Structural Science, Crystal Engineering and Materials, 73, 466–473.

David, W.I.F., Baerlocher, C., McCusker, L.B., and Shankland, K. (2002) Structure Determination from Powder Diffraction Data. Oxford University Press, Incorporated, Oxford, United Kingdom.

Des Cloizeaux, M. (1850) Memoire sur les formes cristallines du wolfram. Annales de Chimie et de Physique, 163–175.

Dickinson, R.G. (1920) The crystal structures of wulfenite and scheelite. Journal of the American Chemical Society, 42, 85–93.

Dunitz, J.D., Schomaker, V., and Trueblood, K.N. (1988) Interpretation of atomic displacement parameters from diffraction studies of crystals. Journal of Physical Chemistry, 92, 856–867.

El Agami, N.L. (2005) Origin and nature of tungsten producing fluids in a granitic hydrothermal system : geochemical and mineralogical study of hubnerite bearing quartz veins, Qash Amir, South Eastern Desert, Egypt. Saudi Geological Survey, 1–26.

Escobar, C., Cid-Dresdner, H., Kittl, P., and Dumler, I. (1971) The relation between “light wolframite" and common wolframite. The American Mineralogist, 56, 489–498.

Guillen, R., Regnard, J.R., and Amosse, J. (1982) Mössbauer study of natural wolframites. Phys

Chem Minerals, 8, 83–86.

Gurmen, E., Daniels, E., and King, J.S. (1971) Crystal structure refinement of $SrMoO_4$, $SrWO_4$, $CaMoO_4$, and $BaWO_4$ by neutron diffraction. The Journal of Chemical Physics, 55, 1093–1097.

Haberlandt, H., and Schroll, E. (1949) Farbung und Fluoreszenz des Wulfenits im Zusammenhang mit dem Gehalt an Chrom und andern Spurenelementen. Experientia, 6, 89–91.

Harlaux, M., Mercadier, J., Marignac, C., Peiffert, C., Cloquet, C., and Cuney, M. (2018) Tracing metal sources in peribatholitic hydrothermal W deposits based on the chemical composition of wolframite: The example of the Variscan French Massif Central. Chemical Geology, 479, 58–85.

Hassan, I., Antao, S.M., and Hersi, A.A. (2003) Single-crystal XRD, TEM, and thermal studies of the satellite reflections in nepheline. Canadian Mineralogist, 41, 759-783.

Hassan, I., Antao, S.M., and Parise, J.B. (2004) Haüyne: phase transition and high-temperature structures obtained from synchrotron radiation and Rietveld refinements. Mineralogical Magazine, 68, 499-513.

Hazen, R.M., Finger, L.W., and Mariathasan, J.W.E. (1985) High-pressure crystal chemistry of scheelite-type tungstates and molybdates. Journal of Physics and Chemistry of Solids, 46, 253–263.

Hibbs, D.E., Jury, C.M., Leverette, P., Plimer, I.R., and Williams, P.A. (2000) An explanation for the origin of hemihedrism in wulfenite : the single-crystal structures of $I4_1/a$ and I-4

tungstenian wulfenites. Mineralogical Magazine, 64, 1057–1062.

Hsu, L.C. (1976) The stability relations of the wolframite series. American Mineralogist, 61, 944–955.

Hurlbut, C.S. (1955) Wulfenite symmetry as shown on crystals from Jugoslavia. American Mineralogist, 40, 857–860.

Jury, C.M., Leverett, P., Williams, P.A., Plimer, I.R., and Hibbs, D.E. (2001) Mineralogical note: The status of "Chillagite." Australian Journal of Mineralogy, 7, 39.

Kay, M.I., Frazer, B.C., and Almodovar, I. (1964) Neutron diffraction refinement of $CaWO_4$. The Journal of Chemical Physics, 40, 504–506.

Kirschbaum, K., Martin, A., and Pinkerton, A.A. (1997) λ/2 Contamination in charge-coupled-device area-detector data. Journal of Applied Crystallography, 30, 514–516.

Knight, K.S. (1992) The crystal structure of russellite; a re-determination using neutron powder diffraction of synthetic Bi_2WO_6. Mineralogical Magazine, 56, 399–409.

Laishevtseva, N.A., Shindel'man, N.K., Khodos, M.Y., Perelyaeva, L.A., and Tkachenko, E.V. (1989) $PbMoO_4$-$PbWO_4$ System. Zhurnal Neorganicheskoj Khimii;, 34, 1291–1294.

Larson, A.C., and Von Dreele, R.B. (2000) General structure analysis system (GSAS). Report LAUR 86-748, Los Alamos National Laboratory, Los Alamos, New Mexico.

Leciejewicz, J. (1965) A neutron crystallographic investigation of lead molybdenum oxide, $PbMoO_4$. Zeitschrift fur Kristallographie, 121, 158–164.

Lee, P.L., Shu, D., Ramanathan, M., Preissner, C., Wang, J., Beno, M.A., Von Dreele, R.B., Ribaud, L., Kurtz, C., Antao, S.M., Jiao, X., and Toby, B.H. (2008) A twelve-analyzer

detector system for high-resolution powder diffraction. Journal of Synchrotron Radiation, 15, 427-432.

Lopez-Moreno, S., Romero, A.H., Rodriguez-Hernandez, P., and Muñoz, A. (2009) Ab initio calculations of the wolframite $MnWO_4$ under high pressure. High Pressure Research, 29, 578–581.

Lugli, C., Medici, L., and Saccardo, D. (1999) Natural wulfenite: structural refinement by single-crystal X-ray diffraction. Neues Jahrbuch fur Mineralogie, Monatshefte, 6, 281–288.

Macavei, J., and Schulz, H. (1993) The crystal structure of wolframite type tungstates at high pressure. Zeitschrift für Kristallographie, 207, 193–208.

Machatschki, F. (1928) IX. Kürzere Originalmitteilungen und Notizen: Über die Kristallgestalt des Magnesiumwolframates. Zeitschrift für Kristallographie, 67, 163–165.

Maczka, M., Filho, A.G.S., Paraguassu, W., Freire, P.T.C., Filho, J.M., and Hanuza, J. (2012) Pressure-induced structural phase transitions and amorphization in selected molybdates and tungstates. Progress in Materials Science, 57, 1335–1381.

Mal, P., Bera, G., Rambabu, P., Turpu, G.R., Chakraborty, B., Ramaniah, L.M., Singh, R.P., Sen, P., and Das, P. (2017) Electronic , magnetic and spectroscopic properties of doped $Mn_{(1-x)}A_xWO_4$ (A = Co, Cu, Ni and Fe) multiferroic: an experimental and DFT study. Journal of Physics: Condensed Matter, 29, 1–10.

Mineral Data Publishing (2005) Hubnerite $Mn^{2+}WO_4$. Mineral Data Publishing, 2005.

Moreau, J.M., Galez, P., Pelgneux, J.P., and Korzhik, M.V. (1996) Structural characterization of $PbWO_4$ and related new phase $Pb_7W_8O_{(32-x)}$. Journal of Alloys and Compounds, 238, 46–48.

Moreiras, D., Pascual, C.M., García-Granda, S., Martín-Izard, A., Roldán, F.V., and Merchán, A.A. y J. (1991) La Stolzita de La Tala : estructura cristalina , reflectancia y microdureza Vickers. Boletin de la Sociedad Espanola de Mineralogia, 14, 23–31.

Nakamura, T., Sugiyama, K., Moriguchi, E., and Shoji, T. (2002) Synthesis of scheelite group minerals in the $CaWO_4$-$CaMoO_4$-$PbMoO_4$-$PbWO_4$ system from aqueous solutions at 100°C. Shigen-to-Sozai, 118, 217–221.

Neiva, A.M.R. (2008) Geochemistry of cassiterite and wolframite from tin and tungsten quartz veins in Portugal. Ore Geology Reviews, 33, 221–238.

Nesse, W.D. (2012) Introduction to Mineralogy, 2nd ed. Oxford University Press, Inc.

Oeder, R., Scharmann, A., and Schwabe, D. (1980) Growth and properties of various scheelite type mixed crystal systems. Journal of Crystal Growth, 49, 349–356.

Olson, H.J. (1966) Oxidation of a sulfide body, Glove Mine, Santa Cruz County, Arizona. Economic Geology, 61, 731–743.

Pačevski, A., Götzinger, M., Dimitrijević, R., and Ljubomir, C. (2007) Oscillatory zoning in wolframite from Osanica locality, Serbia.

Pinnow, D.A., Van Uitert, L.G., Warner, A.W., and Bonner, W.A. (1969) Lead molybdate: A melt-grown crystal with a high figure of merit for acousto-optic device applications. Applied Physics Letters, 15, 83–86.

Quodling, F.M., and Cohen, S.B. (1938) An X-ray examination of chillagite. Journal and Proceedings of the Royal Society of New South Wales, 71, 543–546.

Recnik, A., Zavasnki, J., and Fajmut-Strucl, S. (2014) The Mezica Mine, Koroska (Slovenia).

The Mineralogical Record, 45, 507–548.

Redfern, S.A.T., Bell, A.M.T., Henderson, C.M.B., and Schofield, P.F. (1995) Rietveld study of the structural phase transition in the sanmartinite ($ZnWO_4$)-cuproscheelite ($CuWO_4$) solid solution. European Journal of Mineralogy, 7, 1019–1028.

Renner, B., and Lehmann, G. (1986) Correlation of angular and bond length distortions in TO_4 units in crystals. Zeitschrift fur Kristallographie, 175, 43–59.

Robinson, K., Gibbs, G.V., and Ribbe, P.H. (1971) Quadratic elongation : A quantitative measure of distortion in coordination polyhedra. Science, New Series, 172, 567–570.

Romer, R.L., and Kroner, U. (2016) Phanerozoic tin and tungsten mineralization-Tectonic controls on the distribution of enriched protoliths and heat sources for crustal melting. Gondwana Research, 31, 60–95.

Sasaki, A. (1959) Variation of unit cell parameters in wolframite series. Mineralogical Journal, 2, 375–396.

Schofield, P.F., Knight, K.S., and Cressey, G. (1996) Neutron powder diffraction study of the scintillator material $ZnWO_4$. Journal of Materials Science, 31, 2873–2877.

Schofield, P.F., Knight, K.S., Redfern, S.A.T., and Cressey, G. (1997) Distortion characteristics across the structural phase transition in $(Cu_{1-x}Zn_x)WO_4$. Acta Crystallographica Section B: Structural Science, 53, 102–112.

Sczancoski, J.C., Bomio, M.D.R., Cavalcante, L.S., Joya, M.R., Pizani, P.S., Varela, J.A., Longo, E., Li, M.S., and Andrés, J.A. (2009) Morphology and blue photoluminescence emission of $PbMoO_4$ processed in conventional hydrothermal. The Journal of Physical

Chemistry C, 111, 5812–5822.

Secco, L., Nestola, F., and Dal Negro, A. (2008) The wulfenite—stolzite series: centric or acentric structures? Mineralogical Magazine, 72, 987–990.

Shannon, R.D. (1976) Revised effective ionic radii and systematic studies of interatomic distances in halides and chalcogenides. Acta Crystallographica, 32, 751–767.

Sillen, L., and Nylander, A. (1943) On the oxygen positions in tungstates and molybdates with the scheelite structure. Arkiv fur Kemi, Mineralogi Och Geologi, 17A, 1–27.

Skinner, L.B., Benmore, C.J., Antao, S.M., Soignard, E., Amin, S.A., Bychkov, E., Rissi, E., Parise, J.B., and Yarger, J.L. (2011) Structural changes in vitreous $GeSe_4$ under pressure. Journal of Physical Chemistry C, 116, 2212-2217.

Sleight, A.W. (1972) Accurate cell dimensions for ABO_4 molybdates and tungstates. Acta Crystallographica Section B Structural Science, Crystal Engineering and Materials, 28, 2899–2902.

Soeda, A., Takeno, S., and Watanabe, M. (1979) Mineralogical study on the wolframite series from the Chugoku district, Southwest Japan. I. Relationships between lattice parameters and chemical compositions. The Journal of the Japanese Association of Mineralogists, Petrologists and Economic Geologists, 74, 357–375.

Sugaki, A., Kitakaze, A., and Hayashi, K. (1986) Study on the ore minerals from the Bolivian tin deposits (II) cassiterite and wolframite from the mines in the Potosi and Quechisla Districts. The Science Reports of the Tohoku University, 16, 353–365.

Sun, F., Chen, X., and Zhao, Z. (2019) Synthesis of coarse-grained tungsten carbide directly

from scheelite/wolframite by carbothermal reduction and crystallization. The Minerals, Metals & Materials Society, 7.

Swanson, H.E., Cook, M.I., and Gilfrich, N.T. (1957) Standard X-ray diffraction powder patterns. [Volume VII]. [Data for 53 substances]. National Bureau of Standards, [Washington, D.C.].

Talla, D., Wildner, M., Beran, A., Skoda, R., and Z, L. (2013) On the presence of hydrous defects in differently coloured wulfenites ($PbMoO_4$): an infrared and optical spectroscopic study. Physics and Chemistry of Minerals, 40, 757–769.

Talla, D., Beran, A., Skoda, R., and Losos, Z. (2017) Polarized FTIR spectroscopic examination on hydroxylation in the minerals of the wolframite group, (Fe,Mn,Mg)[W,(Nb,Ta)][O,(OH)]$_4$. American Mineralogist, 102, 867–875.

Thresiamma, G., Sunny, J., Anu Trisa, S., and Suresh, M. (2008) Fascinating morphologies of lead tungstate nanostructures by chimie douce approach. Journal of Nanoparticle Research, 10, 567–575.

Tindle, A.G., and Webb, P.C. (1989) Niobian wolframite from Glen Gairn in the Eastern Highlands A microprobe investigation of Scotland. Geochemica et Cosmochemica Acta, 53, 1921–1935.

Toby, B. (2001) EXPGUI, a graphical user interface for GSAS. Journal of Applied Crystallography, 34, 210–213.

Ulku, V.D. (1967) Untersuchungen und magnetischen zur Kristallstruktur Struktur des Ferberits $FeWO_4$. Zeitschrift fur Kristallographie, 124, 192–219.

Ullman, A.T. (1912) A new mineral. Journal and proceedings of the Royal Society of New South Wales, 46, 186.

Umbsaar, D., and Antao, S. (2020) Crystal chemistry of wulfenite (PbMoO4) and wolframite (Fe,Mn)WO4. In Geoconvention Calgary.

Vegard, L. (1926) CIV. Results of crystal analysis . The London, Edinburgh, and Dublin Philosophical Magazine and Journal of Science, 1, 1151–1193.

Vegard, L., and Refsum, A. (1927) Further investigations on the structure of crystals belonging to the scheelite group. Det Norske Vid. Akad.Skr. in Oslo. Math.-Nat. Kl., 207–208.

Vernaleken, A., Cohen, M.G., and Metcalf, H. (2007) Interferometric measurement of acoustic velocity in PbMoO4 and TeO2. Applied Optics, 46, 7117–7119.

Vesselinov, I. (1996) The significance of wulfenite morphology as shown on crystals from Mezica, Slovenia. Geochemistry, Mineralogy, and Petrology, 31, 29–39.

Wang, J., Toby, B.H., Lee, P.L., Ribaud, L., Antao, S.M., Kurtz, C., Ramanathan, M., Von Dreele, R.B., and Beno, M.A. (2008) A dedicated powder diffraction beamline at the advanced photon source: commissioning and early operational results. Review of Scientific Instruments, 79, 085105.

Werner, A.B.T., Sinclair, W.D., and Amey, E.. (2014) International strategic mineral issues summary report—tungsten (ver. 1.1, November 2014). U.S. Geological Survey Circular 930–O, 74.

Xu, K., Xue, J., Ding, Y., and Lu, G. (1995) Discovery of stolzite in China and refinement of its crystal structure. Acta Geologica Sinica, 8, 111–117.

Zalkin, A., and Templeton, D.H. (1964) X-ray diffraction refinement of the calcium tungstate structure. The Journal of Chemical Physics, 40, 501–504.

Zaman, M., Schubert, M., and Antao, S. (2012) Elevated radionuclide concentrations in heavy mineral-rich beach sands in the Cox's Bazar region, Bangladesh and related possible radiological effects. Isotopes In Environmental and Health Studies, 48, 512-525.

Zhuravlev, V.D., Reznitskikh, O.G., Velikodnyi, Y.A., Patrusheva, T.A., and Sivtsova, O. V (2011) Analysis of solid solutions stability in scheelite-type molybdates and tungstates. Journal of Solid State Chemistry, 184, 2785–2789.

Appendices

For Tables A1-A12 (shown below):

*Ionic radii from Shannon (1976)
%Hu = %Hübnerite = Mn-content = Mn/(Mn+Fe) x 100%
SD = standard deviation among 10 spot analyses

Wulfenite samples (Tables A1-A7) are listed in order of increasing Pb-content: 1X, 4X, 6X, 2X, 5X, 7U, 8U

Wolframite samples (Tables A8-A12) are listed in order of increasing Mn-content: 7X, 3X, 8X, 9X

Table A1: EPMA results for Sample 1X from Taco Mine, Lucia, Utah presented as wt. % oxides and calculated *apfu* on the basis of 4 oxygen atoms. Atoms are grouped into either A or B sites in the general ABO_4 formula.

Sample 1X: Taco Mine, Utah														
Oxide (wt. %)	1-1	1-2	1-3	1-4	1-5	1-6	1-7	1-8	1-9	1-10	Avg	Min	Max	SD
PbO	60.67	59.98	60.38	59.23	59.92	60.34	60.17	60.74	59.79	59.40	60.06	59.23	60.74	0.50
BaO	0.00	0.00	0.00	0.00	0.02	0.00	0.02	0.03	0.02	0.00	0.01	0.00	0.03	0.01
CaO	0.00	0.00	0.01	0.01	0.01	0.00	0.01	0.01	0.00	0.00	0.00	0.00	0.01	0.01
ZnO	0.00	0.00	0.02	0.00	0.00	0.00	0.00	0.00	0.00	0.00	0.00	0.00	0.02	0.00
MoO_3	39.83	39.74	39.55	38.70	38.90	39.03	39.24	39.57	39.19	39.13	39.29	38.70	39.83	0.37
WO_3	0.01	0.00	0.03	0.03	0.00	0.08	0.09	0.06	0.00	0.11	0.04	0.00	0.11	0.04
SO_3	0.00	0.00	0.04	0.00	0.00	0.00	0.00	0.00	0.07	0.00	0.01	0.00	0.07	0.02
CrO_3	0.00	0.00	0.01	0.00	0.00	0.00	0.00	0.00	0.00	0.00	0.00	0.00	0.01	0.00
V_2O_5	0.00	0.00	0.06	0.04	0.04	0.06	0.06	0.00	0.05	0.11	0.04	0.00	0.11	0.04
Total	**100.51**	**99.72**	**100.09**	**98.01**	**98.89**	**99.51**	**99.59**	**100.40**	**99.12**	**98.75**	**99.46**	**98.01**	**100.51**	**0.78**
	apfu	*apfu*	*apfu*	*apfu*	*apfu*	*apfu*	*apfu*	*apfu*	*apfu*	*apfu*	Avg	Min	Max	SD
Pb^{2+} (1.29 Å)	0.987	0.980	0.985	0.989	0.994	0.995	0.989	0.992	0.984	0.980	0.987	0.980	0.995	0.005
Ba^{2+} (1.42 Å)	0.000	0.000	0.000	0.000	0.000	0.000	0.000	0.001	0.000	0.000	0.000	0.000	0.001	0.000
Ca^{2+} (1.12 Å)	0.000	0.000	0.001	0.001	0.001	0.000	0.000	0.000	0.000	0.000	0.000	0.000	0.001	0.000
Zn^{2+} (0.90 Å)	0.000	0.000	0.001	0.000	0.000	0.000	0.000	0.000	0.000	0.000	0.000	0.000	0.001	0.000
ΣA	**0.987**	**0.980**	**0.986**	**0.989**	**0.995**	**0.995**	**0.990**	**0.992**	**0.984**	**0.980**	**0.988**	**0.980**	**0.995**	**0.006**
Mo^{6+} (0.41 Å)	1.004	1.007	1.000	1.002	1.000	0.998	1.000	1.002	1.000	1.001	1.001	0.998	1.007	0.002
W^{6+} (0.42 Å)	0.000	0.000	0.000	0.000	0.000	0.001	0.001	0.001	0.000	0.002	0.001	0.000	0.002	0.001
S^{6+} (0.12 Å)	0.000	0.000	0.002	0.000	0.000	0.000	0.000	0.000	0.003	0.000	0.001	0.000	0.003	0.001
Cr^{6+} (0.26 Å)	0.000	0.000	0.000	0.000	0.000	0.000	0.000	0.000	0.000	0.000	0.000	0.000	0.000	0.000
V^{5+} (0.36 Å)	0.000	0.000	0.002	0.002	0.002	0.003	0.003	0.000	0.002	0.005	0.002	0.000	0.005	0.001
ΣB	**1.004**	**1.007**	**1.005**	**1.004**	**1.002**	**1.002**	**1.004**	**1.003**	**1.006**	**1.007**	**1.004**	**1.002**	**1.007**	**0.002**
Total	**1.991**	**1.987**	**1.991**	**1.993**	**1.997**	**1.997**	**1.994**	**1.995**	**1.990**	**1.988**	**1.992**	**1.987**	**1.997**	**0.004**

Table A2: EPMA results for Sample 4X from Glove Mine, Santa Cruz County, Arizona presented as wt. % oxides and calculated *apfu* on the basis of 4 oxygen atoms. Atoms are grouped into either A or B sites in the general ABO_4 formula.

Sample 4X: Glove Mine, Arizona														
Oxide (wt. %)	4-1	4-2	4-3	4-4	4-5	4-6	4-7	4-8	4-9	4-10	Avg	Min	Max	SD
PbO	60.55	60.04	59.83	59.77	60.02	60.82	60.52	59.98	60.55	60.63	60.27	59.77	60.82	0.38
BaO	0.00	0.01	0.03	0.00	0.07	0.00	0.00	0.00	0.00	0.00	0.01	0.00	0.07	0.02
CaO	0.01	0.00	0.00	0.01	0.00	0.02	0.02	0.01	0.01	0.01	0.01	0.00	0.02	0.01
ZnO	0.00	0.01	0.02	0.01	0.03	0.00	0.00	0.00	0.01	0.00	0.01	0.00	0.03	0.01
MoO_3	39.44	39.41	39.11	39.52	39.28	39.74	39.17	39.09	39.22	39.67	39.37	39.09	39.74	0.23
WO_3	0.00	0.08	0.00	0.00	0.01	0.00	0.00	0.00	0.00	0.00	0.01	0.00	0.08	0.03
SO_3	0.06	0.00	0.00	0.05	0.00	0.00	0.00	0.00	0.00	0.01	0.01	0.00	0.06	0.02
CrO_3	0.00	0.00	0.00	0.05	0.00	0.00	0.00	0.00	0.00	0.00	0.01	0.00	0.05	0.01
V_2O_5	0.00	0.05	0.07	0.14	0.05	0.06	0.08	0.06	0.13	0.07	0.07	0.00	0.14	0.04
Total	**100.05**	**99.60**	**99.06**	**99.55**	**99.46**	**100.63**	**99.79**	**99.13**	**99.91**	**100.39**	**99.76**	**99.06**	**100.63**	**0.51**
	apfu	*apfu*	*apfu*	*apfu*	*apfu*	*apfu*	*apfu*	*apfu*	*apfu*	*apfu*	Avg	Min	Max	SD
Pb^{2+} (1.29 Å)	0.990	0.984	0.988	0.975	0.987	0.988	0.995	0.991	0.993	0.987	0.988	0.975	0.995	0.006
Ba^{2+} (1.42 Å)	0.000	0.000	0.001	0.000	0.002	0.000	0.000	0.000	0.000	0.000	0.000	0.000	0.002	0.001
Ca^{2+} (1.12 Å)	0.001	0.000	0.000	0.000	0.000	0.001	0.001	0.000	0.001	0.001	0.001	0.000	0.001	0.000
Zn^{2+} (0.90 Å)	0.000	0.000	0.001	0.001	0.001	0.000	0.000	0.000	0.000	0.000	0.000	0.000	0.001	0.000
ΣA	**0.991**	**0.985**	**0.989**	**0.976**	**0.990**	**0.990**	**0.996**	**0.991**	**0.994**	**0.988**	**0.989**	**0.976**	**0.996**	**0.006**
Mo^{6+} (0.41 Å)	1.000	1.002	1.001	1.000	1.001	1.001	0.998	1.001	0.998	1.001	1.000	0.998	1.002	0.001
W^{6+} (0.42 Å)	0.000	0.001	0.000	0.000	0.000	0.000	0.000	0.000	0.000	0.000	0.000	0.000	0.001	0.000
S^{6+} (0.12 Å)	0.003	0.000	0.000	0.002	0.000	0.000	0.000	0.000	0.000	0.000	0.001	0.000	0.003	0.001
Cr^{6+} (0.26 Å)	0.000	0.000	0.000	0.002	0.000	0.000	0.000	0.000	0.000	0.000	0.000	0.000	0.002	0.001
V^{5+} (0.36 Å)	0.000	0.002	0.003	0.005	0.002	0.002	0.003	0.002	0.005	0.003	0.003	0.000	0.005	0.002
ΣB	**1.003**	**1.005**	**1.004**	**1.009**	**1.004**	**1.004**	**1.002**	**1.003**	**1.003**	**1.005**	**1.004**	**1.002**	**1.009**	**0.002**
Total	**1.994**	**1.991**	**1.993**	**1.985**	**1.993**	**1.994**	**1.998**	**1.994**	**1.997**	**1.992**	**1.993**	**1.985**	**1.998**	**0.004**

Table A3: EPMA results for Sample 6X from Mezica (Mies) Mine, Slovenia presented as wt. % oxides and calculated *apfu* on the basis of 4 oxygen atoms. Atoms are grouped into either A or B sites in the general ABO_4 formula.

Sample 6X: Mezica (Mies) Mine, Slovenia														
Oxide (wt. %)	6-1	6-2	6-3	6-4	6-5	6-6	6-7	6-8	6-9	6-10	Avg	Min	Max	SD
PbO	61.09	60.47	60.50	60.61	60.03	60.71	60.84	61.06	60.82	60.80	60.69	60.03	61.09	0.31
BaO	0.00	0.00	0.00	0.00	0.00	0.03	0.00	0.00	0.00	0.02	0.01	0.00	0.03	0.01
CaO	0.01	0.00	0.00	0.00	0.02	0.03	0.01	0.01	0.01	0.00	0.01	0.00	0.03	0.01
ZnO	0.02	0.00	0.00	0.02	0.00	0.00	0.00	0.01	0.00	0.00	0.00	0.00	0.02	0.01
MoO_3	38.83	38.39	39.11	39.77	39.76	38.61	38.94	38.56	39.58	38.66	39.02	38.39	39.77	0.51
WO_3	0.00	0.09	0.06	0.04	0.00	0.00	0.11	0.00	0.05	0.10	0.04	0.00	0.11	0.04
SO_3	0.04	0.00	0.06	0.05	0.07	0.00	0.15	0.00	0.02	0.14	0.05	0.00	0.15	0.05
CrO_3	0.00	0.00	0.00	0.00	0.00	0.00	0.00	0.00	0.00	0.00	0.00	0.00	0.00	0.00
V_2O_5	0.24	0.26	0.12	0.10	0.08	0.21	0.17	0.27	0.12	0.08	0.17	0.08	0.27	0.07
Total	**100.23**	**99.22**	**99.85**	**100.58**	**99.95**	**99.59**	**100.22**	**99.92**	**100.61**	**99.80**	**100.00**	**99.22**	**100.61**	**0.43**
	apfu	*apfu*	*apfu*	*apfu*	*apfu*	*apfu*	*apfu*	*apfu*	*apfu*	*apfu*	Avg	Min	Max	SD
Pb^{2+} (1.29 Å)	1.003	1.004	0.992	0.982	0.975	1.004	0.995	1.009	0.989	1.002	0.996	0.975	1.009	0.011
Ba^{2+} (1.42 Å)	0.000	0.000	0.000	0.000	0.000	0.001	0.000	0.000	0.000	0.001	0.000	0.000	0.001	0.000
Ca^{2+} (1.12 Å)	0.001	0.000	0.000	0.000	0.001	0.002	0.001	0.001	0.001	0.000	0.001	0.000	0.002	0.001
Zn^{2+} (0.90 Å)	0.001	0.000	0.000	0.001	0.000	0.000	0.000	0.000	0.000	0.000	0.000	0.000	0.001	0.000
ΣA	**1.004**	**1.004**	**0.993**	**0.983**	**0.977**	**1.007**	**0.995**	**1.010**	**0.990**	**1.003**	**0.997**	**0.977**	**1.010**	**0.011**
Mo^{6+} (0.41 Å)	0.989	0.988	0.995	1.000	1.002	0.991	0.987	0.988	0.998	0.988	0.992	0.987	1.002	0.006
W^{6+} (0.42 Å)	0.000	0.002	0.001	0.001	0.000	0.000	0.002	0.000	0.001	0.002	0.001	0.000	0.002	0.001
S^{6+} (0.12 Å)	0.002	0.000	0.003	0.002	0.003	0.000	0.007	0.000	0.001	0.006	0.002	0.000	0.007	0.002
Cr^{6+} (0.26 Å)	0.000	0.000	0.000	0.000	0.000	0.000	0.000	0.000	0.000	0.000	0.000	0.000	0.000	0.000
V^{5+} (0.36 Å)	0.010	0.010	0.005	0.004	0.003	0.008	0.007	0.011	0.005	0.003	0.007	0.003	0.011	0.003
ΣB	**1.000**	**1.000**	**1.003**	**1.006**	**1.008**	**0.999**	**1.003**	**0.999**	**1.004**	**1.000**	**1.002**	**0.999**	**1.008**	**0.003**
Total	**2.005**	**2.005**	**1.996**	**1.990**	**1.985**	**2.006**	**1.998**	**2.008**	**1.994**	**2.003**	**1.999**	**1.985**	**2.008**	**0.008**

Table A4: EPMA results for Sample 2X from Laurion, Greece presented as wt. % oxides and calculated *apfu* on the basis of 4 oxygen atoms. Atoms are grouped into either A or B sites in the general ABO_4 formula.

Sample 2X: Laurion, Greece														
Oxide (wt. %)	2-1	2-2	2-3	2-4	2-5	2-6	2-7	2-8	2-9	2-10	Avg	Min	Max	SD
PbO	60.76	60.12	60.29	59.23	59.36	59.76	60.49	60.97	59.83	59.98	60.08	59.23	60.97	0.57
BaO	0.00	0.02	0.00	0.05	0.02	0.00	0.00	0.00	0.09	0.00	0.02	0.00	0.09	0.03
CaO	0.01	0.02	0.00	0.01	0.00	0.00	0.02	0.00	0.01	0.00	0.01	0.00	0.02	0.01
ZnO	0.00	0.00	0.03	0.00	0.00	0.01	0.00	0.01	0.00	0.00	0.00	0.00	0.03	0.01
MoO_3	38.71	38.54	38.58	38.19	37.62	38.57	38.21	38.41	38.00	38.18	38.30	37.62	38.71	0.33
WO_3	0.03	0.00	0.05	0.00	0.00	0.02	0.00	0.12	0.00	0.00	0.02	0.00	0.12	0.04
SO_3	0.00	0.09	0.00	0.00	0.04	0.00	0.00	0.12	0.10	0.00	0.03	0.00	0.12	0.05
CrO_3	0.09	0.09	0.03	0.02	0.16	0.08	0.00	0.01	0.04	0.00	0.05	0.00	0.16	0.05
V_2O_5	0.24	0.31	0.44	0.43	0.09	0.00	0.46	0.50	0.42	0.30	0.32	0.00	0.50	0.17
Total	**99.83**	**99.20**	**99.42**	**97.94**	**97.29**	**98.44**	**99.18**	**100.15**	**98.48**	**98.46**	**98.84**	**97.29**	**100.15**	**0.88**
	apfu	*apfu*	*apfu*	*apfu*	*apfu*	*apfu*	*apfu*	*apfu*	*apfu*	*apfu*	Avg	Min	Max	SD
Pb^{2+} (1.29 Å)	1.000	0.991	0.993	0.988	1.005	0.997	1.003	0.999	0.995	1.002	0.997	0.988	1.005	0.006
Ba^{2+} (1.42 Å)	0.000	0.001	0.000	0.001	0.000	0.000	0.000	0.000	0.002	0.000	0.000	0.000	0.002	0.001
Ca^{2+} (1.12 Å)	0.000	0.001	0.000	0.001	0.000	0.000	0.001	0.000	0.001	0.000	0.000	0.000	0.001	0.000
Zn^{2+} (0.90 Å)	0.000	0.000	0.001	0.000	0.000	0.000	0.000	0.000	0.000	0.000	0.000	0.000	0.001	0.000
ΣA	**1.001**	**0.993**	**0.994**	**0.990**	**1.005**	**0.997**	**1.004**	**0.999**	**0.998**	**1.002**	**0.998**	**0.990**	**1.005**	**0.005**
Mo^{6+} (0.41 Å)	0.988	0.985	0.985	0.988	0.987	0.998	0.983	0.976	0.980	0.989	0.986	0.976	0.998	0.006
W^{6+} (0.42 Å)	0.001	0.000	0.001	0.000	0.000	0.000	0.000	0.002	0.000	0.000	0.000	0.000	0.002	0.001
S^{6+} (0.12 Å)	0.000	0.004	0.000	0.000	0.002	0.000	0.000	0.005	0.004	0.000	0.002	0.000	0.005	0.002
Cr^{6+} (0.26 Å)	0.003	0.003	0.001	0.001	0.006	0.003	0.000	0.000	0.002	0.000	0.002	0.000	0.006	0.002
V^{5+} (0.36 Å)	0.010	0.013	0.018	0.018	0.004	0.000	0.019	0.020	0.017	0.012	0.013	0.000	0.020	0.007
ΣB	**1.001**	**1.005**	**1.005**	**1.006**	**0.999**	**1.001**	**1.002**	**1.004**	**1.003**	**1.001**	**1.003**	**0.999**	**1.006**	**0.002**
Total	**2.002**	**1.997**	**1.999**	**1.996**	**2.004**	**1.998**	**2.006**	**2.003**	**2.002**	**2.003**	**2.001**	**1.996**	**2.006**	**0.003**

Table A5: EPMA results for Sample 5X from Touissit, Morocco presented as wt. % oxides and calculated *apfu* on the basis of 4 oxygen atoms. Atoms are grouped into either A or B sites in the general ABO_4 formula.

Sample 5X: Touissit, Morocco														
Oxide (wt. %)	5-1	5-2	5-3	5-4	5-5	5-6	5-7	5-8	5-9	5-10	Avg	Min	Max	SD
PbO	61.06	60.41	59.95	60.79	61.25	60.51	60.48	60.75	61.28	60.99	60.75	59.95	61.28	0.42
BaO	0.07	0.00	0.00	0.00	0.00	0.00	0.00	0.00	0.00	0.00	0.01	0.00	0.07	0.02
CaO	0.04	0.00	0.00	0.00	0.01	0.01	0.00	0.02	0.00	0.02	0.01	0.00	0.04	0.01
ZnO	0.00	0.00	0.00	0.00	0.00	0.00	0.00	0.01	0.00	0.00	0.00	0.00	0.01	0.00
MoO_3	39.15	39.30	39.08	39.36	38.93	39.04	39.07	37.53	39.24	39.10	38.98	37.53	39.36	0.52
WO_3	0.02	0.22	0.25	0.19	0.12	0.13	0.13	0.22	0.17	0.06	0.15	0.02	0.25	0.07
SO_3	0.00	0.00	0.03	0.00	0.00	0.06	0.06	0.00	0.03	0.00	0.02	0.00	0.06	0.03
CrO_3	0.00	0.01	0.00	0.00	0.00	0.00	0.00	0.00	0.00	0.00	0.00	0.00	0.01	0.00
V_2O_5	0.02	0.11	0.06	0.04	0.10	0.05	0.00	0.15	0.04	0.00	0.06	0.00	0.15	0.05
Total	**100.37**	**100.05**	**99.37**	**100.38**	**100.40**	**99.80**	**99.74**	**98.68**	**100.77**	**100.17**	**99.97**	**98.68**	**100.77**	**0.61**
	apfu	*apfu*	*apfu*	*apfu*	*apfu*	*apfu*	*apfu*	*apfu*	*apfu*	*apfu*	Avg	Min	Max	SD
Pb^{2+} (1.29 Å)	1.002	0.988	0.986	0.994	1.007	0.995	0.995	1.025	1.001	1.004	1.000	0.986	1.025	0.011
Ba^{2+} (1.42 Å)	0.002	0.000	0.000	0.000	0.000	0.000	0.000	0.000	0.000	0.000	0.000	0.000	0.002	0.001
Ca^{2+} (1.12 Å)	0.003	0.000	0.000	0.000	0.000	0.000	0.000	0.001	0.000	0.001	0.001	0.000	0.003	0.001
Zn^{2+} (0.90 Å)	0.000	0.000	0.000	0.000	0.000	0.000	0.000	0.000	0.000	0.000	0.000	0.000	0.000	0.000
ΣA	**1.007**	**0.988**	**0.986**	**0.994**	**1.007**	**0.995**	**0.995**	**1.027**	**1.001**	**1.005**	**1.001**	**0.986**	**1.027**	**0.012**
Mo^{6+} (0.41 Å)	0.997	0.996	0.997	0.998	0.992	0.995	0.997	0.982	0.994	0.997	0.995	0.982	0.998	0.005
W^{6+} (0.42 Å)	0.000	0.004	0.004	0.003	0.002	0.002	0.002	0.004	0.003	0.001	0.002	0.000	0.004	0.001
S^{6+} (0.12 Å)	0.000	0.000	0.002	0.000	0.000	0.003	0.003	0.000	0.001	0.000	0.001	0.000	0.003	0.001
Cr^{6+} (0.26 Å)	0.000	0.000	0.000	0.000	0.000	0.000	0.000	0.000	0.000	0.000	0.000	0.000	0.000	0.000
V^{5+} (0.36 Å)	0.001	0.005	0.002	0.002	0.004	0.002	0.000	0.006	0.002	0.000	0.002	0.000	0.006	0.002
ΣB	**0.998**	**1.005**	**1.005**	**1.002**	**0.998**	**1.002**	**1.002**	**0.992**	**1.000**	**0.998**	**1.000**	**0.992**	**1.005**	**0.004**
Total	**2.005**	**1.993**	**1.991**	**1.996**	**2.005**	**1.997**	**1.997**	**2.019**	**2.001**	**2.003**	**2.001**	**1.991**	**2.019**	**0.008**

Table A6: EPMA results for Sample 7U from Los Lamentos, Chihuahua, Mexico presented as wt. % oxides and calculated *apfu* on the basis of 4 oxygen atoms. Atoms are grouped into either A or B sites in the general ABO_4 formula.

Sample 7U Los Lamentos, Mexico Oxide (wt. %)	7-1	7-2	7-3	7-4	7-5	7-6	7-7	7-8	7-9	7-10	Avg	Min	Max	SD
PbO	60.29	60.48	60.57	60.87	60.60	60.49	60.53	60.67	59.93	60.48	60.49	59.93	60.87	0.25
BaO	0.00	0.02	0.00	0.00	0.00	0.01	0.05	0.03	0.00	0.00	0.01	0.00	0.05	0.02
CaO	n	n	n	n	n	n	n	n	n	n	n	n	n	n
ZnO	0.01	0.00	0.00	0.00	0.00	0.00	0.00	0.00	0.00	0.01	0.00	0.00	0.01	0.00
MoO_3	38.44	38.48	38.72	38.80	38.44	38.83	39.27	38.71	38.74	38.09	38.65	38.09	39.27	0.31
WO_3	0.04	0.00	0.00	0.26	0.00	0.03	0.00	0.10	0.14	0.02	0.06	0.00	0.26	0.09
SO_3	0.07	0.05	0.00	0.18	0.17	0.05	0.00	0.00	0.00	0.10	0.06	0.00	0.18	0.07
CrO_3	n	n	n	n	n	n	n	n	n	n	n	n	n	n
V_2O_5	0.05	0.06	0.06	0.05	0.08	0.06	0.02	0.01	0.02	0.04	0.05	0.01	0.08	0.02
Total	**98.90**	**99.08**	**99.34**	**100.17**	**99.29**	**99.47**	**99.86**	**99.53**	**98.83**	**98.74**	**99.32**	**98.74**	**100.17**	**0.46**
	apfu	*apfu*	*apfu*	*apfu*	*apfu*	*apfu*	*apfu*	*apfu*	*apfu*	*apfu*	Avg	Min	Max	SD
Pb^{2+} (1.29 Å)	1.004	1.007	1.005	0.998	1.004	1.000	0.995	1.006	0.996	1.013	1.003	0.995	1.013	0.006
Ba^{2+} (1.42 Å)	0.000	0.000	0.000	0.000	0.000	0.000	0.001	0.001	0.000	0.000	0.000	0.000	0.001	0.000
Ca^{2+} (1.12 Å)	n	n	n	n	n	n	n	n	n	n	n	n	n	n
Zn^{2+} (0.90 Å)	0.001	0.000	0.000	0.000	0.000	0.000	0.000	0.000	0.000	0.000	0.000	0.000	0.001	0.000
ΣA	**1.005**	**1.007**	**1.005**	**0.998**	**1.004**	**1.000**	**0.996**	**1.007**	**0.996**	**1.013**	**1.003**	**0.996**	**1.013**	**0.006**
Mo^{6+} (0.41 Å)	0.993	0.993	0.996	0.986	0.988	0.995	1.001	0.996	0.998	0.989	0.994	0.986	1.001	0.005
W^{6+} (0.42 Å)	0.001	0.000	0.000	0.004	0.000	0.001	0.000	0.002	0.002	0.000	0.001	0.000	0.004	0.001
S^{6+} (0.12 Å)	0.003	0.002	0.000	0.008	0.008	0.002	0.000	0.000	0.000	0.005	0.003	0.000	0.008	0.003
Cr^{6+} (0.26 Å)	n	n	n	n	n	n	n	n	n	n	n	n	n	n
V^{5+} (0.36 Å)	0.002	0.002	0.002	0.002	0.003	0.003	0.001	0.001	0.001	0.002	0.002	0.001	0.003	0.001
ΣB	**0.999**	**0.998**	**0.999**	**1.001**	**0.999**	**1.000**	**1.001**	**0.998**	**1.001**	**0.996**	**0.999**	**0.996**	**1.001**	**0.002**
Total	**2.004**	**2.005**	**2.004**	**1.999**	**2.003**	**2.001**	**1.997**	**2.005**	**1.998**	**2.009**	**2.002**	**1.997**	**2.009**	**0.004**

Table A7: EPMA results for Sample 8U from Red Cloud Mine, La Paz, County, Arizona presented as wt. % oxides and calculated *apfu* on the basis of 4 oxygen atoms. Atoms are grouped into either A or B sites in the general ABO_4 formula.

Sample 8U Red Cloud Mine, Arizona Oxide (wt. %)	8-1	8-2	8-3	8-4	8-5	8-6	8-7	8-8	8-9	8-10	Avg	Min	Max	SD
PbO	60.48	60.40	60.34	60.46	60.97	60.99	60.10	59.85	60.71	60.40	60.47	59.85	60.99	0.35
BaO	0.00	0.00	0.00	0.00	0.00	0.07	0.00	0.00	0.00	0.01	0.01	0.00	0.07	0.02
CaO	n	n	n	n	n	n	n	n	n	n	n	n	n	n
ZnO	0.00	0.00	0.00	0.00	0.00	0.00	0.00	0.00	0.00	0.03	0.00	0.00	0.03	0.01
MoO_3	38.40	38.54	38.55	38.59	38.68	38.88	38.79	38.70	38.81	38.87	38.68	38.40	38.88	0.16
WO_3	0.29	0.00	0.14	0.17	0.40	0.02	0.00	0.00	0.16	0.17	0.14	0.00	0.40	0.14
SO_3	0.02	0.01	0.00	0.00	0.02	0.05	0.00	0.03	0.00	0.03	0.02	0.00	0.05	0.02
CrO_3	n	n	n	n	n	n	n	n	n	n	n	n	n	n
V_2O_5	0.01	0.04	0.02	0.01	0.00	0.00	0.02	0.00	0.00	0.00	0.01	0.00	0.04	0.01
Total	**99.20**	**99.00**	**99.06**	**99.23**	**100.07**	**100.01**	**98.91**	**98.58**	**99.68**	**99.52**	**99.32**	**98.58**	**100.07**	**0.49**
	apfu	*apfu*	*apfu*	*apfu*	*apfu*	*apfu*	*apfu*	*apfu*	*apfu*	*apfu*	Avg	Min	Max	SD
Pb^{2+} (1.29 Å)	1.007	1.006	1.005	1.005	1.007	1.006	0.999	0.997	1.005	0.998	1.004	0.997	1.007	0.004
Ba^{2+} (1.42 Å)	0.000	0.000	0.000	0.000	0.000	0.002	0.000	0.000	0.000	0.000	0.000	0.000	0.002	0.000
Ca^{2+} (1.12 Å)	n	n	n	n	n	n	n	n	n	n	n	n	n	n
Zn^{2+} (0.90 Å)	0.000	0.000	0.000	0.000	0.000	0.000	0.000	0.000	0.000	0.001	0.000	0.000	0.001	0.000
ΣA	**1.007**	**1.006**	**1.005**	**1.005**	**1.007**	**1.008**	**0.999**	**0.997**	**1.005**	**1.000**	**1.004**	**0.997**	**1.008**	**0.004**
Mo^{6+} (0.41 Å)	0.992	0.996	0.995	0.995	0.990	0.995	1.000	0.999	0.996	0.996	0.995	0.990	1.000	0.003
W^{6+} (0.42 Å)	0.005	0.000	0.002	0.003	0.006	0.000	0.000	0.000	0.003	0.003	0.002	0.000	0.006	0.002
S^{6+} (0.12 Å)	0.001	0.001	0.000	0.000	0.001	0.002	0.000	0.001	0.000	0.001	0.001	0.000	0.002	0.001
Cr^{6+} (0.26 Å)	n	n	n	n	n	n	n	n	n	n	n	n	n	n
V^{5+} (0.36 Å)	0.000	0.002	0.001	0.000	0.000	0.000	0.001	0.000	0.000	0.000	0.000	0.000	0.002	0.001
ΣB	**0.998**	**0.998**	**0.999**	**0.998**	**0.998**	**0.997**	**1.001**	**1.001**	**0.998**	**1.000**	**0.999**	**0.997**	**1.001**	**0.001**
Total	**2.005**	**2.005**	**2.003**	**2.004**	**2.004**	**2.005**	**1.999**	**1.998**	**2.003**	**2.000**	**2.003**	**1.998**	**2.005**	**0.003**

Table A8: EPMA results for Sample 7X from Tong Wah (Tae Wha) Mine, Korea presented as wt. % oxides and calculated *apfu* on the basis of 4 oxygen atoms. Atoms are grouped into either A or B sites in the general ABO_4 formula.

Sample 7X: Tong Wah (Tae Wha) Mine, Korea														
Oxide (wt. %)	7-1	7-2	7-3	7-4	7-5	7-6	7-7	7-8	7-9	7-10	Avg	Min	Max	SD
MnO	15.47	15.25	14.84	15.12	15.28	15.57	14.59	15.26	14.95	15.12	15.14	14.59	15.57	0.29
FeO	8.58	8.62	9.02	8.73	8.49	8.30	9.22	8.60	8.80	8.78	8.71	8.30	9.22	0.26
ZnO	0.07	0.03	0.00	0.06	0.00	0.00	0.02	0.00	0.00	0.05	0.02	0.00	0.07	0.03
MgO	0.02	0.02	0.00	0.00	0.02	0.02	0.06	0.00	0.00	0.01	0.02	0.00	0.06	0.02
NiO	0.00	0.01	0.01	0.01	0.05	0.02	0.02	0.04	0.03	0.04	0.02	0.00	0.05	0.02
CaO	0.00	0.00	0.00	0.00	0.00	0.01	0.00	0.00	0.00	0.02	0.00	0.00	0.02	0.01
PbO	0.00	0.00	0.00	0.00	0.00	0.00	0.00	0.00	0.00	0.00	0.00	0.00	0.00	0.00
WO_3	76.46	75.79	76.35	75.98	75.96	76.34	75.56	76.10	76.61	75.90	76.11	75.56	76.61	0.33
MoO_3	0.00	0.00	0.00	0.00	0.00	0.00	0.00	0.00	0.00	0.00	0.00	0.00	0.00	0.00
SO_3	0.00	0.11	0.00	0.08	0.11	0.00	0.00	0.06	0.23	0.03	0.06	0.00	0.23	0.08
TiO_2	0.00	0.00	0.00	0.00	0.00	0.00	0.15	0.01	0.01	0.00	0.02	0.00	0.15	0.05
V_2O_3	0.00	0.00	0.00	0.01	0.01	0.00	0.00	0.00	0.00	0.00	0.00	0.00	0.01	0.00
Cr_2O_3	0.00	0.02	0.03	0.00	0.00	0.02	0.00	0.00	0.00	0.00	0.01	0.00	0.03	0.01
Total	**100.60**	**99.85**	**100.24**	**100.00**	**99.92**	**100.28**	**99.62**	**100.07**	**100.64**	**99.95**	**100.12**	**99.62**	**100.64**	**0.32**
	apfu	*apfu*	*apfu*	*apfu*	*apfu*	*apfu*	*apfu*	*apfu*	*apfu*	*apfu*	Avg	Min	Max	SD
Mn^{2+} (0.83 Å)*	0.657	0.651	0.632	0.645	0.652	0.663	0.624	0.651	0.632	0.646	0.645	0.624	0.663	0.012
Fe^{2+} (0.78 Å)	0.360	0.363	0.379	0.368	0.358	0.349	0.390	0.362	0.367	0.370	0.367	0.349	0.390	0.011
Zn^{2+} (0.74 Å)	0.002	0.001	0.000	0.002	0.000	0.000	0.001	0.000	0.000	0.002	0.001	0.000	0.002	0.001
Mg^{2+} (0.72 Å)	0.001	0.002	0.000	0.000	0.001	0.002	0.005	0.000	0.000	0.001	0.001	0.000	0.005	0.001
Ni^{2+} (0.69 Å)	0.000	0.000	0.000	0.001	0.002	0.001	0.001	0.001	0.001	0.002	0.001	0.000	0.002	0.001
Ca^{2+} (1.00 Å)	0.000	0.000	0.000	0.000	0.000	0.001	0.000	0.000	0.000	0.001	0.000	0.000	0.001	0.000
Pb^{2+} (1.19 Å)	0.000	0.000	0.000	0.000	0.000	0.000	0.000	0.000	0.000	0.000	0.000	0.000	0.000	0.000
ΣA	**1.020**	**1.017**	**1.012**	**1.015**	**1.013**	**1.015**	**1.020**	**1.014**	**1.000**	**1.021**	**1.015**	**1.000**	**1.021**	**0.006**
W^{6+} (0.60 Å)	0.993	0.990	0.996	0.992	0.991	0.995	0.989	0.993	0.991	0.992	0.992	0.989	0.996	0.002
Mo^{6+} (0.59 Å)	0.000	0.000	0.000	0.000	0.000	0.000	0.000	0.000	0.000	0.000	0.000	0.000	0.000	0.000
S^{6+} (0.29 Å)	0.000	0.004	0.000	0.003	0.004	0.000	0.000	0.002	0.009	0.001	0.002	0.000	0.009	0.003
Ti^{4+} (0.61 Å)	0.000	0.000	0.000	0.000	0.000	0.000	0.006	0.000	0.000	0.000	0.001	0.000	0.006	0.002
V^{3+} (0.64 Å)	0.000	0.000	0.000	0.000	0.000	0.000	0.000	0.000	0.000	0.000	0.000	0.000	0.000	0.000
Cr^{3+} (0.62 Å)	0.000	0.001	0.001	0.000	0.000	0.001	0.000	0.000	0.000	0.000	0.000	0.000	0.001	0.000
ΣB	**0.993**	**0.995**	**0.997**	**0.995**	**0.996**	**0.995**	**0.995**	**0.995**	**1.000**	**0.993**	**0.995**	**0.993**	**1.000**	**0.002**
Total	**2.014**	**2.012**	**2.008**	**2.010**	**2.009**	**2.010**	**2.015**	**2.009**	**2.000**	**2.014**	**2.010**	**2.000**	**2.015**	**0.004**
%Hu	64.61	64.17	62.50	63.68	64.56	65.50	61.58	64.24	63.24	63.56	63.77	61.58	65.50	1.13

Table A9: EPMA results for Sample 3X from Oregon Mine, Boulder, Colorado presented as wt. % oxides and calculated *apfu* on the basis of 4 oxygen atoms. Atoms are grouped into either A or B sites in the general ABO_4 formula.

Sample 3X: Oregon Mine, Boulder, Colorado														
Oxide (wt. %)	3-1	3-2	3-3	3-4	3-5	3-6	3-7	3-8	3-9	3-10	Avg	Min	Max	SD
MnO	17.82	17.70	18.48	17.66	19.05	20.16	18.18	19.21	17.54	20.07	18.59	17.54	20.16	0.99
FeO	5.82	5.93	5.01	5.89	4.24	3.27	5.20	4.28	6.27	3.42	4.93	3.27	6.27	1.08
ZnO	0.02	0.00	0.00	0.02	0.06	0.03	0.00	0.02	0.06	0.04	0.02	0.00	0.06	0.02
MgO	0.03	0.00	0.00	0.00	0.00	0.02	0.00	0.00	0.00	0.00	0.00	0.00	0.03	0.01
NiO	0.00	0.07	0.02	0.00	0.02	0.04	0.03	0.02	0.01	0.04	0.02	0.00	0.07	0.02
CaO	0.00	0.00	0.03	0.00	0.01	0.00	0.03	0.00	0.00	0.00	0.01	0.00	0.03	0.01
PbO	0.00	0.00	0.00	0.00	0.00	0.00	0.00	0.00	0.00	0.00	0.00	0.00	0.00	0.00
WO_3	76.33	76.39	76.30	76.47	75.81	76.05	75.58	75.99	76.45	76.00	76.14	75.58	76.47	0.30
MoO_3	0.00	0.00	0.00	0.00	0.00	0.00	0.00	0.00	0.00	0.00	0.00	0.00	0.00	0.00
SO_3	0.10	0.00	0.11	0.26	0.14	0.04	0.10	0.20	0.04	0.21	0.12	0.00	0.26	0.08
TiO_2	0.00	0.00	0.00	0.00	0.02	0.00	0.07	0.06	0.00	0.00	0.01	0.00	0.07	0.03
V_2O_3	0.01	0.00	0.00	0.00	0.00	0.00	0.00	0.04	0.00	0.00	0.00	0.00	0.04	0.01
Cr_2O_3	0.00	0.00	0.00	0.00	0.00	0.00	0.00	0.00	0.00	0.00	0.00	0.00	0.00	0.00
Total	**100.12**	**100.09**	**99.95**	**100.31**	**99.34**	**99.61**	**99.19**	**99.81**	**100.37**	**99.78**	**99.86**	**99.19**	**100.37**	**0.39**
	apfu	*apfu*	*apfu*	*apfu*	*apfu*	*apfu*	*apfu*	*apfu*	*apfu*	*apfu*	Avg	Min	Max	SD
Mn^{2+} (0.83 Å)	0.759	0.755	0.788	0.748	0.817	0.864	0.781	0.818	0.746	0.856	0.793	0.746	0.864	0.044
Fe^{2+} (0.78 Å)	0.244	0.250	0.211	0.247	0.179	0.138	0.221	0.180	0.263	0.144	0.208	0.138	0.263	0.045
Zn^{2+} (0.74 Å)	0.001	0.000	0.000	0.001	0.002	0.001	0.000	0.001	0.002	0.001	0.001	0.000	0.002	0.001
Mg^{2+} (0.72 Å)	0.002	0.000	0.000	0.000	0.000	0.001	0.000	0.000	0.000	0.000	0.000	0.000	0.002	0.001
Ni^{2+} (0.69 Å)	0.000	0.003	0.001	0.000	0.001	0.002	0.001	0.001	0.000	0.001	0.001	0.000	0.003	0.001
Ca^{2+} (1.00 Å)	0.000	0.000	0.002	0.000	0.000	0.000	0.001	0.000	0.000	0.000	0.000	0.000	0.002	0.001
Pb^{2+} (1.19 Å)	0.000	0.000	0.000	0.000	0.000	0.000	0.000	0.000	0.000	0.000	0.000	0.000	0.000	0.000
ΣA	**1.006**	**1.008**	**1.001**	**0.996**	**0.999**	**1.006**	**1.004**	**1.000**	**1.011**	**1.002**	**1.003**	**0.996**	**1.011**	**0.005**
W^{6+} (0.60 Å)	0.994	0.997	0.995	0.992	0.994	0.997	0.993	0.990	0.995	0.991	0.994	0.990	0.997	0.002
Mo^{6+} (0.59 Å)	0.000	0.000	0.000	0.000	0.000	0.000	0.000	0.000	0.000	0.000	0.000	0.000	0.000	0.000
S^{6+} (0.29 Å)	0.004	0.000	0.004	0.010	0.005	0.001	0.004	0.007	0.002	0.008	0.005	0.000	0.010	0.003
Ti^{4+} (0.61 Å)	0.000	0.000	0.000	0.000	0.001	0.000	0.003	0.002	0.000	0.000	0.001	0.000	0.003	0.001
V^{3+} (0.64 Å)	0.000	0.000	0.000	0.000	0.000	0.000	0.000	0.002	0.000	0.000	0.000	0.000	0.002	0.000
Cr^{3+} (0.62 Å)	0.000	0.000	0.000	0.000	0.000	0.000	0.000	0.000	0.000	0.000	0.000	0.000	0.000	0.000
ΣB	**0.998**	**0.997**	**1.000**	**1.001**	**1.001**	**0.998**	**1.000**	**1.002**	**0.996**	**0.999**	**0.999**	**0.996**	**1.002**	**0.002**
Total	**2.004**	**2.005**	**2.001**	**1.997**	**2.000**	**2.004**	**2.003**	**2.001**	**2.008**	**2.002**	**2.002**	**1.997**	**2.008**	**0.003**
%Hu	75.63	75.13	78.88	75.22	81.98	86.19	77.97	81.98	73.91	85.60	79.24	73.91	86.19	4.47

Table A10: EPMA results for Sample 8X from Silverton, Colorado presented as wt. % oxides and calculated *apfu* on the basis of 4 oxygen atoms. Atoms are grouped into either A or B sites in the general ABO_4 formula.

Sample 8X: Silverton, Colorado														
Oxide (wt. %)	8-1	8-2	8-3	8-4	8-5	8-6	8-7	8-8	8-9	8-10	Avg	Min	Max	SD
MnO	21.90	22.17	21.16	21.96	21.73	22.35	22.67	21.46	21.41	22.03	21.89	21.16	22.67	0.46
FeO	1.64	1.26	2.31	1.36	1.70	0.87	0.56	2.03	2.12	1.29	1.51	0.56	2.31	0.56
ZnO	0.00	0.02	0.01	0.00	0.00	0.04	0.00	0.02	0.00	0.00	0.01	0.00	0.04	0.01
MgO	0.00	0.00	0.00	0.00	0.01	0.00	0.02	0.01	0.00	0.00	0.00	0.00	0.02	0.01
NiO	0.05	0.06	0.03	0.00	0.01	0.05	0.01	0.02	0.02	0.05	0.03	0.00	0.06	0.02
CaO	0.00	0.00	0.00	0.00	0.01	0.00	0.00	0.00	0.00	0.00	0.00	0.00	0.01	0.00
PbO	0.00	0.00	0.00	0.00	0.00	0.00	0.00	0.00	0.00	0.00	0.00	0.00	0.00	0.00
WO_3	76.46	76.25	76.07	76.41	76.02	76.31	76.45	76.48	76.25	76.19	76.29	76.02	76.48	0.16
MoO_3	0.00	0.00	0.00	0.00	0.00	0.00	0.00	0.00	0.00	0.00	0.00	0.00	0.00	0.00
SO_3	0.02	0.28	0.00	0.00	0.00	0.00	0.06	0.04	0.02	0.05	0.05	0.00	0.28	0.09
TiO_2	0.00	0.00	0.00	0.00	0.00	0.00	0.00	0.00	0.00	0.00	0.00	0.00	0.00	0.00
V_2O_3	0.00	0.00	0.00	0.00	0.00	0.01	0.00	0.00	0.00	0.00	0.00	0.00	0.01	0.00
Cr_2O_3	0.00	0.00	0.01	0.00	0.01	0.01	0.00	0.00	0.00	0.03	0.01	0.00	0.03	0.01
Total	**100.07**	**100.04**	**99.59**	**99.74**	**99.48**	**99.64**	**99.76**	**100.06**	**99.83**	**99.64**	**99.78**	**99.48**	**100.07**	**0.21**
	apfu	*apfu*	*apfu*	*apfu*	*apfu*	*apfu*	*apfu*	*apfu*	*apfu*	*apfu*	Avg	Min	Max	SD
Mn^{2+} (0.83 Å)	0.934	0.941	0.907	0.940	0.932	0.958	0.969	0.915	0.915	0.943	0.935	0.907	0.969	0.019
Fe^{2+} (0.78 Å)	0.069	0.053	0.098	0.058	0.072	0.037	0.024	0.085	0.090	0.054	0.064	0.024	0.098	0.023
Zn^{2+} (0.74 Å)	0.000	0.001	0.000	0.000	0.000	0.001	0.000	0.001	0.000	0.000	0.000	0.000	0.001	0.000
Mg^{2+} (0.72 Å)	0.000	0.000	0.000	0.000	0.001	0.000	0.002	0.001	0.000	0.000	0.000	0.000	0.002	0.001
Ni^{2+} (0.69 Å)	0.002	0.003	0.001	0.000	0.001	0.002	0.000	0.001	0.001	0.002	0.001	0.000	0.003	0.001
Ca^{2+} (1.00 Å)	0.000	0.000	0.000	0.000	0.000	0.000	0.000	0.000	0.000	0.000	0.000	0.000	0.000	0.000
Pb^{2+} (1.19 Å)	0.000	0.000	0.000	0.000	0.000	0.000	0.000	0.000	0.000	0.000	0.000	0.000	0.000	0.000
ΣA	**1.005**	**0.997**	**1.007**	**0.998**	**1.006**	**0.998**	**0.994**	**1.002**	**1.006**	**0.999**	**1.001**	**0.994**	**1.007**	**0.004**
W^{6+} (0.60 Å)	0.998	0.990	0.998	1.001	0.998	1.000	1.000	0.998	0.997	0.998	0.998	0.990	1.001	0.003
Mo^{6+} (0.59 Å)	0.000	0.000	0.000	0.000	0.000	0.000	0.000	0.000	0.000	0.000	0.000	0.000	0.000	0.000
S^{6+} (0.29 Å)	0.001	0.011	0.000	0.000	0.000	0.000	0.002	0.002	0.001	0.002	0.002	0.000	0.011	0.003
Ti^{4+} (0.61 Å)	0.000	0.000	0.000	0.000	0.000	0.000	0.000	0.000	0.000	0.000	0.000	0.000	0.000	0.000
V^{3+} (0.64 Å)	0.000	0.000	0.000	0.000	0.000	0.001	0.000	0.000	0.000	0.000	0.000	0.000	0.001	0.000
Cr^{3+} (0.62 Å)	0.000	0.000	0.000	0.000	0.000	0.000	0.000	0.000	0.000	0.001	0.000	0.000	0.001	0.000
ΣB	**0.998**	**1.001**	**0.998**	**1.001**	**0.998**	**1.001**	**1.002**	**0.999**	**0.998**	**1.001**	**1.000**	**0.998**	**1.002**	**0.002**
Total	**2.003**	**1.998**	**2.004**	**1.999**	**2.004**	**1.999**	**1.996**	**2.002**	**2.004**	**2.000**	**2.001**	**1.996**	**2.004**	**0.003**
%Hu	93.12	94.71	90.27	94.23	92.83	96.29	97.62	91.48	91.09	94.54	93.61	90.27	97.62	2.32

Table A11: EPMA results for Sample 9X from Pasto Bueno, Peru presented as wt. % oxides and calculated *apfu* on the basis of 4 oxygen atoms. Atoms are grouped into either A or B sites in the general ABO_4 formula.

Sample 9X: Pasto Bueno, Peru														
Oxide (wt. %)	9-1	9-2	9-3	9-4	9-5	9-6	9-7	9-8	9-9	9-10	Avg	Min	Max	SD
MnO	23.41	n	23.58	23.49	23.56	23.25	23.37	23.35	23.26	23.43	23.41	23.25	23.58	0.12
FeO	0.08	n	0.05	0.09	0.10	0.07	0.05	0.06	0.09	0.08	0.07	0.05	0.10	0.02
ZnO	0.04	n	0.05	0.04	0.08	0.04	0.02	0.05	0.05	0.01	0.04	0.01	0.08	0.02
MgO	0.00	n	0.00	0.00	0.00	0.00	0.00	0.00	0.03	0.00	0.00	0.00	0.03	0.01
NiO	0.01	n	0.04	0.01	0.01	0.03	0.00	0.00	0.00	0.04	0.02	0.00	0.04	0.02
CaO	0.00	n	0.00	0.00	0.00	0.00	0.00	0.01	0.00	0.00	0.00	0.00	0.01	0.00
PbO	0.00	n	0.00	0.00	0.00	0.00	0.00	0.00	0.00	0.00	0.00	0.00	0.00	0.00
WO_3	76.47	n	76.57	76.08	76.50	75.96	76.01	75.62	75.63	75.61	76.05	75.61	76.57	0.39
MoO_3	0.00	n	0.00	0.00	0.00	0.00	0.00	0.00	0.00	0.00	0.00	0.00	0.00	0.00
SO_3	0.25	n	0.13	0.26	0.04	0.05	0.00	0.00	0.01	0.00	0.08	0.00	0.26	0.11
TiO_2	0.02	n	0.00	0.01	0.02	0.00	0.03	0.00	0.01	0.01	0.01	0.00	0.03	0.01
V_2O_3	0.00	n	0.00	0.00	0.00	0.00	0.00	0.00	0.00	0.00	0.00	0.00	0.00	0.00
Cr_2O_3	0.00	n	0.00	0.00	0.00	0.01	0.01	0.02	0.00	0.00	0.00	0.00	0.02	0.01
Total	**100.28**		**100.42**	**99.98**	**100.31**	**99.41**	**99.48**	**99.12**	**99.08**	**99.17**	**99.69**	**99.08**	**100.42**	**0.55**
	apfu		*apfu*	*apfu*	*apfu*	*apfu*	*apfu*	*apfu*	*apfu*	*apfu*	Avg	Min	Max	SD
Mn^{2+} (0.83 Å)	0.991	n	1.000	0.998	1.002	0.997	1.002	1.005	1.001	1.008	1.000	0.991	1.008	0.005
Fe^{2+} (0.78 Å)	0.003	n	0.002	0.004	0.004	0.003	0.002	0.003	0.004	0.003	0.003	0.002	0.004	0.001
Zn^{2+} (0.74 Å)	0.001	n	0.002	0.001	0.003	0.001	0.001	0.002	0.002	0.000	0.002	0.000	0.003	0.001
Mg^{2+} (0.72 Å)	0.000	n	0.000	0.000	0.000	0.000	0.000	0.000	0.002	0.000	0.000	0.000	0.002	0.001
Ni^{2+} (0.69 Å)	0.000	n	0.002	0.000	0.000	0.001	0.000	0.000	0.000	0.001	0.001	0.000	0.002	0.001
Ca^{2+} (1.00 Å)	0.000	n	0.000	0.000	0.000	0.000	0.000	0.001	0.000	0.000	0.000	0.000	0.001	0.000
Pb^{2+} (1.19 Å)	0.000	n	0.000	0.000	0.000	0.000	0.000	0.000	0.000	0.000	0.000	0.000	0.000	0.000
ΣA	**0.997**		**1.005**	**1.004**	**1.009**	**1.003**	**1.005**	**1.010**	**1.009**	**1.013**	**1.006**	**0.997**	**1.013**	**0.005**
W^{6+} (0.60 Å)	0.991	n	0.993	0.989	0.995	0.997	0.998	0.996	0.996	0.995	0.994	0.989	0.998	0.003
Mo^{6+} (0.59 Å)	0.000	n	0.000	0.000	0.000	0.000	0.000	0.000	0.000	0.000	0.000	0.000	0.000	0.000
S^{6+} (0.29 Å)	0.009	n	0.005	0.010	0.002	0.002	0.000	0.000	0.000	0.000	0.003	0.000	0.010	0.004
Ti^{4+} (0.61 Å)	0.001	n	0.000	0.000	0.001	0.000	0.001	0.000	0.000	0.000	0.000	0.000	0.001	0.000
V^{3+} (0.64 Å)	0.000	n	0.000	0.000	0.000	0.000	0.000	0.000	0.000	0.000	0.000	0.000	0.000	0.000
Cr^{3+} (0.62 Å)	0.000	n	0.000	0.000	0.000	0.001	0.000	0.001	0.000	0.000	0.000	0.000	0.001	0.000
ΣB	**1.001**		**0.998**	**0.999**	**0.997**	**0.999**	**0.999**	**0.997**	**0.997**	**0.996**	**0.998**	**0.996**	**1.001**	**0.002**
Total	**1.998**		**2.003**	**2.002**	**2.006**	**2.002**	**2.004**	**2.007**	**2.006**	**2.009**	**2.004**	**1.998**	**2.009**	**0.003**
%Hu	99.68		99.80	99.62	99.57	99.70	99.80	99.75	99.62	99.67	99.69	99.57	99.80	0.08

Table A12: Sample 3X from Oregon Mine, Boulder, Colorado split into two potential phases: wolframite (Mn-content < 80%) and hübnerite (Mn-content > 80%). Patterns in trace element abundances are unclear

Sample 3X:
Oregon Mine, Boulder, Colorado

	Wolframite						Hubnerite									
Oxide (wt. %)	3-9	3-2	3-4	3-1	3-7	3-3	3-8	3-5	3-10	3-6	Avg	Min	Max	SD	Avg Wolf	Avg Hu
MnO	17.54	17.70	17.66	17.82	18.18	18.48	19.21	19.05	20.07	20.16	18.59	17.54	20.16	0.99	17.90	19.62
FeO	6.27	5.93	5.89	5.82	5.20	5.01	4.28	4.24	3.42	3.27	4.93	3.27	6.27	1.08	5.69	3.80
ZnO	0.06	0.00	0.02	0.02	0.00	0.00	0.02	0.06	0.04	0.03	0.02	0.00	0.06	0.02	0.02	0.04
MgO	0.00	0.00	0.00	0.03	0.00	0.00	0.00	0.00	0.00	0.02	0.00	0.00	0.03	0.01	0.01	0.00
NiO	0.01	0.07	0.00	0.00	0.03	0.02	0.02	0.02	0.04	0.04	0.02	0.00	0.07	0.02	0.02	0.03
CaO	0.00	0.00	0.00	0.00	0.03	0.03	0.00	0.01	0.00	0.00	0.01	0.00	0.03	0.01	0.01	0.00
PbO	0.00	0.00	0.00	0.00	0.00	0.00	0.00	0.00	0.00	0.00	0.00	0.00	0.00	0.00	0.00	0.00
WO_3	76.45	76.39	76.47	76.33	75.58	76.30	75.99	75.81	76.00	76.05	76.14	75.58	76.47	0.30	76.25	75.96
MoO_3	0.00	0.00	0.00	0.00	0.00	0.00	0.00	0.00	0.00	0.00	0.00	0.00	0.00	0.00	0.00	0.00
SO_3	0.04	0.00	0.26	0.10	0.10	0.11	0.20	0.14	0.21	0.04	0.12	0.00	0.26	0.08	0.10	0.15
TiO_2	0.00	0.00	0.00	0.00	0.07	0.00	0.06	0.02	0.00	0.00	0.01	0.00	0.07	0.03	0.01	0.02
V_2O_3	0.00	0.00	0.00	0.01	0.00	0.00	0.04	0.00	0.00	0.00	0.00	0.00	0.04	0.01	0.00	0.01
Cr_2O_3	0.00	0.00	0.00	0.00	0.00	0.00	0.00	0.00	0.00	0.00	0.00	0.00	0.00	0.00	0.00	0.00
Total	**100.37**	**100.09**	**100.31**	**100.12**	**99.19**	**99.95**	**99.81**	**99.34**	**99.78**	**99.61**	**99.86**	**99.19**	**100.37**	**0.39**	**100.00**	**99.63**
	apfu	*apfu*	*apfu*	*apfu*	*apfu*	*apfu*	*apfu*	*apfu*	*apfu*	*apfu*	Avg	Min	Max	SD		
Mn^{2+} (0.83 Å)	0.746	0.755	0.748	0.759	0.781	0.788	0.818	0.817	0.856	0.864	0.793	0.746	0.864	0.044	0.76	0.84
Fe^{2+} (0.78 Å)	0.263	0.250	0.247	0.244	0.221	0.211	0.180	0.179	0.144	0.138	0.208	0.138	0.263	0.045	0.24	0.16
Zn^{2+} (0.74 Å)	0.002	0.000	0.001	0.001	0.000	0.000	0.001	0.002	0.001	0.001	0.001	0.000	0.002	0.001	0.00	0.00
Mg^{2+} (0.72 Å)	0.000	0.000	0.000	0.002	0.000	0.000	0.000	0.000	0.000	0.001	0.000	0.000	0.002	0.001	0.00	0.00
Ni^{2+} (0.69 Å)	0.000	0.003	0.000	0.000	0.001	0.001	0.001	0.001	0.001	0.002	0.001	0.000	0.003	0.001	0.00	0.00
Ca^{2+} (1.00 Å)	0.000	0.000	0.000	0.000	0.001	0.002	0.000	0.000	0.000	0.000	0.000	0.000	0.002	0.001	0.00	0.00
Pb^{2+} (1.19 Å)	0.000	0.000	0.000	0.000	0.000	0.000	0.000	0.000	0.000	0.000	0.000	0.000	0.000	0.000	0.00	0.00
ΣA	**1.011**	**1.008**	**0.996**	**1.006**	**1.004**	**1.001**	**1.000**	**0.999**	**1.002**	**1.006**	**1.003**	**0.996**	**1.011**	**0.005**	**1.00**	**1.00**
W^{6+} (0.60 Å)	0.995	0.997	0.992	0.994	0.993	0.995	0.990	0.994	0.991	0.997	0.994	0.990	0.997	0.002	0.99	0.99
Mo^{6+} (0.59 Å)	0.000	0.000	0.000	0.000	0.000	0.000	0.000	0.000	0.000	0.000	0.000	0.000	0.000	0.000	0.00	0.00
S^{6+} (0.29 Å)	0.002	0.000	0.010	0.004	0.004	0.004	0.007	0.005	0.008	0.001	0.005	0.000	0.010	0.003	0.00	0.01
Ti^{4+} (0.61 Å)	0.000	0.000	0.000	0.000	0.003	0.000	0.002	0.001	0.000	0.000	0.001	0.000	0.003	0.001	0.00	0.00
V^{3+} (0.64 Å)	0.000	0.000	0.000	0.000	0.000	0.000	0.002	0.000	0.000	0.000	0.000	0.000	0.002	0.000	0.00	0.00
Cr^{3+} (0.62 Å)	0.000	0.000	0.000	0.000	0.000	0.000	0.000	0.000	0.000	0.000	0.000	0.000	0.000	0.000	0.00	0.00
ΣB	**0.996**	**0.997**	**1.001**	**0.998**	**1.000**	**1.000**	**1.002**	**1.001**	**0.999**	**0.998**	**0.999**	**0.996**	**1.002**	**0.002**	**1.00**	**1.00**
Total	**2.008**	**2.005**	**1.997**	**2.004**	**2.003**	**2.001**	**2.001**	**2.000**	**2.002**	**2.004**	**2.002**	**1.997**	**2.008**	**0.003**	**2.00**	**2.00**
%Hu	73.91	75.13	75.22	75.63	77.97	78.88	81.98	81.98	85.60	86.19	79.24	73.91	86.19	4.47	76.12	83.94